The Role of Hydrogen and Ammonia in Decarbonizing the Steel and Power Sectors

D205690

KHUSNIDDIN ALIKULOV ZARIFOVICH

A Dissertation Submitted to
the Graduate School of Advanced Science and Engineering
of Hiroshima University in Partial Fulfilment
of the Requirement for the Degree
of Doctor of Philosophy in Engineering

April 2024

Table of Contents

List of Figures

List of Tables

List of Equations

ABSTRACT

Decarbonizing current conventional and fossil fuel-based steel and power sectors is crucial for the sustainable development of the industrial sectors in the future. In the steel sector, several research works, and pilot projects are ongoing to transform the Direct Reduction Iron Ore – Electric Arc Furnace route into the Hydrogen Direct Reduction Iron Ore – Electric Arc Furnace route. On the other hand, there are various research works and projects investigating the stable operation of existing gas turbine units with ammonia and hydrogen fuel blends. The present study focuses on three clusters of research works. Firstly, the optimization of iron ore reduction with hydrogen fuel in a laboratory condition to achieve stoichiometric values for the route. In the second part of the research works, four scenarios with different fuel blending options are applied to existing gas turbine units with an installed capacity of 7.6 MW. In the third part of the current studies, technical and economic comparisons of the steel and power sectors are investigated under the use of 100% hydrogen fuel instead of conventional fuel, and the effect of using each 1 kg of hydrogen in the sectors is analyzed.

The first part of the research work aims to evaluate the energy and mass balance of the Hydrogen Direct Reduction Iron – Electric Arc Furnace route to identify optimal energy utilization and achieve stoichiometric hydrogen consumption per ton of liquid steel (tls) production under laboratory conditions. The route used 54.00 kg of H_2 and 2.68 MWh to reduce 1,428.00 kg of Fe_2O_3 and produce 1 tls. The experiments were conducted at temperatures of 750, 760, 770, 780, 790, and 800 °C, using 2.3622 g of Fe_2O_3, 1 L/min of H_2, 0.001 MPa, and residence times of 1, 2, 3, 3.5, 4, 5, 7, 10, and 15 minutes. Specifically, an experiment using two samples, each containing 2.3622 g of Fe_2O_3, at 770 °C, 0.001 MPa, with a residence time of 7 minutes and 1 L/min of H_2, resulted in reduction yields of 99.7 % and 99.33 %. Another experiment, using a single feedstock and a residence time of 3.5 minutes under the same conditions, yielded an 85.71% reduction. In conclusion, an approach utilizing 4.7244 g of Fe_2O_3 and a residence time of 7 minutes at 770 °C demonstrated a higher reduction yield compared to the one using 2.3622 g of Fe_2O_3 with a residence time of 3.5 minutes.

In the second part of the research, the effects of fuel blends comprising ammonia and hydrogen on the technical, economic, and environmental indicators of an existing 7.6 MW output power gas turbine unit were investigated and analyzed. Four models, each with different fuel-blending options, were designed using Aspen HYSYS and Ansys®Chemkin Pro to analyze the technical and chemical processes. The fuel blends for Scenarios 1, 2, 3, and 4 were 100% natural gas (NG), 30% ammonia (NH_3) and 70% NG, 30% hydrogen (H_2) and 70% NG, and 30% NH_3, 30% H_2, and 40% NG, respectively. Based on the technical and CO_2 emission values of each model developed in Aspen HYSYS, the focus was on Scenario 4 with ammonia and hydrogen co-firing. This scenario exhibited the highest electric efficiency (36.63%) and the lowest CO_2 emissions (3,979.00 kg CO2/h) but had higher costs (0.19 $/kWh) for generated electricity compared to other scenarios. Economic evaluations of all scenarios provided a clear understanding of each fuel cost and Levelized Cost of Electricity (LCOE). Initially, Scenario 2, with ammonia co-firing, appeared to be an attractive option for further implementation. However, detailed analyses of the combustion process in each model dramatically changed the final decision and provided a good reason to focus on hydrogen fuel, which significantly reduced NOx emissions. In conclusion, Scenario 3 with hydrogen co-firing demonstrated attractive performance and favorable combustion kinetics.

In the third part, three clusters of research works were conducted. In the first cluster, the mass and energy balance of the existing metallurgical complex based on the Tebinbulak mine were calculated and identified. In the second cluster, an existing gas turbine unit was selected for the complete replacement of natural gas with hydrogen, finding the most optimal mass and energy balance in the cycle through the Aspen HYSYS model. Additionally, chemical kinetics in the hydrogen combustion process were simulated using Ansys®Chemkin Pro to research emissions. In the last cluster, a comparative economic analysis was conducted to identify the levelized cost of production of the route and the levelized cost of electricity of the cycle. Findings in the economic analysis provided good insight into the details of capital and operational expenditure of each industrial sector, helping understand the impact of consuming each kg of hydrogen in the plants. The outcomes of this study serve as a solid foundation for future research works aimed at reducing the cost of hydrogen-based steel and power sectors. Moreover, the results of this study can also assist ongoing large-scale hydrogen and ammonia projects in Uzbekistan in designing novel hydrogen-based industries with cost-effective solutions.

Considering all the findings, in the case of Uzbekistan, there is limited opportunity to apply hydrogen in the steel manufacturing sector due to the unavailability of a suitable steel plant route at this moment. Most available steel manufacturing can be put into operation by 2027. On the other hand, the power sector in Uzbekistan has several gas turbine units in operation with a capacity ranging from 7.6 MW to 650 MW. An additional and alternative fuel to the gas turbine can be ammonia, but significant NOx emissions are a challenging point to replace natural gas. Therefore, in the short term, hydrogen combustion can be a potential option for replacing natural gas in the power sector. In both cases, the capital and operational expenditure of electrolyzer, compression, and storage units exceed the investment cost of target technologies. Instead of producing, storing, and compressing hydrogen fuel on project sites, it is also feasible to import hydrogen fuel from sellers for the successful implementation of 100% hydrogen-based steel and power plants. On the other hand, water scarcity in the region makes it challenging to produce hydrogen with electrolyzer units on-site. Alternatively, a large-scale hydrogen production project in Kazakhstan can be the optimal solution to meet the hydrogen consumption demand of each project. However, hydrogen transportation for long distances is not feasible at this moment, and ammonia can be a potential hydrogen carrier, which also requires energy for cracking it after transportation to a project site. Taking into consideration all conditions, 30% hydrogen co-firing in the selected gas turbine technology is possible to implement and meet all emission regulations set by the manufacturer. The reason for this ultimate statement is the possibility of meeting the required amount of hydrogen and the operation of all existing parts, including the combustor of the gas turbine. In any case, electrolyzer, compression, and storage units are required.

Acknowledgement

I would like to express my gratitude to several people who contributed to the successful implementation of my research goals.

Firstly, I extend my heartfelt thanks to Prof. Tran Dang Xuan, who supervised and guided me through every phase of my research, from its inception to its ultimate defense. Even in the final moments, Prof. Tran Dang Xuan continued to motivate me, ensuring the success of my ongoing research, and providing support in addressing academic and practical challenges. His mentorship has been invaluable, teaching me to confront challenges and tackle them with innovative solutions throughout my academic journey.

Secondly, I am deeply grateful to Prof. Ichihashi Masaru, Dr. Nguyen Van Quan, Asis. Prof. Dr. Hoang Anh La and Assoc. Prof. Kim Wookyung for their valuable advice, insightful comments, constructive feedback, specific suggestions, and extensive discussions, which have played a crucial role in achieving meaningful and significant results in all my research endeavors.

Thirdly, I would like to express my gratitude to the JDS scholarship for providing me with the financial support for the successful implementation of my Ph.D. in Japan at Hiroshima University. Additionally, I extend my thanks to my laboratory members and many friends for their assistance and support in learning new topics, methodologies, visualization techniques, and in preparing well-organized research articles.

Finally, I am especially grateful to my family and daughters for supporting and motivating me during difficult and successful moments throughout my academic life in Japan. I could not have achieved my research goals without their love and continuous support.

Chapter 1. General Introduction

1.1Background

The ongoing global warming, climate change, and depletion of natural resources worldwide have compelled humanity to seek environmentally friendly approaches to decarbonize existing industrial sectors, ensuring their sustainability in the coming decades. Figure 1 illustrates global greenhouse gas emissions by sectors, with energy sectors contributing 73.2%.[1]. Examining emissions from the energy sector, both iron & steel and fuel combustion in power

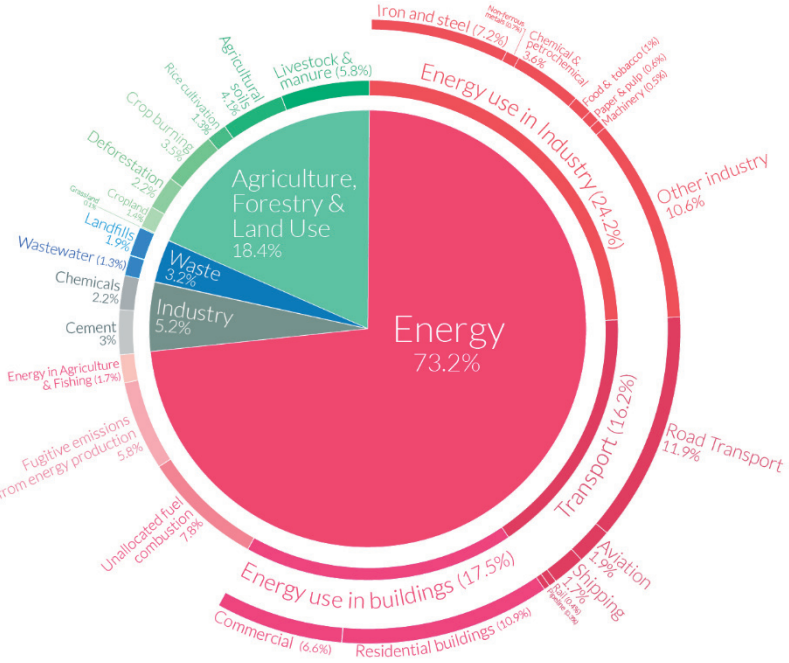

Figure 1. Global Greenhouse gas emission by sector, Source: Climate Watch (2020)

sectors contribute 7.2 % and 7.8 %, respectively, to total industrial emissions. To address emissions from these industrial sectors, various decarbonization approaches are being implemented and developed to achieve full-scale decarbonization, aiming to replace fossil fuel-based industries. For example, Vercammen discussed potential approaches such as applying carbon capture and storage (CCS) units to existing conventional steel-making plants and advancing the development of hydrogen direct reduction iron ore – electric arc furnace (HDRI-EAF) route-based steel-making plants for the future. Additionally, it was noted that conventional steel-making plants emit 1.8 metric tons of CO_2 to produce 1 metric ton of steel. [2].

In the power sector, renewable energy technologies have become more affordable, experiencing a cost drop of up to 80% in solar technologies and 40% in wind energy technologies. However, the output of solar and wind energy technologies depends on meteorological parameters, leading to fluctuations in output power and, consequently, impacting the power grid stability [3]. Finkelstein et al. reported the possibility of addressing excess energy generated by renewable energy technologies (e.g., solar, wind, etc.) through the promotion of Power to Gas to Power (P2G2P). This involves producing green hydrogen for industrial sectors, with the potential to decarbonize by using hydrogen as a reducing agent in the steel sector or directly combusting it in power units [3]. Currently, hydrogen fuel is primarily utilized by chemical industries for producing ammonia and refining petroleum. The available technology for hydrogen production (grey

hydrogen) now is based on the Steam Methane Reforming (SMR) method, which uses natural gas as a feed material and produces CO2 as a by-product. Kurrer reported that the current cost of 1 kg of grey hydrogen ranges from 1.5 to 2.0 euros, based on the cost of natural gas in the European market. On the other hand, green hydrogen production with renewable sources is priced between 3.6 and 5.3 euros per kg of H_2, with future perspectives aiming to reduce it to 1.8 euros/kgH_2 by 2030 [4]. Global hydrogen consumption, as reported by the International Energy Agency (IEA), reached 95 million tons in 2022. Figure 2 illustrates the worldwide use of hydrogen across various industrial sectors and regions during the same year. Most of the hydrogen produced using

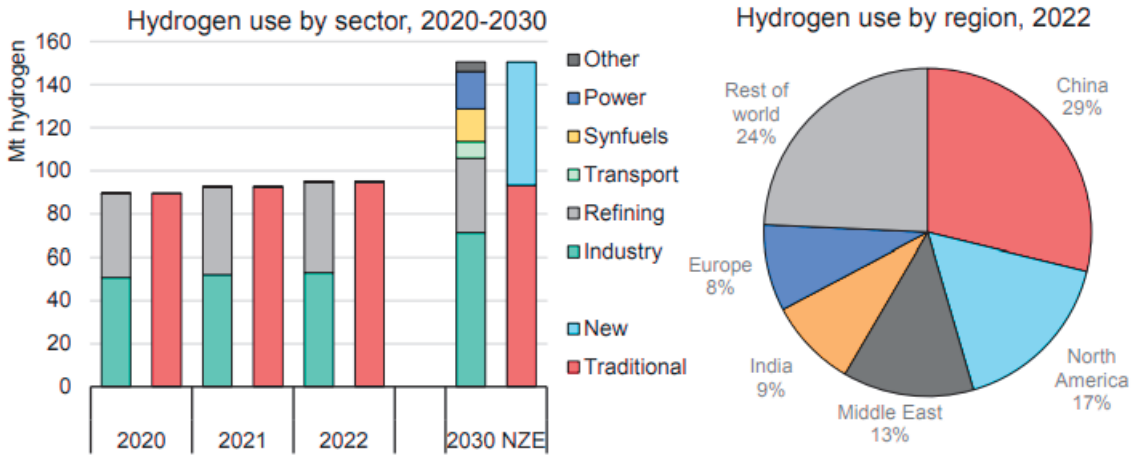

Figure 2. Global hydrogen use by sectors and regions in 2022, Source: IEA (2023)

conventional methods, such as Steam Methane Reforming (SMR), was utilized in petroleum refining and other industries, including the ammonia industry. However, there is an anticipated increase in global hydrogen production to approximately 150 million tons per year by 2030, with nearly 40% of this coming from new production methods. In terms of regional consumption, China led the way, accounting for 29% of the global hydrogen consumption in 2022 [5].

In terms of ammonia-based decarbonization initiatives, JERA reported the successful operation of the first commercial ammonia co-firing in a coal-fired power plant in Japan. This plant employs ammonia for combustion, substituting 20% of the coal in its fuel mix. As a result, it achieves a 20% reduction in CO_2 emissions from the coal-fired power plant. JERA has outlined

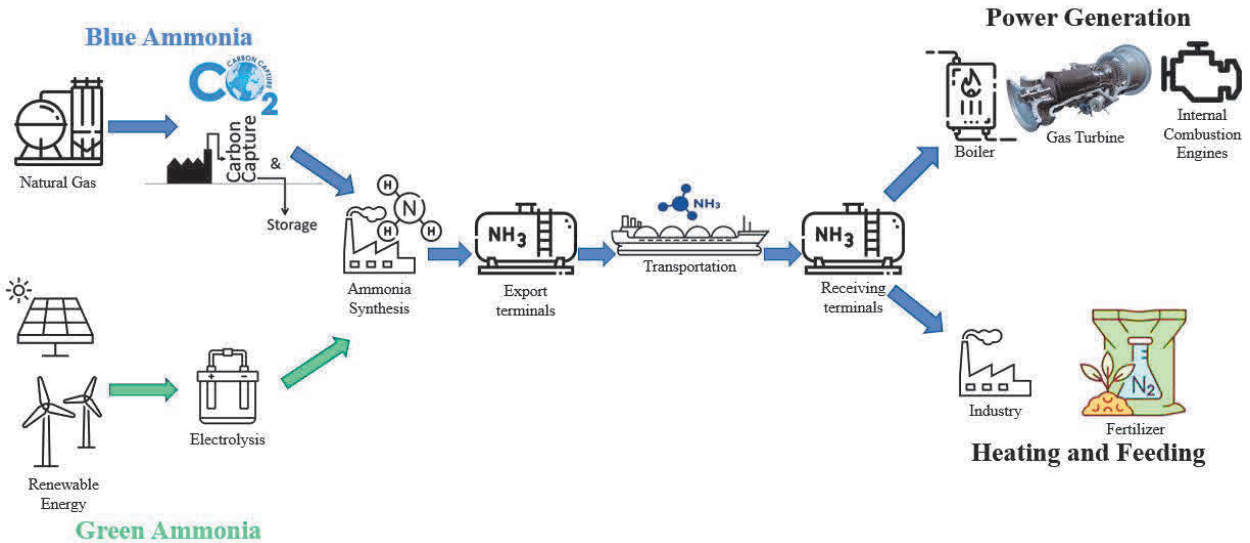

Figure 3. Ammonia value chain (Fujimori & Suda, 2022).

plans to further increase the ammonia share, aiming for 50-60% in the fuel mixture. Consequently, ammonia is emerging as a promising decarbonizing fuel for the power sector in the future [6]. It was reported that global ammonia production is approximately 200 million tons per year, and most of it goes to fertilizer production, accounting for more than 70% of total production. Currently, there are two main methods of producing ammonia in the world: blue and green ammonia production options (Figure 3) [7]. Blue ammonia, produced from fossil fuels, accounts for more than 96% of the total ammonia produced worldwide. Currently, 70% of globally produced hydrogen through the Steam Methane Reforming process is used for ammonia production. Therefore, the production of blue ammonia emits 2.5–2.9 kg CO_2-eq/kg NH_3. From an economic perspective, the cost of producing 1 ton of ammonia can reach 500 USD when the source material, hydrogen, costs 2.5 USD/kg. Otherwise, conventional ammonia and hydrogen production costs are at 0.38 USD/kg NH_3 and 2.00 USD/kg H_2, respectively [8]. If the energy content of 1 kg of ammonia is 18.6 megajoules (MJ) and 1 kg of hydrogen has 120 MJ, then the cost of ammonia per 1 kg at 0.38 USD will be reasonably proportional to the cost of 1 kg of hydrogen at 2.5 USD [9]. Shah reported the cost of green hydrogen at USD 5.5 per kg, and this cost can decrease to 3 USD in countries with good solar irradiation and resources. In comparison, the cost of grey hydrogen amounted to 2.00 USD per kg [10]. The terminologies such as “grey”, “blue” and “green” for each fuel (i.e., hydrogen and ammonia) describe Steam Methane Reforming (SMR) based process, SMR including carbon capture and storage (CCS), and electrolyzer based process, respectively. In the case of SMR process, natural gas and steam are reacted under catalytic conditions to produce hydrogen (H_2) and carbon monoxide (CO) [11].

Equation 1. Steam Methane Reforming process.

$$CH_4 + H_2O \rightarrow CO + 3H_2 \quad (1)$$

The mixture of product gas will then need to be sent to the water-gas shift reaction to increase the yield of hydrogen by converting carbon monoxide to hydrogen gas.

Equation 2. Water-gas shift reaction.

$$CO + H_2O \rightarrow CO_2 + H_2 \quad (2)$$

Up to this stage, grey hydrogen is produced. To produce grey ammonia, the next stage involves synthesizing ammonia in a Haber-Bosch reactor, which combines the produced hydrogen and nitrogen from the air under high pressure (200-300 atmospheres) and high temperature (400-500 °C) conditions with an iron-based catalytic process. Up to this stage, grey hydrogen and ammonia are produced for further utilization. If additional carbon capture and storage units are included in each process, the processes of ammonia and hydrogen can be considered a 'blue' process. To decarbonize grey hydrogen and grey ammonia production, it is possible to produce green hydrogen from an electrolyzer unit by splitting water into hydrogen and oxygen. This will also utilize electricity from renewable energy sources to power the entire process [12]. Ultimately, the use of renewable electricity for hydrogen production serves as the starting point for the green hydrogen and green ammonia production processes. It is forecasted to achieve 2 USD/kg of green H_2 by 2025 and 1 USD/kg of green H_2 by 2030 [12]. In the case of green ammonia, IRENA and AEA reported the cost of renewable or green ammonia ranging from 720 to 1400 per tonne (0.72-1.4 USD/kg NH_3) in 2022, with future perspectives on reducing to USD 310-610 per tonne (0.31-0.61USD/kg NH_3) by 2050 [13].

1.2 HDRI process

Direct Reduction of Iron Ore – Electric Arc Furnace (DRI-EAF) route emerged in the beginning of the 20th century. The initial direct reduction of iron ore plant received its patent in 1918 and bears the Höganäs tunnel furnace process for reducing fine iron ore with carbon. In the 1930s, another process, called the Krupp-Renn process, was developed for reducing iron ore with carbon in a rotary kiln. The next significant step occurred in Söderfors, Sweden, with the development of the Wiberg process to reduce lumpy iron ore and produce 25,000 tons of sponge iron per year [14]. In the 1950s, industrial-scale direct reduction iron ore processes emerged, and a wider range of processes took shape in the 1970s. Table 1 contains the most important direct reduction processes developed by different companies in the middle of the 1970s [14].

Table 1. List of important direct reduction processes.

1.	Allis-Chalmers-Process	Rotary kiln, natural gas (Allis- Chalmers)
2.	Armco-Process	Shaft furnace, natural gas (Armco Steel)
3.	Esso-Fior-Process	Fluidized bed, natural gas (Esso Research)
4.	HIB-Process	Fluidized bed, natural gas (US Steel)
5.	HyL-Process	Retorts, natural gas (Hojalata y Lamina)
6.	Kawasaki-Process	Grate kiln, coke (Kawasaki Steel)
7.	Kinglor-Metor-Process	Outside heated chamber furnace, coal (Monteforno, Danieli)
8.	Koho-Process	Grate kiln, C-containing pellets (Nippon Steel)
9.	Krupp-Eisenschwamm-Process	Rotary kiln, coal (Fried. Krupp)
10.	Midrex-Process	Shaft furnace, natural gas (Midland-Ross)
11.	NCS-Process	Shaft furnace, natural gas (Nippon Steel)
12.	Purofer-Process	Shaft furnace, natural gas (Thyssen Purofer)
13.	SDR-Process	Rotary kiln, fine coke (Sumitomo)
14.	SL/RN-Process	Rotary kiln, coal (Lurgi)
15.	SPM-Process	Rotary kiln, coal (Kubota, Sumitomo)

Out of all mentioned processes, only 3 of them, namely HyL, Midrex and SL/RN processes, have

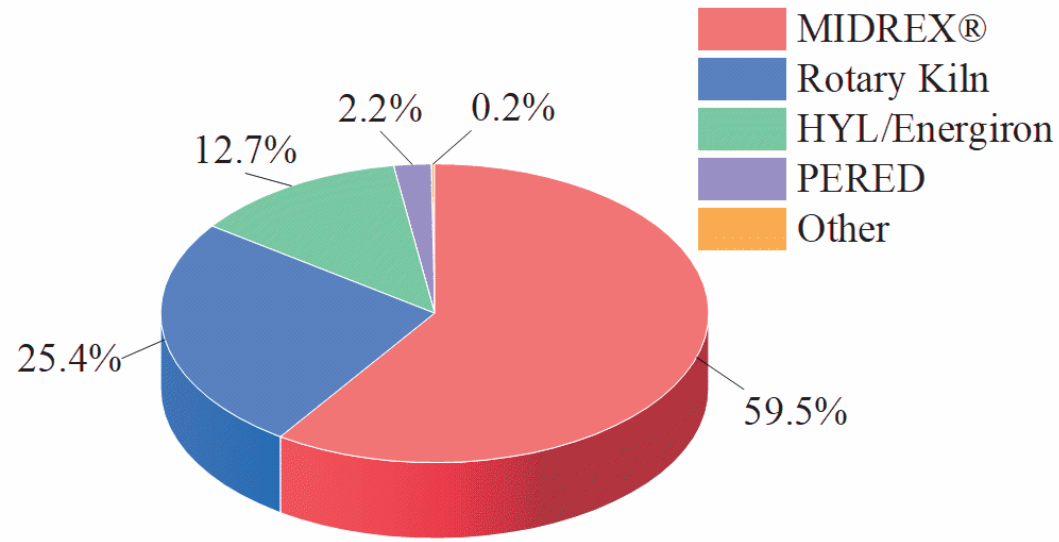

Figure 4. Type of direct reduction iron ore process. Source: Midrex (2022).

been developed for industrial scale since 1976. Current global DRI production accounts for 119.2

Mt per year and Figure 4 depicts share of DRI by processes, where MIDREX process is dominating in the world [15]. Figure 5 depicts the process flow sheet of Midrex DRI technology. In this process,

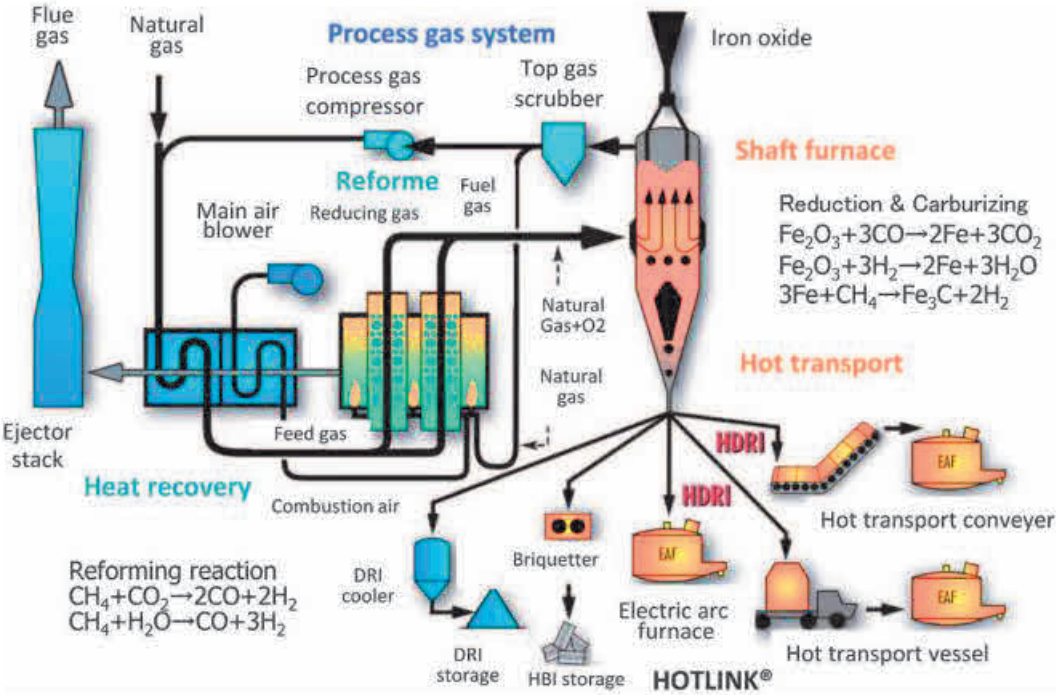

Figure 5. Midrex process flow sheet. Source: Kobelco (2015).

the reducing agent is natural gas. After reforming methane into carbon monoxide and hydrogen gases, the reducing gases CO and H_2 are sent to the shaft furnace from the edge side to counter the iron oxide pellets moving from top to bottom. The reduction is a so-called counter-current process, where sponge iron moves down for further processing in the electric arc furnace [16]. In terms of

Figure 6. Main steel production pathways. Source: IEEFA (2022).

CO_2 emissions from the steel sector, there are differences. As illustrated in Figure 6, the blast furnace – basic oxygen furnace (BF - BOF) route emits nearly 2.2 metric tons of CO_2 per ton of crude steel, and this route contributes to global steel production with a share of 73 %. In the case of the DRI-EAF route emissions, it has 1.4 tons of CO_2 per ton of crude steel, while the EAF alone,

working with scraps, can emit 0.3 tons of CO_2 emissions per ton of crude steel. In terms of energy consumption, BF-BOF, DRI-EAF, and EAF routes consume 22.7 GJ/t, 21.8 GJ/t, and 5.2 GJ/t, respectively. On the other hand, the share of each route in global steel production amounted to 73.2 %, 4.8 %, and 21.5 %, respectively. The reason for the 21.5 % share of the EAF route in global steel production is related to the continuous recycling of metal scraps [17]. To decarbonize the steel sector, several research and industrial projects are under development, namely COURSE50 (Japan), the Hybrit Project (Sweden), H2 Green Steel (Sweden), ArcelorMittal Projects (Luxembourg), Tata Steel's HIsarna Project (Netherlands), etc. [18-22]. One of the emerging environmentally friendly steel making processes is hydrogen direct reduction iron ore – electric arc furnace (HDRI-EAF) route. Considering the significant CO_2 emissions from the conventional steel sector, the HDRI-EAF route has showcased a positive impact on the steel industry. This is attributed to its use of hydrogen as a reducing agent, replacing carbon-intensive fossil fuels and reducing CO_2 emissions by 95-100 % [23,24]. The process offers an opportunity to incorporate renewable energy to produce green hydrogen, aligning with the demand for sustainable products in the market [25,26].

Equation 3. Reaction of iron ore reduction with hydrogen.

$$Fe_2O_3 + 3H_2 \rightarrow 2Fe + 3H_2O \quad (3)$$

The process flow of HDRI-EAF is depicted in Figure 7, where hydrogen fuel is produced by an

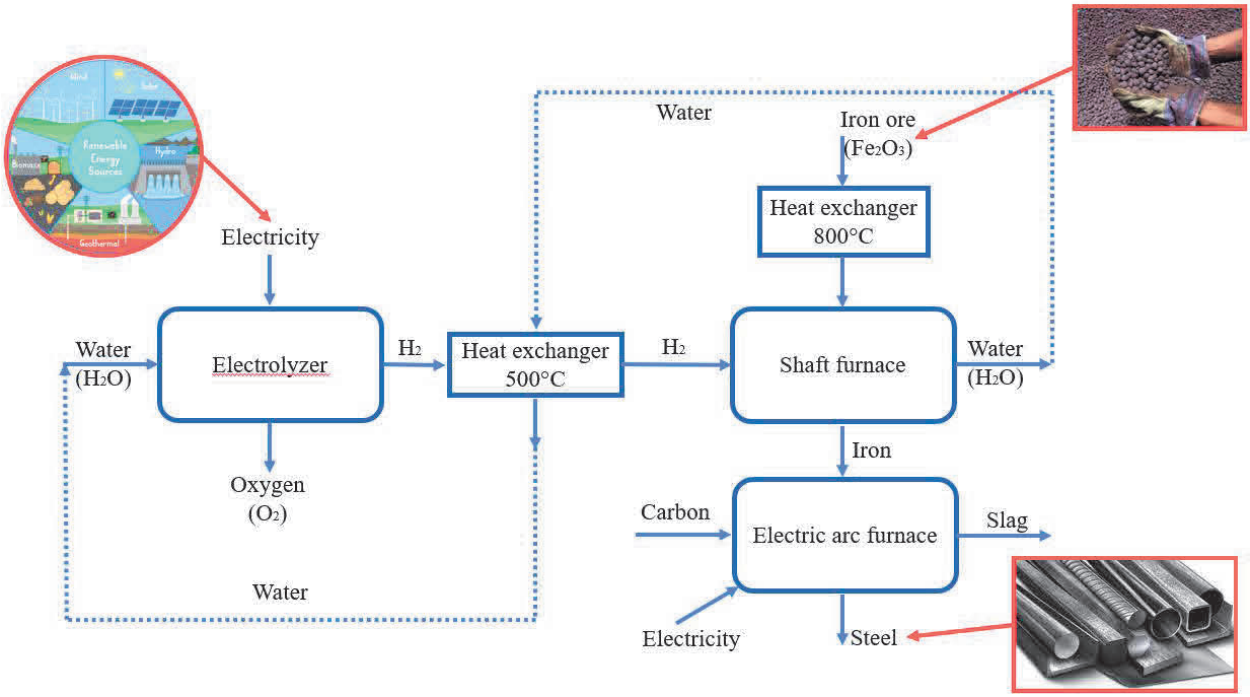

Figure 7. Process flow of HDRI-EAF.

electrolyzer using electricity from renewable sources. The produced hydrogen fuel will then flow to the hydrogen exchanger to utilize the heat of exhaust gases from the shaft furnace. Preheated iron ore at 800 °C will move from the top of the shaft furnace to the bottom, and the reaction between iron ore and hydrogen will take place. As a result of the reaction, sponge iron will be the preliminary product, which will immediately be sent to the EAF for crude steel production. Additionally, carbon or char will be introduced to the EAF to achieve the designated carbon content (0.02-2.14%) in the crude steel.

1.3 Hydrogen and ammonia-fired gas turbines

In 1791, John Barber received a patent for the world's first gas turbine unit, which, ultimately, was not commercialized during his lifetime. It wasn't until 1939 that the idea reached a maturity level for power production, a development spearheaded by the Brown Boveri Company in Neuchâtel, Switzerland [27]. In 1937, Dr. Hans von Ohain initiated research on the combustion of gaseous hydrogen in jet engines. The results of von Ohain's experimental work highlighted the absence of combustion issues with hydrogen (H_2) combustion. Nevertheless, challenges related to metal burnout were predominantly observed [28].

Since one part of the current study investigates hydrogen and ammonia blends for a gas turbine in a combined heat and power plant in Uzbekistan, it is important to describe the process. A Combined Heat and Power (CHP) plant is designed to produce heat while generating electricity in the system. The generated heat is typically used for heating residential buildings and the industrial sector as well [29]. Among the available technologies used in CHP plants, the most widely used types are based on reciprocating engines, gas turbines, microturbines, fuel cells, and steam turbines. The overall efficiency of CHP plants typically ranges between 65% and 85%. CHP plants with the highest capacities often employ gas turbine technologies, which operate based on the Brayton cycle. The overall and electrical efficiencies of these plants range between 65% and 71% and 24% and 36%, respectively. [30]. A gas turbine comprises three main units: an air compressor, combustor, and gas turbine. Figure 8 shows the process flow diagram of the Brayton

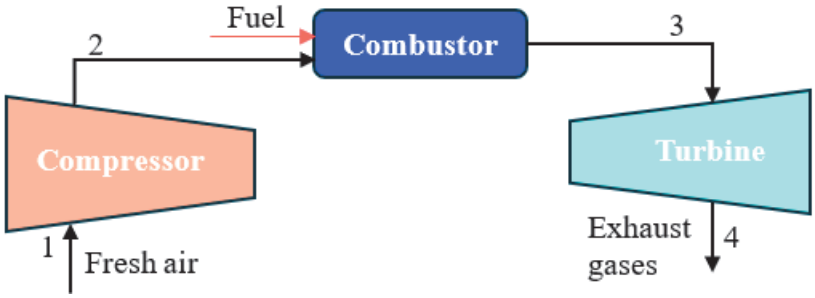

Figure 8. Overview diagram of Bryton cycle.

cycle, which begins with compressing air to increase its pressure. This compressed air is then mixed with fuel (e.g., natural gas, biofuel, hydrogen, ammonia, etc.). The mixture of fuel and air is combusted in the combustion chamber under constant pressure, generating hot gas. The hot gas product is expanded in the gas turbine, performing work to generate electricity and simultaneously run the compressing unit. It is important to emphasize that the air compressor is considered the energy-intensive part of the cycle [31]. Figure 9 depicts the Brayton cycle, which consists of four processes outlined in PV and TS diagrams, namely process 1 → 2: Isentropic compression, process 2 →3: Heat addition, process 3 →4: Isentropic expansion, and process 4 → 1: Heat rejection. As for the first process (i.e., 1 → 2: Isentropic Compression), ambient air is sent to the compressor, and after the compression of air, the pressure increases from P1 to P2, but the volume V1 reduces to V2 while the temperature changes from T1 to T2. On the other hand, entropy in the system remains unchanged, S1=S2. Then, in the second process (i.e., 2 → 3: Heat addition), compressed air and fuel enter the combustor. Combustion takes place under constant pressure (P2=P3), and the amount of heat increases due to the rise in temperature from T2 to T3 and the expansion of volume from V2 to V3. In this case, entropy also increases from S2 to S3. In the next process (i.e., 3 → 4: Isentropic expansion), the heated gas with high pressure expands in a turbine under an adiabatic

process, where no heat and mass exchange take place in the system. While the gas expands in a turbine, rotating blades perform a certain amount of work, gradually reducing the gas's internal energy. At the same time, pressure drops from P3 to P4, and temperature drops from T3 to T4. On

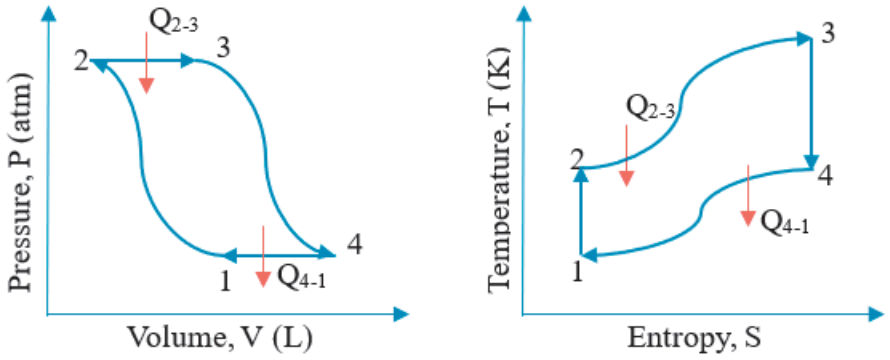

Figure 9. Brayton cycle PV and TS diagrams.

the other hand, volume starts increasing from V3 to V4. The whole process is an isentropic process, where entropy is constant (S3=S4). In the last process (i.e., 4 → 1: Heat rejection), heat rejection takes place under an isobaric process or constant pressure (P4=P1). Volume decreases from V4 to V1 due to heat rejection, and the gas also loses temperature from T4 to T1. At the same time, entropy drops from S4 to S1.

When considering decarbonization strategies for existing gas turbine units, there are various approaches to attain this objective. One method involves substituting or maximizing the utilization of alternative fuels, such as ammonia or hydrogen. Another strategy entails the adoption of carbon capture and storage (CCS) technologies for capturing and storing emissions. From a technical perspective, it is also viable to enhance the overall gas turbine process by improving combustion efficiency or incorporating renewable energy technologies into the system, particularly for a recuperated gas turbine cycle [32]. For example, Matsumoto et al. explored gas turbines utilizing hydrogen and ammonia as part of efforts to decarbonize gas turbine-based power plants in the future. The study highlighted the successful validation of a 20% volume hydrogen co-firing gas turbine within one of Mitsubishi Heavy Industry (MHI)'s gas turbine units installed in the USA. Additionally, they addressed the ongoing development of various combustor types to

Combustor type	Diffusion combustor	Premixed combustor	
		Multi-nozzle	Multi-cluster
Configuration	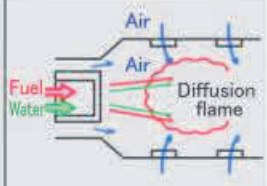	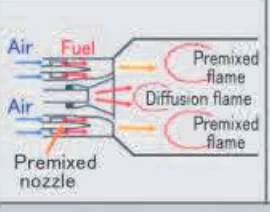	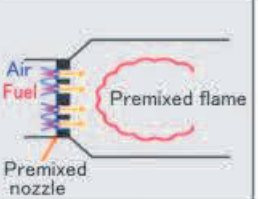
Measures against NOx	Water injection is required as flame temperature increases locally	Low risk due to uniform flame temperature	
Measures against flashback	Low risk due to diffused flame	High risk due to wide flame propagation area	Low risk due to narrower flame propagation area
Performance	Efficiency loss due to water injection	No water injection required, therefore, no efficiency loss	
Overall evaluation	Requires processed water. Technological hurdle is lower than premixed type.	Technological hurdle toward 100% single-fuel firing hydrogen is high, as reliability concern due to flashbacks cannot be eliminated.	Performance is good, but technological hurdle is higher than diffusion due to significant new development elements.

Figure 10. MHI's gas turbine combustors for hydrogen combustion.

ensure stable and efficient combustion when using different volumes of hydrogen and ammonia fuels (Figure 10) [33]. In Figure 10, two categories of combustors are delineated: diffusion and premixed combustors. Regarding diffusion combustors, MHI has already demonstrated the feasibility of efficiency decline, albeit with stable combustion. Conversely, premixed combustors, incorporating two burner types—multi-nozzle and multi-cluster—are in the developmental phase to achieve full-scale hydrogen combustion. Both burners within the premixed combustor necessitate thorough investigations to ensure low NOx emissions and prevent flashback phenomena.

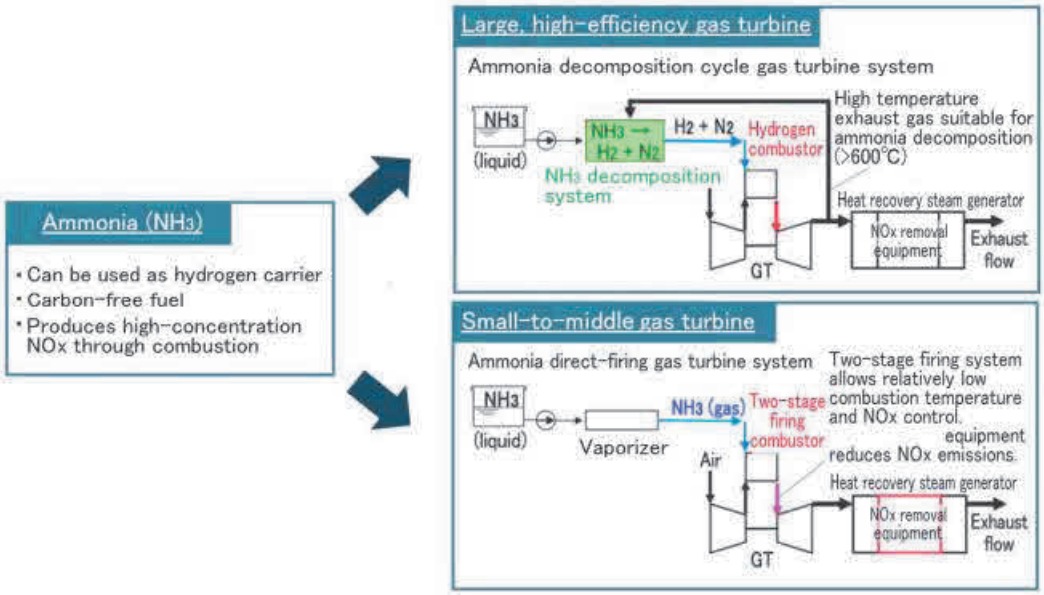

Figure 11. Ammonia utilization methods for a gas turbine unit.

Regarding ammonia co-firing gas turbine technologies, MHI contemplates two approaches tailored to different gas turbine capacities. For large-scale gas turbines, MHI proposes ammonia cracking or decomposition, wherein hydrogen, a byproduct of ammonia decomposition, is combusted in the gas turbine combustor. On the other hand, for small-scale gas turbine units, ammonia can be directly combusted in two stages. The process involves initially combusting a

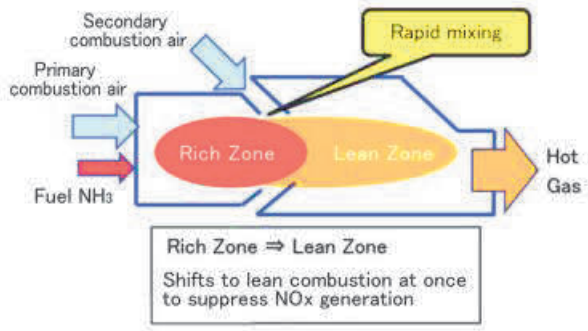

Figure 12. Two-stage rich-lean combustion scheme. Source: Matsumoto et al. (2022)

portion of air along with the entire supplied ammonia, followed by reintroducing a portion of air into the combustion chamber to reduce NOx emissions. Figure 12 illustrates the specifics of MHI's ammonia combustion using a two-air-staging approach to achieve low NOx emissions.

1.4 Research Objectives

In light of the expanding economies globally, there is a persistent rise in the demand for steel and power, leading to substantial CO_2 emissions. To mitigate the impact of global warming and foster sustainable development on a global scale, it becomes imperative to formulate innovative strategies for decarbonizing industries with high carbon intensity. This study establishes the following research objectives to prioritize decarbonization approaches specifically tailored to the industries in Uzbekistan:

- Evaluate the energy and mass balance of hydrogen-based steel production.
- Optimize the iron ore reduction process for optimal steel production based on the results from the energy and mass balance of the HDRI route.
- Develop multi-fuel combustion models for the existing gas turbine at the Fergana Combined Heat and Power (CHP) plant.
- Identify the costs associated with steel and electricity production in hydrogen-assisted steel and power plants.
- Discuss findings and compare the two approaches of using alternative fuels for decarbonizing the steel and power sectors in the future.

Chapter 2. Experimental Optimization Works on Reducing Iron Ore with Hydrogen

2.1 Introduction

Iron and steel production emit 7 % of global and 16 % of total industrial emissions of CO_2 [23], and conventional steel production, based on the Blast Furnace-Basic Oxygen Furnace (BF-BOF) route accounts for 70.8 % of global ore-based steel production [34]. The BF-BOF route mainly uses carbon-intensive coke for reducing iron ore and producing steel; therefore, the route is considered one of the carbon emitting industries with more than 1.8 tons CO_2 per ton of liquid steel production [23,35]. Along the BF-BOF route, direct reduction of iron ore is also emerging, and up to date, several approaches on this route have been developed, such as direct reduction of iron ore with carbon monoxide by using natural gas or a carbon based reducing agent [36]. There are four types of direct reduction processing, including shaft, rotary kiln, fluidized bed, and retort. In April 2021, Primetals Technologies demonstrated a Hydrogen-based Fine-Ore Reduction (HYFOR) pilot plant at the voestalpine Donavitz steelworks in Austria [37,38]. The pilot plant can reduce fine iron ore with a particle size of less than 0.15 mm and consists of a preheating and oxidation unit, a gas processing plant, and a reduction unit to produce iron. It was also mentioned that the pilot plant is of modular type and can be accommodated on the iron ore mining site, reducing transportation cost of raw materials (e.g., hematite or magnetite) [38]. In addition to the reports from Primetals Technologies, Mitsubishi Heavy Industries (MHI) also published their technical reported in June 2022 about the same project, entitled HYFOR process [39]. The report provided more details on the project, including schematics of the pilot plant and the prospective industrial prototype, which were mentioned and explained. Additionally, four unresolved points were highlighted, namely the required residence time for achieving the desired metallization degree, gas consumption and utilization features in connection of superficial gas velocity and pressure in the reactor, the optimum temperature of the inletting gas for avoiding sticking of particles in the distributing section of reducing gas in the reactor and understanding the reducibility of magnetite in case of a lack of hematite resources. The report also outlined the possibility of building a commercial plant with a capacity of 5-15 tons per hour based on continuous production [39].

In term of the kinetics of iron ore reduction, several factors affect the process, including temperature, pressure, gas composition, grain size, porosity, mineralogy, gangue, etc. [40-42]. Heidari et al. [40,43,44] have discussed several factors influencing the reduction of iron oxides, such as high temperature accelerating the reduction process, while it is also possible to reduce iron ore at low temperatures. In the case of hydrogen as a reducing agent, a higher temperature positively contributes to the thermodynamics and kinetics of the reduction process [45]. For carbon monoxide as a reducing agent, a higher temperature will decrease the yield of the reduction [46,47]. Therefore, it is important to understand the behavior of each reducing agent in the reduction process of iron ore. In most of the previously published papers, the temperature range between 500 °C and 1100 °C was mentioned as an experimental condition for reducing iron oxide. Full reduction of iron oxide is still possible at different above-mentioned temperature profiles within the above-mentioned range, with varying experimental parameters, namely residence time, mass of reducing agent, etc. [44]. Regarding the fastest reduction process of iron ore, a reaction at 900 °C resulted full reduction in 250 seconds or 4 min and 10 seconds [40,48]. Zakeri et al. [49] also revealed 80 % reduction with different amounts of $CaCO_3$ in Fe_2O_3 and the achievability of fast reduction at higher amounts of calcium carbonate (i.e., from 1 % to 10 % of the ore weight). Zakeri et al. also broadly explained the effect of different impurities in iron ore when reduced with hydrogen and CO reducing agents.

Many studies have conducted experiments using not only hematite (Fe_2O_3) but also magnetite (Fe_3O_4) and wüstite (FeO) to produce iron and steel [44]. This is because of the availability of iron oxide in different countries. Since the reduction of hematite to iron consists of

three phases changing steps, namely, $Fe_2O_3 \rightarrow Fe_3O_4 \rightarrow FeO \rightarrow Fe$ steps, the formation of FeO takes place at temperatures above 570 °C, which is very slow in terms of reduction kinetics [43]. Regarding magnetite reduction with hydrogen, Zheng et al. [50] investigated and analyzed parameters affecting the reduction process such as oxidation temperature (i.e., 800 °C), oxidant content (i.e., 1.5 wt. % of MgO powder), and reducing gas velocity (i.e., 0.45 m/s).

As one part of the current study highlights the hydrogen-based reduction of iron ore, it is important to evaluate and understand the potential of hydrogen production for the process, which varies from country to country. The stoichiometric consumption of hydrogen in the reduction process is 54 kg per ton of liquid steel production. The current available and large-scale production of hydrogen is based on Steam Methane Reforming (SMR). The SMR process requires fossil fuel for producing hydrogen fuel, which is currently not welcomed by many countries in the world. Many new projects in this direction prioritize using an electrolyzer for producing green hydrogen [43].

Firstly, a process flow diagram is designed, and the mass and energy balance of the process are determined for each unit.

Secondly, the experimental apparatus is designed in a lab condition, and conditions for experiments are set up, taking into consideration the mass and energy balance.

Finally, a series of experiments is conducted, and optimal conditions are found by elaborating on the strategy of experiments.

2.2 Materials and methods

2.2.1 Structure of HDRI experiments

Figure 13 depicts the process flow diagram of the experimental apparatus, continuing the previously developed research works of Alikulov and Xuan Tran [51]. The experimental conditions have been established based on the mass balance of the process, namely 54 kg of H_2 for reducing

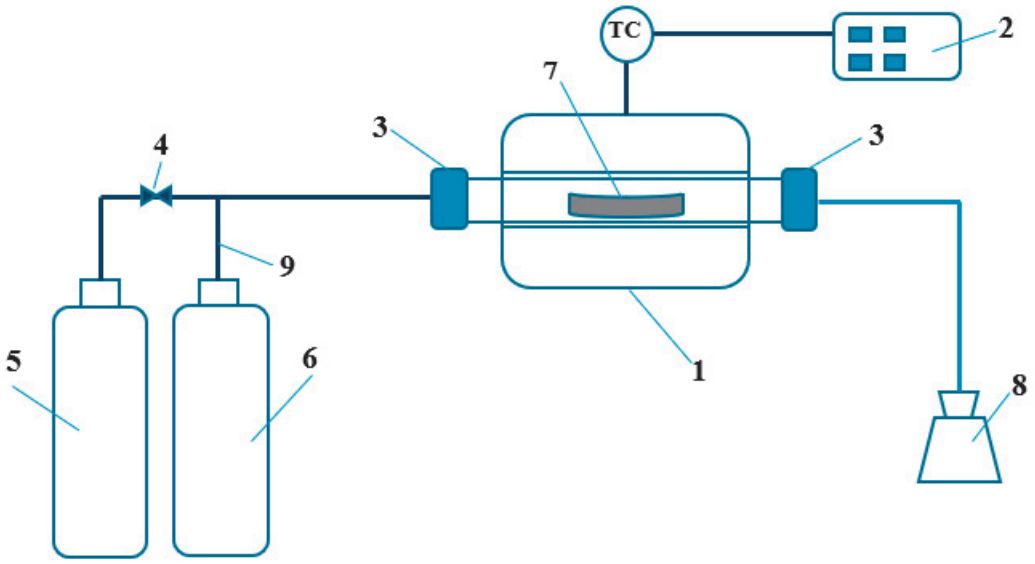

Figure 13. Process flow diagram of the experimental apparatus.

1,428.00 kg of Fe_2O_3. The corresponding value of 0.037815 g or 0.423 L of H_2 was determined for reducing 1 g of Fe_2O_3. Since the mass flow controller metric is in Standard Liter per Minute (SLM), the value of 0.423 L of H_2 for reducing 1 g of Fe_2O_3 is multiplied by the residence time of each experiment. If the designed flow rate control range of the mass flow meter is between 5 - 100 % of the nominal value of 20 SLM, then a controlling value of at least 1 SLM must be set up. Ultimately, 1 liter of H_2 has been set up for reducing 2.3622 g of Fe_2O_3. For any residence time value, the amount of the feedstock remained the same, and the final decision on optimization was based on multiplying the hydrogen flow rate by the designated residence time. In this research work, initially, residence times of 5 min, 10 min and 15 min were selected for temperatures ranging

from 750 to 800 °C. After conducting a series of experiments, it was decided to focus on 770 °C by conducting more detailed timely experiments within the range of 1 min to 7 min, etc. The pressure of the experiments was set at 0.001 MPa. As for the operating pressure at 0.001 MPa and 1 L/min of H2, the safe operation of experiments for the reduction process in this study was at 0.001 MPa or lower values. There are several reasons that did not allow experiments above 0.001 MPa. For instance, sealing assembling tools cannot provide stable sealing above 0.001 MPa, which is dangerous when using hydrogen in the process. Regarding the structure of the experimental apparatus, Figure 1 depicts details including a ceramic tube electric furnace (1), temperature controller (2), sealing assembling tools (3), mass flow controller (4), hydrogen cylinder (5), nitrogen cylinder (6), CB boat (7), water container (8), and mechanical valve (9) for controlling the mass flow of nitrogen.

2.2.2 Specification of route units

In the HDRI-EAF process, hydrogen serves as a reducing agent to produce sponge iron, and the reaction is endothermic, demanding energy for its operation. In this study, a process flow diagram was constructed, drawing from previous research [23]. The diagram comprises various units, such as an electrolyzer, a heat exchanger for hydrogen preheating, an iron ore reducer, a preheater for iron ore, and an electric arc furnace. Additionally, specific materials are necessary to run the process, including water, electricity, iron ore, and char.

Initially, energy and mass balances of the process were calculated based on the stoichiometric reactions, namely Equations (3) [52] and (4).

$$Fe_2O_3 + 3H_2 \rightarrow 2Fe + 3H_2O \qquad \Delta Hr = +99.5\ kJ/mol \tag{3}$$

Equation 4. Reaction of hydrogen production from water electrolysis.

$$H_2O \rightarrow H_2 + \frac{1}{2}O_2 \qquad \Delta Hr = +242\ KJ/mol \tag{4}$$

Where, Fe_2O_3, H_2, Fe, H_2O and O_2 represent iron ore, hydrogen, sponge iron, water, and oxygen, respectively.

First, H_2O is split into H_2 and O_2 using an electrolyzer. Then, hydrogen is utilized in the reduction process of iron ore, with the target product being 1 ton (1,000.00 kg) of steel production (0.999 Fe : 0.001 C).

Several assumptions are made:

- Incompressible fluid.
- Ideal gas/ low-pressure gases.
- No moving parts, horizontal unit and kinetic energy changes are neglected.
- Steady flow heat transfer.
- Processes under constant pressure.

2.2.2.1 Balance on the reactive process (electrolyzer)

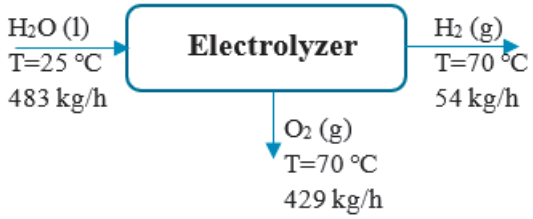

Figure 14. Process flow diagram of Electrolyzer.

Figure 14 depicts the process flow diagram of the electrolyzer.

According to references, H_2 (g) and O_2 (g) are assumed to be at 25 °C and 1 atm [53]. Table 2 presents the streams of mass and energy in the electrolyzer unit.

Table 2. Inlet and outlet enthalpies and mass and energy balance in Electrolyzer.

Substance	M_{in} (kg/h)	H_{in} (kJ/kg)	M_{out} (kg/h)	H_{out} (kJ/kg)
H_2O	483	H1	-	-
H_2	-	-	54	H_2
O_2	-	-	429	H_3

Specific enthalpies of each material:

Equation 5. Enthalpy of H_2O at 25°C.

H_2O (l, 25 °C):

$$\widehat{H}_1=\left(\Delta H^0_{f\,298.15\,H_2O(l)}\right)=-285.830\,\frac{kJ}{mol}=-285.830\,\frac{kJ}{mol}\times\frac{1\ mol}{18\times10^{-3}kg}=-15{,}879.44\ \frac{kJ}{kg} \quad (5)$$

Equation 6. Enthalpy of H_2 at 70°C.

H2 (g, 70 °C):

$$\widehat{H}_2=\left(\Delta H^0_{f\,343.15\,H_2(g)}\right)=1.296\,\frac{kJ}{mol}=1.296\,\frac{kJ}{mol}\times\frac{1\ mol}{2\times10^{-3}kg}=648\ \frac{kJ}{kg} \quad (6)$$

Equation 7. Enthalpy of O_2 at 70°C.

O2 (g, 70 °C):

$$\widehat{H}_3=\left(\Delta H^0_{f\,343.15\,O_2(g)}\right)=1.344\,\frac{kJ}{mol}=1.344\,\frac{kJ}{mol}\times\frac{1\ mol}{32\times10^{-3}kg}=42\ \frac{kJ}{kg} \quad (7)$$

Equation 8. Energy balance in electrolyzer.

Energy balance of electrolyzer based on the first law of thermodynamics [53,54]:

$$Q-W_s=\triangle H+\triangle E_k+\triangle E_p,\ \text{if } W_s=0,\triangle E_k=0 \text{ and } \triangle E_p=0 \text{ then } Q=\triangle H \quad (8)$$

Equation 9. Required energy for electrolyzer.

Energy required for the electrolyzer is found from following equation [53,54]:

$$\triangle H=\sum\left(m_{out}\times\widehat{H}_{out}\right)-\sum\left(m_{in}\times\widehat{H}_{in}\right)=\left(54\,\frac{kg}{h}\times648\,\frac{kJ}{kg}\right)+\left(429\,\frac{kg}{h}\times42\,\frac{kg}{h}\right)=7722.78\,\frac{MJ}{h} \quad (9)$$

2.2.2.2 Balance on the non-reactive process of HDRI-EAF (hydrogen preheater)

Figure 15 depicts the hydrogen preheater to help understand the process within the preheater.

Energy values of the hydrogen preheater are found from the following Equations [53,54]: Then the enthalpies of each point are calculated.

H_2 (g, 70 °C):

Figure 15. Process flow diagram of hydrogen preheater.

Equation 10. Enthalpy of H_2 at 500°C.

$$\widehat{H}_2=1.296\,\frac{kJ}{mol}=1.296\,\frac{kJ}{mol}\times\frac{1\ mol}{2\times10^{-3}kg}=648\,\frac{kJ}{kg}\ \text{(Eq. 6 is identical to Eq. 6.)} \quad (6)$$

H_2 (g, 500 °C):

$$\widehat{H}_2 = 13.83\,\frac{\text{kJ}}{\text{mol}} = 13.83\,\frac{\text{kJ}}{\text{mol}} \times \frac{1\text{ mol}}{2\times10^{-3}\text{kg}} = 6915.00\,\frac{kJ}{kg} \quad (10)$$

If Q equals ΔH from Equation (8) as assumed earlier, then the energy required for the hydrogen preheater is found from the following equation:

Equation 11. Energy of hydrogen preheater.

$$Q = \triangle H = \sum(m_{out} \times \widehat{H}_{out}) - \sum(m_{in} \times \widehat{H}_{in}) = 54\,\frac{kg}{h} \times \left(6915\,\frac{kJ}{kg} - 648\,\frac{kJ}{kg}\right) = 338{,}418\,\frac{kJ}{h} = 338.42\,\frac{MJ}{h} \quad (11)$$

2.2.2.3 Balance on the non-reactive process of HDRI-EAF (iron ore preheater)

Energy values of iron ore (hematite) preheater is found from following equations [53]: Figure 16 depicts the process in iron ore preheater.

Figure 16. Process flow diagram of Iron ore preheater.

Equation 12. Enthalpy of Fe_2O_3 at 800 °C.

Fe_2O_3 (s, 800 °C):

$$\widehat{H}_{\text{hematite}} = \int_{25+273.15K}^{800+273.15K} (C_p)_{Fe_2O_3}\,dT = (103.4\times10^{-3} + 6.711\times10^{-5}T - 17.72\times10^{2}T^{-2})\,dT = 111.504\,\frac{\text{kJ}}{\text{mol}} = 111.504\,\frac{\text{kJ}}{\text{mol}} \times \frac{1\text{ mol}}{159.69\times10^{-3}\text{kg}} = 698.253\,\frac{\text{kJ}}{\text{kg}} \quad (12)$$

Reference data: $C_p\left[\frac{kJ}{mol\times kJ}\right] = a + bT + cT^{-2}, where\ for\ Fe_2O_3, a = 103.4 \times 10^{-3}, b = 6.711 \times 10^{-5}, c = -17.72 \times 10^{2}$ and range of temperature is between 273 K and 1097 K.

Equation 13. Energy required for iron ore preheater.

If Q=△H in Equation 8 as assumed earlier, then the energy required for the iron ore preheater is found from following equation:

$$Q = \triangle H = \sum(m_{out} \times \widehat{H}_{out}) - \sum(m_{in} \times \widehat{H}_{in}) = 1428\,\frac{kg}{h} \times \left(698.253\,\frac{kJ}{kg} - 0\,\frac{kJ}{kg}\right) = 997105.284\,\frac{kJ}{h} = 997.105\,\frac{MJ}{h} \quad (13)$$

2.2.2.4 Balance on the reactive process (reducer unit)

Figure 17 illustrates the reducer unit to aid in understanding the ongoing process.

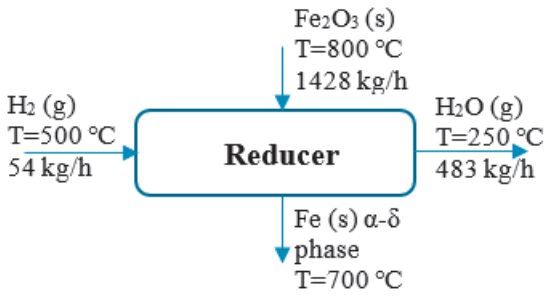

Figure 17. Process flow diagram of Reducer.

References state that H2 (g), O_2 (g) and Fe (s) are at 25 °C and 1 atm [53]. Table 3 displays the stream of energy and mass in the reducer.

Table 3. Inlet and outlet enthalpies and mass and energy balance in reducer.

Substance	M_{in} (kg/h)	H_{in} (kJ/kg)	M_{out} (kg/h)	H_{out} (kJ/kg)
H_2	54	H_4	-	-
Fe_2O_3	1428	H_5	-	-
Fe (α-δ phase)	-	-	999	H_6
H_2O	-	-	483	H_7

Specific enthalpies of each material [53]:

Equation 14. Enthalpy of Fe_2O_3 at 800°C.

H_2 (g, 500 ℃): Equation 10 is identical to above-mentioned Equation 10.

$$\widehat{H}_4=\left(\Delta H^0_{f\,773.15\,H_2(g)}\right)=13.83\,\frac{kJ}{mol}=13.83\,\frac{kJ}{mol}\times\frac{1\ mol}{2\times10^{-3}kg}=6915\ \frac{kJ}{kg} \tag{10}$$

Fe_2O_3 (s, 800 ℃):

$$\widehat{H}_5=\left(\Delta H^0_{f\,298.15\,Fe_2O_3(g)}\right)+\int_{25+273.15K}^{800+273.15K}(C_p)_{Fe_2O_3}\,dT=(-822.2\,\frac{kJ}{mol}\times\frac{1\ mol}{159.69\times10^{-3}kg})+ \tag{14}$$
$$698.253\,\frac{kJ}{kg}=-4450.473\,\frac{kJ}{kg}$$

Equation 15. Enthalpy of Fe at 700°C.

Fe (s, 700 ℃) is found by using Shomate equation:

$$\widehat{H}_6=\Delta H^0_{f\,298.15\,Fe}+\int_{298.15K}^{973.15K}(C_p)_{Fe_2O_3}\,dT=0+\int_{0.29815}^{0.973.15}(a+bT+cT^2+ \tag{15}$$
$$dT^3+eT^{-2})\,dT\ =22.521\,\frac{kJ}{mol}\times\frac{1mol}{55.845\times10^{-3}kg}=403.27\,\frac{kJ}{kg}$$

Condition: T=temperature (K) / 1000, Coefficients within the range of 298-700 K (α-δ phase): (a=18.42868, b=24.64301, c=-8.913720, d=9.664706, e=-0.012643) and within the range of 700 K-1042 K (α-δ phase): (a=-57767.65, b=137919.7, c=-122773.2, d=38682.42, e=3993.080) [55].

Equation 16. Enthalpy of H_2O at 250°C.

H_2O (g, 250 ℃):

$$\widehat{H}_7=\left(\Delta H^0_{f\,298.15\,H_2O(g)}\right)+\int_{298.15K}^{523.15K}(C_p)_{H_2O}\,dT= \tag{16}$$
$$-241.818\,\frac{kJ}{mol}\times\frac{1\ mol}{18\times10^{-3}kg}+7.79\,\frac{kJ}{mol}\times\frac{1\ mol}{18\times10^{-3}kg}=-13001.55\,\frac{kJ}{kg}$$

Equation 17. Energy for reducing iron ore.

If Q=△H from Equation (8) as assumed earlier, then the energy required for reducing the iron ore is determined by the following equation:

$$Q=\triangle H=\sum(m_{out}\times\widehat{H}_{out})-\sum(m_{in}\times\widehat{H}_{in})=\left[\left(999\,\frac{kg}{h}\times\right.\right. \tag{17}$$
$$\left.\left.403.277\,\frac{kJ}{kg}\right)+\left(483\,\frac{kJ}{h}\times\left(-13001.55\,\frac{kJ}{kg}\right)\right)\right]-$$
$$\left[\left(54\,\frac{kg}{h}\times6915\,\frac{kJ}{kg}\right)+\left(1428\,\frac{kg}{h}\times\left(-4450.473\,\frac{kJ}{kg}\right)\right)\right]=$$
$$104990.517\,\frac{kJ}{h}=104.991\,\frac{MJ}{h}$$

2.1.2.5 Balance on reactive process (electric arc furnace)

Figure 18 depicts the process flow diagram of the EAF, indicating the input and output materials.

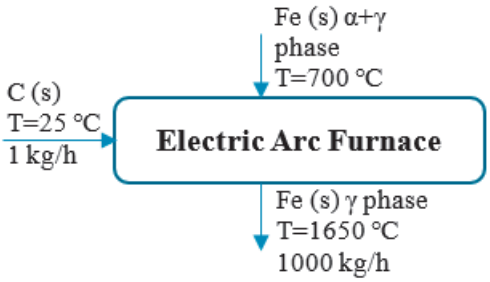

Figure 18. Process flow diagram of EAF.

References state that C (s) and Fe (s) are at 25 °C and 1 atm [53]. Table 4 presents the energy and mass stream in the EAF tool of the route.

Table 4. Inlet and outlet enthalpies and mass and energy balance in the EAF.

Substance	Min (kg/h)	Hin (kJ/kg)	Mout (kg/h)	Hout (kJ/kg)
Fe (α-δ phase)	999	H6	-	-
C	1	H8	-	-
Fe (γ phase)	-	-	1000	H9

Fe (s, 700 °C, α-δ phase): Equation 15 is identical to above-mentioned Equation 15.

$$\widehat{H}_6 = \Delta H^0_{f\,298.15\,Fe} + \int_{298.15K}^{973.15K} (C_p)_{Fe_2O_3}\, dT = 403.277\ \frac{\text{kJ}}{\text{kg}} \tag{15}$$

Equation 18. Enthalpy of C at 25°C.
C (s, 25 °C):

$$\widehat{H}_8 = H^0_{f\,298.15\,C} = 0 \tag{18}$$

Equation 19. Enthalpy of Fe at 1650 °C.
Fe (s, 1650 °C):

$$\widehat{H}_9 = \Delta H^0_{f\,298.15\,Fe} + \int_{298.15K}^{1923.15K} (C_p)_{Fe}\, dT = (0 + \int_{298.15K}^{1923.15K} dT) = \tag{19}$$
$$(a + bT + CT^2 + dT^3 + eT^{-2})dT =$$
$$\int_{298.15K}^{1809K} \int_{0.29815}^{1.809} (a + bT + CT^2 + dT^3 + eT^{-2})dT = 49.542\frac{kJ}{mol} = 49.542\frac{kJ}{mol} \times$$
$$\frac{1mol}{55.845\times10^{-3}kg} = 887.134\frac{kJ}{kg}$$

Assumption: H_{Fe}, 1923.15 K is not different from H_{Fe}, 1809 K because of limitation of experimental data. T=temperature (K)/1000. Coefficients within the range of 298 K - 1809 K (γ phase): (a=23.97449, b=8.36775, c=0.000277, d=-0.000086, e=-0.000005) [55].

Equation 20. Energy required for EAF.
If Q=△H from Equation (4) as assumed earlier, then the energy required for the conversion of sponge iron to steel is determined by following equation [53]:

$$Q = \triangle H = \sum(m_{out} \times \widehat{H}_{out}) - \sum(m_{in} \times \widehat{H}_{in}) = \tag{20}$$
$$\left[\left(1000\frac{kg}{h} \times 887.134\frac{kJ}{kg}\right)\right] - \left[\left(1\frac{kg}{h} \times 0\frac{kJ}{kg}\right) + \left(999\frac{kg}{h} \times 403.277\frac{kJ}{kg}\right)\right] =$$
$$484260.277\frac{kJ}{h} = 484.26\frac{MJ}{h}$$

2.2.2.6 Yield of reduction of iron ore

After calculating the mass and energy balance of the HDRI-EAF process, experiments are conducted to understand the behavior of iron ore reduction and optimize the reduction process using the following Equation [56,57]:

Equation 21. Yield of reduction of iron ore.

$$R = \frac{\Delta W_o}{W_o^i} x100\ \% = \frac{W_o^i - \Delta W_o^H}{W_o^i} x100\ \% \quad (21)$$

Where R represents the yield of reduction, ΔW_o^H is the total weight loss during hydrogen reduction, and W_o^i is the total weight of O_2 present in Fe_2O_3. Iron ore is assumed to be pure hematite without any other compositions. The composition of Fe_2O_3 is 69.9 % Fe and 30.1 % O_2.

2.3 Results and Discussion

Mass and energy balance and optimized reduction process results are presented. It is assumed that the reducer is in a static and horizontal state. Energy consumption and the speed of reduction are compared with previous studies and discussed to demonstrate the novel approach.

2.3.1 Process flow of HDRI-EAF

The mass and energy balance of the HDRI-EAF, composing electrolyzer, hydrogen and iron ore preheaters, reducer of iron ore and electric arc furnace, is depicted in Figure 19. All values are calculated based on the target amount of the product, namely 1 ton of liquid steel production. In the mass and energy balance, it is assumed that there are no hydrogen losses, and the required

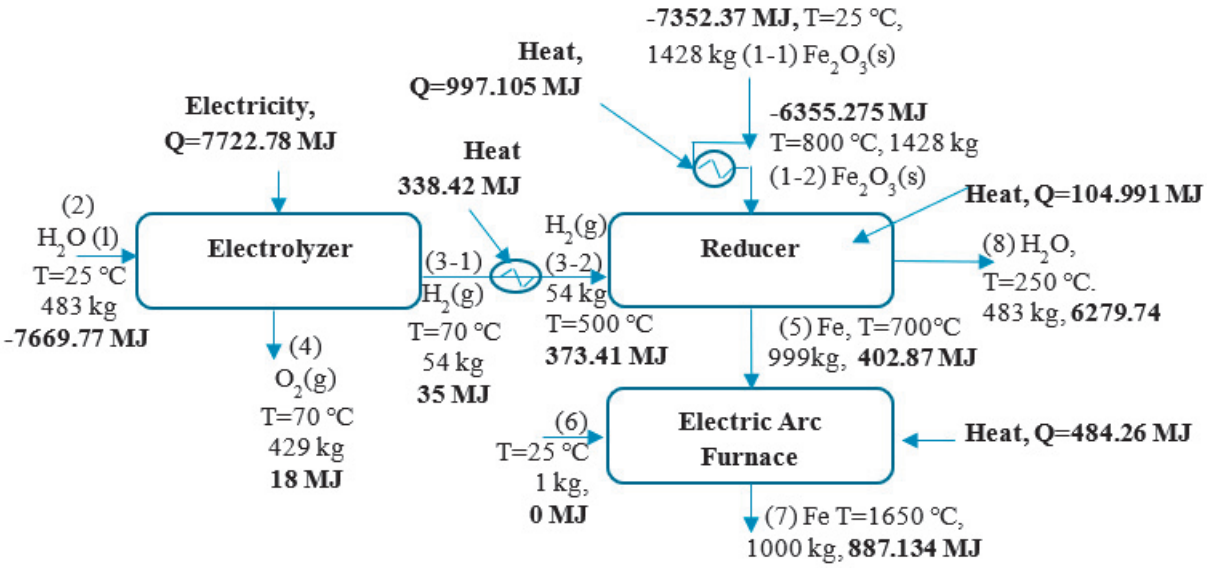

Figure 19. Process flow diagram of Hydrogen Direct Iron Reduction.

amount of hydrogen for running the process is calculated from stoichiometric values. Additionally, the mass of slag, CO, and CO_2 are neglected in the calculation because the main objective of the study is to find stoichiometric values and conduct experiments to determine the most optimal reduction mode of the process. The reason for using an electrolyzer in the process is to design the process flow diagram based on green renewable energy and to avoid fossil fuel-based hydrogen production approaches. Source of electricity for running the electrolyzer is not specified, while previous studies [23,43,57-61] emphasized the use of wind, solar and other renewable energy sources for the decarbonization of HDRI-EAF. The mass of necessary materials, i.e., 1,428.00 kg of Fe_2O_3,

1 kg of Carbon (C), 54 kg of H_2, 483 kg of H_2O to produce 1 ton of liquid steel, is also depicted in Figure 19.

2.3.2 Energy consumption of HDRI-EAF

Since the HDRI-EAF mainly consumes electricity for running the whole process, the analysis of energy consumption aspects is very important for process feasibility and commercialization. Results of the current study state that the electrolyzer needs 7,722.78 MJ (2,145.21 kWh), the hydrogen preheater 338.42 MJ (94 kWh), the iron ore preheater 997.105 MJ (276.97 kWh), the reducer 104.991 MJ (29 kWh), and the EAF 484.26 MJ (134.51 kWh) of energy to produce of 1 ton of liquid steel within the HDRI-EAF process. The calculations did not include the energy requirement of hydrogen storage of the process. In total, the energy requirement of HDRI-EAF based on the findings is 9,647.556 MJ/tls or 2,679.69 kWh/tls. Table 5 summarizes the flow of energy and mass in the HDRI-EAF process based on the results of the current study.

Table 5. Summary of energy and mass balance of the process.

Stream	Mass flow (ton/tls)	Temperature (°C)	Energy (kWh)	ΔH (kJ/kg)	Short description	Process step
1	1.428	800	276.99	698.294	Iron ore pellets entering Reducer after heating	Reducer
2	0.483	25	29.089	104.72	Water entering electorlyzer	Electrolyzer
3-1	0.054	70	9.73	649.15	H_2 exiting Electrolyzer	
3-2	0.054	500	94	6266.8	H_2 entering Reducer	Reducer
4	0.429	70	4.966	41.674	O_2 exiting Electrolyzer	Electrolyzer
5	0.999	700	98.24	354.03	Sponge iron exiting Reducer and entering EAF	EAF
6	0.001	25	19.4	69872.66	Char entering EAF	EAF
7	1	1650	268.60	967.96	Molten steel exiting EAF	EAF
8	0.483	250	57.96	432.055	H_2O exiting Reducer	Reducer

A previous study already reported the total Specific Energy Consumption (SEC) requirement of HDRI-EAF without a hydrogen storage system, amounting to 3.72 MWh/tls, which exceeds the 1.01 MWh SEC found in this research [23]. Moreover, the SEC of the conventional steel manufacturing industry based on the BF-BOF route consumes 3.48 MWh/tls [23]. Another study's

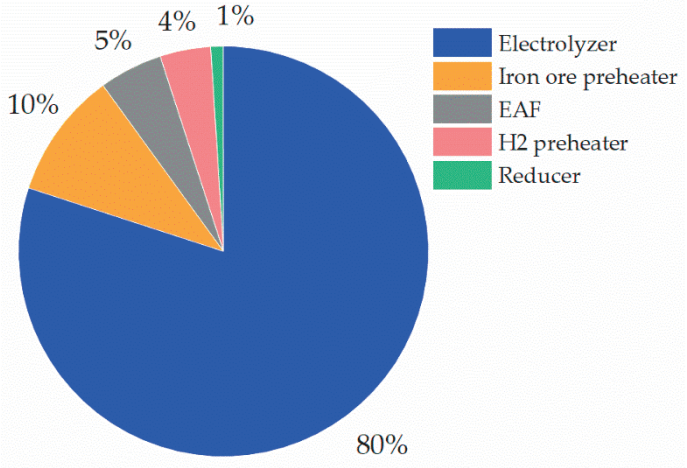

Figure 20. Energy consumption of HDRI-EAF in %.

report mentioned the SEC of HDRI-EAF totaling 3.48 MWh/tls, while the SEC of BF-BOF was 3.68 MWh/tls [61]. In addition, the minimum value of total SEC in the direct reduction of iron process, accounting for 12.2 GJ/tls or 3.388 MWh/tls, was reported, but a higher amount of total SEC in the Blast Furnace, totaling to 15.7 GJ/tls or 4.361 MWh/tls, was reported by the research [61]. From the SEC of the current research findings, as mentioned in Figure 20, the highest energy demand was found in the Electrolyzer, which consumes 80 % energy of the SEC. The next energy consumptions were found in the hydrogen preheater with 1.74 kWh SEC per kg of H_2, in the iron ore preheater with 0.19 kWh SEC per kg of Fe_2O_3, and in the EAF with 0.13 kWh SEC per kg of sponge iron processing. Based on the above-mentioned SEC in each unit, it is advisable to build a strategy for reducing energy consumption in the HDRI-EAF towards decarbonization and the commercialization of the process. Li et al. [57] mentioned in their studies that the heat energy of the effluent from the shaft furnace composing H_2 and H_2O, can be used in the heat exchanger of H_2 and recycled to the electrolyzer or H_2 storage units.

2.3.3 Optimization of reduction process in lab condition

After identifying the key input values of the HDRI-EAF process, taking into consideration the energy and mass balance calculation, the conditions for the experiment were decided and outlined in Table 6.

Table 6. Condition of experiments.

Feedstock	Fe2O3 (2.3622 g)
Reducing agent: H_2	Mass flow: 1 L/min
Heating and cooling gas: N_2	Mass flow: Throughout the experiment
Pressure:	0,001 MPa/0,01 bar
Residence time	1, 2, 3, 3.5, 4, 5, 7, 10 and 15 min.
Temperature	750 ℃, 760 ℃, 770 ℃, 780 ℃, 790 ℃ and 800 ℃
Reduced product	Sponge iron (Fe)
Yield of reduction (R)	14.9 % - 100 %
Composition of Fe_2O_3	Fe_2O_3 ≧ 96 %, Acid insoluble ≦ 1.5 %, moisture ≦ 1.5 %, Mn ≦ 0.5 %

Fe_2O_3, or red iron ore in the form of powder with the composition mentioned in Table 5, was used as a feedstock in all experiments. As for the reducing gas (H2), 54 kg of H_2 is required for the reduction of 1428 kg of Fe_2O_3 based on data provided in Table 4. Since the nominal value of the mass flow controller is 20 SLM and the flow rate nominal value ranged between 5 and 100 % [62], it is necessary to convert grams of H_2 into liters of H_2 to set the correct experimental condition. If 1 mole of any gas occupies 22.4 L of volume at standard temperature and pressure, then 1 g of Fe_2O_3 will require 0.037815 g of H_2 or 0.4235 L/min of H_2. To conduct experiments under the minimum (5 %) H_2 flow rate control range, which is 1 L/min of H_2, the above-mentioned and converted value 0.4235 L/min must be at least 1 L/min. Then, 2.3622 g of Fe_2O_3 will be required for conducting experiments under 1 L/min of H2 flow rate. Beside the reducing gas, N_2 is used for heating and cooling the feedstock until the designated experimental condition is reached. After each residence time, it is used for cooling the product to avoid the deoxidation of sponge iron (Fe). The validation of the reducibility of Fe_2O_3 with H_2 is confirmed through an experiment by using N_2 at 800 ℃, 0.001 MPa and 5 min of heating time at the designated temperature. As a result of the validation experiment, the mass of the feedstock did not change significantly (2.3622

g → 2.3503 g). Subsequently, all other experiments were conducted with different conditions outlined in Table 6. It was also assumed that in all samples, impurities are neglected, and any reduction yield exceeding 100 % is attributed to these neglected impurities.

2.3.3.1 Experiment of reducing Iron ore at different temperatures each with 5 min of residence time

Initial experiments were conducted with temperature conditions of 750 °C, 760 °C, 770 °C, 780 °C, 790 °C, 800 °C, each with a residence time of 5 minutes. These experiments aimed to understand the range of experimental conditions to focus on in future research investigations. Figure 12 depicts the outcome of the experiments, where the reduction efficiency in all cases was consistently near 100 %. The most attractive case was an experiment of reducing iron ore under the condition of 770 °C and 5 minutes of residence time, highlighted with a red dot in Figure 21.

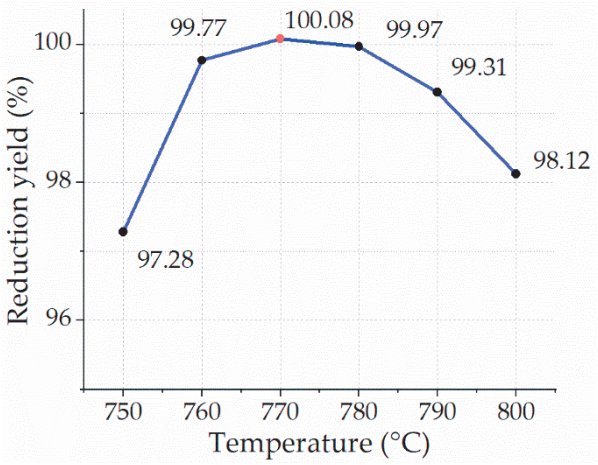

Figure 21. Yield of reduction in 5 minutes with H_2 at different temperature profiles.

One of the previously published papers reported approximately 23 % reduction yield of LKAB-KPRS Iron ore pellets (diameter = 14 mm) with H_2 with the experimental conditions of 770 °C, 5 minutes of residence time, 4.7 g of mass, H_2/He (60/40 vol.) and 2 L/min mass flow of gases. The reduction yield increased from 14 % to 25 % in the temperature profile between 600 °C and 950 °C respectively. In the case of reducing CVRD-DR pellets (diameter = 14 mm), the reduction yield with 5 minutes of residence time, 4.7 g of mass, H_2/He (60/40 vol.), and 2 L/min mass flow of gases in the temperature profile between 600 °C and 950 °C ranged from approximately 10 % to 20 % [43]. On the other hand, Heidari et al. [40,48] presented their findings on reducing iron ore with 100 % hydrogen on a laboratory scale, mentioning that a 95 % reduction degree can be achieved in 300 seconds or 5 minutes at 700 °C. Their findings closely align with the results found in this study. Cavaliere et al. [63] also mentioned in their study the reduction of iron ore at 1000 °C and 1 bar, resulting in nearly 100 % reduction until 15 minutes of residence time. A reason for the parabolic behavior of the figure is related to chemical and physical mechanisms, namely insufficient (short) residence time at elevated temperature, which can lead to constraints for hydrogen to diffuse through the entire particle and form sintering of iron. This, in turn, decreases the surface area available for the reaction with hydrogen. As a result, the yield of reduction will be reduced. Similar phenomena are also highlighted in studies by Bhaskar et al. [23,57,64].

2.3.3.2 Experiment of reducing Iron ore at different temperatures each with 10 min of residence time

Next batch of experiments was conducted with a residence time of 10 minutes in each temperature profile. The yield of reduction in each temperature profile was nearly close to full reduction (Figure 22). It is important to mention that the stoichiometric value of consuming

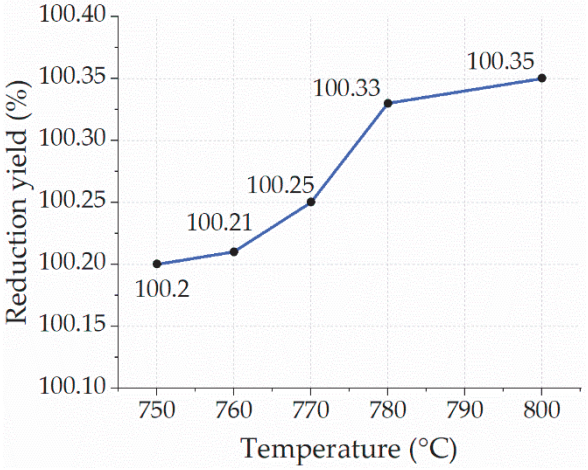

Figure 22. Yield of reduction in 10 minutes with H_2 at different temperature profiles.

hydrogen per unit of iron ore was calculated as 1 L/min for reducing 2.3622 g of Fe_2O_3. In this case, the mass flow of hydrogen was 10 L per reduction scenario. Despite assuming pure iron ore in this study, the results show a yield of reduction slightly exceeding 100 %. The obtained numbers prove that there are no significant changes in each temperature profile despite a two-fold increase in residence time.

In a previous study reducing iron ore at 800 °C, some data were provided stating that the highest reduction yield (85 %) can be achieved after reaching 50-minutes residence time. Afterwards, no other significant reduction was observed. Initial reduction values in 10 minutes of residence time demonstrated more than 80 % of the reduction yield [42]. The outcomes suggest a different approach or condition is required to reach a 100 % reduction yield. The findings of the current study provided significant value towards the optimization of the process. Another case study of reducing iron ore pellets from two different manufacturers provided a 50 % and 40 % reduction yield at 770 °C with 4.7 g of feedstock mass, and a 2 L/min of H_2/He (60/40 vol.) mass flow [43]. Despite almost the same condition, the outcome was lower than the one found based on experiments in this study.

2.3.3.3 Experiment of reducing Fe_2O_3 at different temperatures each with 15 min of residence time

The next case involved increasing the residence time from 10 minutes to 15 minutes for each temperature profile. Figure 23 depicts the yield of reduction of iron ore for each temperature profile ranging from 750 °C to 800 °C. The yield of reduction remained unchanged and demonstrated full reduction in almost all cases except for the case of 750 °C, where the yield of reduction nearly approached 100 %. Since the residence time is threefold increased for the current scenario, the specific consumption of hydrogen was also 15 times increased compared to stochiometric values. Findings of Sohn [65] with 100 % H_2 reduction condition of Fe_2O_3 provided different conversion yield, namely 95 %, 96 %, 85 %, 85 and 100 % at 500 °C, 600 °C, 700 °C, 800 °C and 900 °C, respectively. At 800 °C, the reduction of Fe2O3 with a residence time of 15

minutes did not differ from the one at 700 °C. The results are very similar to the ones found in this study's reduction case with a residence time of 15 minutes.

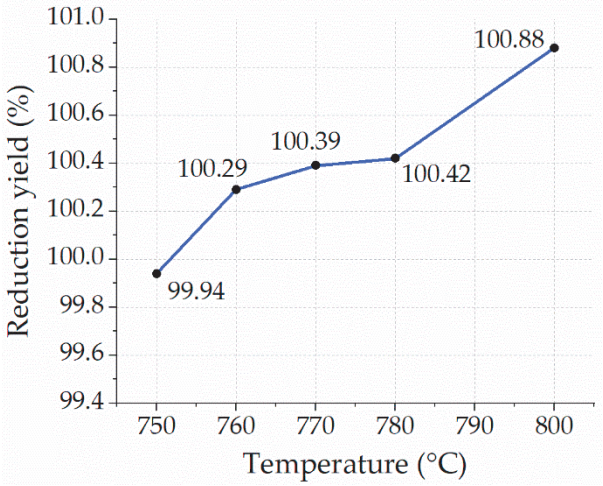

Figure 23. Yield of reduction in 15 minutes with H_2 at different temperature profiles.

2.3.3.4 Experiment of reducing Fe_2O_3 at 770 °C each with varying residence time

After running experiments for each cluster of residence time, including 5, 10 and 15 minutes, it was decided to continue with further detailed experiments at 770 °C, which was selected due to the full reduction yield and lower temperature point compared to other scenarios. Figure 24 illustrates the yield of reduction at each residence time (i.e., 1, 2, 3, 3.5, 4, 5 and 7 minutes). After observing the outcome of all experiments, the yield of reduction with the resistance time of 5 and 7 minutes demonstrated nearly the same values as the yield of reduction with residence times 10 and 15 minutes. As for the reduction process with residence times of 1 minute, 2 minutes, 3 minutes, 4 minutes, and 5 minutes, the yield was 14.9 %, 55.59 %, 75.5 %, 85.71 % and 90.36 %, respectively. Despite a 100.08 % yield of reduction within the residence time of 5 minute, demonstrating full reduction, doubling the amount of Fe_2O_3 mass did not help to reach full reduction of each feedstock sample, resulting in 87.76 % in the first sample and 86.14 % in the second sample of the experiment. Therefore, the further strategy was to double the number of samples with a residence time of 7 minutes instead of 5 minutes. As a result, the reduction yield

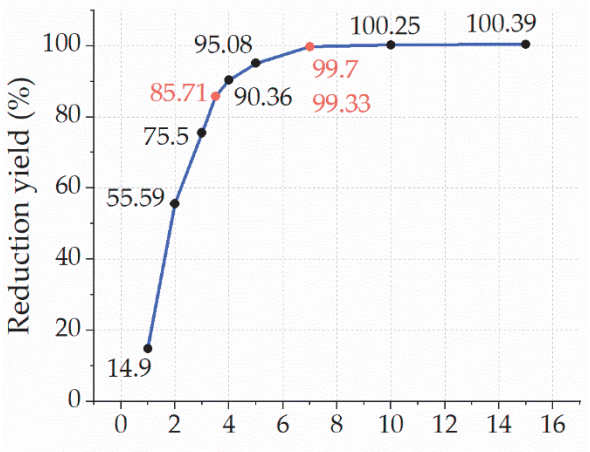

Figure 24. Yield of reduction of Fe_2O_3 at T=770 °C within a residence time (1-15 minutes).

could achieve nearly full reduction yield at the level of 99.70 % in the first sample and 99.33 % in the second sample, as mentioned with a red dot in Figure 24. If the number of the same samples is doubled and the reduction yield of each sample is achieved nearly 100 % reduction yield, the specific consumption of hydrogen under the optimal reduction process can be 3.5 L/min of hydrogen for reducing a unit of the feedstock, which means the real value is 3.5 times more than the stochiometric value. To understand the behavior of the reduction process with 3.5 minutes of residence time, another experiment was conducted at 770 ℃ with a single sample under the condition of 100 % H_2 supply, which showed an 85.71 % reduction yield and is mentioned with a red dot in Figure 24. Comparing these findings to previous studies, Wagner et al. [48] could reach a reduction degree of nearly 90 % of iron ore with 100 % H_2 at 800℃ within 3.5 minutes or 210 seconds. Another temperature profile at 700 ℃ showed a 70 % yield of reduction within 210 seconds [40,48]. As for the outcome of this study and the experiment at 770 ℃ with two identical feedstocks under the condition of a 100 % H_2 reducing agent, a residence time of 7 minutes demonstrated the most optimal reduction yield. As a result, the findings in terms of reduction time can be equivalent to the one with 3.5 minutes per a single unit of the feedstock. The findings have been published in the Energies journal (Energies 2024, 17(5), 1242).

2.4 Conclusion

Research work included the energy and mass balance of HDRI-EAF, analysis of energy consumption indicators of the process, and lab-scale experiments for optimizing the yield of reduction with an emphasis on residence time, temperature, and mass flow of H_2. After discussing the outcome of energy and mass balance and conducted experimental works, the following research findings are summarized:

- The total energy demand of steel production based on HDRI-EAF, without considering energy for hydrogen storage, accounted for 2,679.69 kWh/tls, significantly lower than previously published values.
- The energy and mass balance of the HDRI-EAF process included the following energy-consuming units: 2,145.21 kWh for electrolyzer, 94 kWh for hydrogen preheater, 276.97 kWh for Fe_2O_3 preheater, 29 kWh for reducer, and 134.51 kWh for EAF.
- Energy analyses provided a good understanding of Specific Energy Consumption (SEC) of each unit and proved that the electrolyzer unit consumes 80% of the total SEC of the process. The unit-based SEC in the hydrogen preheater accounted for 1.74 kWh SEC per kg of H_2, in the iron ore pre-heater totaled 0.19 kWh SEC per kg of Fe_2O_3, and in the EAF amounted to 0.13 kWh SEC per kg of pig iron processing. The breakdown of the total SEC of the process can help lead future energy system optimization research within the HDRI-EAF process.
- After calculating and identifying the energy and mass balance of HDRI-EAF processes, lab-scale experiments were conducted to reach stoichiometric values by optimizing conditions. The conditions of experiments were set as 2.3622 g of feedstock (Fe_2O_3), 1 L/min of reducing gas (H_2) mass flow, throughout the experiment providing heating and cooling gas (N_2), 0.001 MPa of working pressure, 1, 2, 3, 3.5, 4, 5, 7, 10, and 15 min of residence time, and a temperature of 750, 760, 770, 780, 790, and 800 ℃. The selected feedstock (Fe_2O_3) had the following composition: Fe_2O_3 ≧ 96%, Acid insoluble ≦ 1.5%, moisture ≦ 1.5%, Mn ≦ 0.5%.

- A set of experiments was conducted by revising residence time, temperature, and the number of feedstock samples. The experiments resulted in yields of reduction ranged between 14.9% - 100%, where the optimal condition was found as 1 L/min of hydrogen mass flow, 0.001 MPa of working pressure, twofold of feedstock each with 2.3622 g of Fe_2O_3, residence time 7 min, yield of reduction of each sample, 99.70% in the first sample and 99.33% in the second sample. Comparing with the stoichiometric value of the reduction process, lab-scale enables to achieve 3.5 L/min hydrogen consumption by the process for reducing 2.3622 g of Fe_2O_3. The results are 3.5 times more than the stoichiometric value but still a more optimized value compared to previous studies.

Chapter 3. Development of a Multi Fuel-Fired Gas Turbine in the Existing Power Unit of Fergana Combined Heat and Power Plant

3.1 Introduction

Research on gaseous hydrogen combustion in jet engines began in 1937 by Dr. Hans von Ohain. The outcome of von Ohain's research experiments emphasized no combustion issues with hydrogen (H_2) combustion; however, issues pertaining to metal burnout were mostly observed [28]. Studies by Wang et al. [66] on researching combustion and emission characteristics for hydrogen and methane blended fuel mix with different compositions in a 2.5 MW concentric staged low-pollution combustor resulted in a reduction of CH_2O and C_2H_2 emissions under 30-40 % hydrogen blending ratios. More detailed research on the combustion characteristics of hydrogen-fired gas turbines was conducted in the middle of the 1980s. Sampath and Shum [67] investigated hydrogen combustion in a can-type combustor equipped with two different fuel injectors (i.e., multi-hole and swirl types). More than 400 experiments were conducted by considering different ranges of fuel-to-air ratios, inlet pressure and temperature, and combustor loading, and the discussion of results covered metal temperature, flame characteristics, combustion efficiency, stability, and NOx emissions. Sampath and Shum [67] reported the excellent combustion characteristics of hydrogen in a gas turbine, including good combustion efficiency, ignition, and stable performance. However, NOx emissions under hydrogen co-firing resulted in a higher amount compared with the designed liquid fuel of the turbine. However, multi-hole fuel injectors (micromix burners) were found to be more efficient for hydrogen combustion because of the thorough mixing of fuel and oxidants [68]. Besides research findings of Giacomazzi and Messina [69] on investigating Dry Low Emission gas turbine performance and emissions by co-firing 30% volume (vol.) of H_2, results mentioned only 5 % by mass CO_2 reduction or 75 % by vol. of H_2 is required for reaching 50 % CO_2 reduction. Giacomazzi and Messina [69] in their research findings also listed several issues related to the combustion of hydrogen in gas turbines with the blending of hydrogen in a fuel mix in the range of 0-100 %, and these issues are to control the temperature rise to maintain NOx emissions below 25 parts per million, by volume (ppmv). Of course, this is a challenging goal, as NOx emissions from the combustion of natural gas in gas turbines are below 15 ppmv. However, hydrogen combustion in gas turbines causes more steam in the exhaust, which in turn negatively affects the life span of hot parts with hot corrosion. Additionally, Giacomazzi and Messina [69] mentioned pressing issues on the production site of hydrogen, which is currently costly and not environmentally friendly, namely 99 % of global hydrogen production (70 Mt per year) comes from coal and natural gas. If the production from a fossil fuel-based source is converted to electrolysis-unit-based production, 3,600.00 TWh of electricity will be required per year to reach 70 Mt of hydrogen production per annum. On a comparative scale, 3,600.00 TWh is more than the annually produced electricity in the European Union. As for Technology Readiness Levels (TRL) of hybrid fuel-fired gas turbines, Giacomazzi et al. [69,70] emphasized the importance of the combustion physics of hydrogen and its blends with ammonia in a gas turbine at TRL 2-3, which must be investigated and analyzed. The hydrogen power generation handbook [71] of Mitsubishi Heavy Industries, including several technical reviews on the use of hydrogen in existing gas turbines, reported the outcome of experiments analyzing the combustion characteristics of hydrogen using multi-nozzle, multi-cluster, and diffusion combustors. Among the mentioned combustors, the diffusion flame combustor reached up to 100 % hydrogen combustion, while several drawbacks were observed, such as a drop in cycle efficiency and high NOx emission, but no flashback risk. Until now, multi-nozzle combustors have achieved up to 30 vol. % of hydrogen co-firing with the absence of drops in cycle efficiency and low NOx emission, but with high flashback risk due to large flame propagating area. The last available multi-cluster combustor with a premixed flame combustion method can achieve 100 vol. % of hydrogen combustion with no drops in cycle efficiency, low NOx emissions, and low flashback risk. In addition, ammonia is

used as a hydrogen carrier because of its higher density than that of liquefied hydrogen. In this case, an ammonia cracking unit is used, and it requires 46 kJ/mol of the heat of reaction for cracking 1 mole of raw ammonia with the drawbacks of combusting ammonia in a gas turbine, such as low combustion speed (approximately 1/5 of the methane combustion speed) and cracked fuel with nitrogen content causing more NOx emissions as a result [72]. Moreover, the use of ammonia in a gas turbine combustor also requires upsizing the dimensions of the combustor for the complete combustion of an ammonia-blended fuel mixture.

As for challenges with ammonia combustion, Erdemir and Dincer mentioned three main issues: high autoignition temperature (651°C), low flame speed (0.15 m/s), and slow chemical kinetics [73]. Erdemir and Dincer [73] also provided solutions for the aforementioned issues in the combustion of ammonia, namely, mixing ammonia with other traditional fuels, including hydrogen, to solve difficult ignition and slow chemical kinetics issues. In addition to preheating and increasing the compression ratio of ammonia, it is possible to overcome the low flame speed and high ignition temperature. Erdemir and Dincer [73] also emphasized the option of blending ammonia with other fuels, especially hydrogen, to resolve the three major issues mentioned above and boost the output power of the internal combustion engine. In terms of investigating ammonia combustion in gas turbines, Aalrebei et al. [74] conducted case studies comparing NH_3-H_2 / air and CH4 / air fuel and air blending and combustion performance approaches. It was also important to identify the operating region for reducing emissions under the NH_3-H_2 / air gas turbine cycle. In this case, the interval between two points of equivalence ratio at = 0.5, and at = 1.25 was investigated, and the equivalence ratio at 1.25, increased the NH_3 emission molar fraction, while the cycle efficiency was lower compared of the CH_4 / air gas turbine at a rate higher than 0.75. As a result, the study concluded that an NH_3-H_2 / air gas turbine with an equivalence ratio ⌀ < 0.75 has high system efficiency and low emission values. Ditaranto et al. [75] investigated the impact of recirculating exhaust gas of hydrogen-fired gas turbines for reducing NOx emissions. The recirculation of exhaust gas to the inlet of the air compressor was applied to reduce the oxygen concentration in the compressed air and the temperature of the combustion case. Simulations were performed with dry, wet, and wet cooling of the exhaust gas options, and with it was concluded that applying exhaust gas recirculation instead of nitrogen dilution will contribute to increasing the power plant's total efficiency while maintaining NOx emission at a favorable level. Lee et al. [76] also investigated ammonia co-firing combustors designed for conventional and gas turbine units and concluded that it is necessary to conduct future experiments on ammonia co-firing in gas turbines with a pressure higher than 20 bar. Bayramoglu et al. conducted a numerical study on the effect of blending up to 15% volume of H_2 and NH_3 with methane to evaluate emissions. The findings revealed an increase in NOx emissions up to 3,790.00 ppm with a 15% NH_3 blending option in a diesel engine [77]. Another study, conducted by Karam Ghareh Gheshlaghi and Tahsini, investigated the effect of different H_2 compositions (ranging from 5% to 30%) in methane on an existing gas turbine with a 5 MW installed capacity. The results indicated that a higher percentage of H_2 by volume leads to increased NOx emissions, attributed to the elevated temperature in the flame zone [78]. The development of a combined cycle gas turbine within an existing power plant with a Rankine cycle was investigated to increase the electrical efficiency of the overall cycle [79]. Matjanov investigated the effect of gas turbine inlet air cooling for maintaining higher efficiency of combined heat and power plants in Uzbekistan during the summer season [80]. Until now, several research works have been conducted on investigating the combustion kinetics of multi-fuel combustion, including fuel blends of methane, H_2, and NH_3 [81-88]. However, studies covering technical performance, combustion kinetics, and economic indicators have not been conducted in existing gas turbine technology for practically acceptable fuel mixture shares (up to 30% volume of H_2, etc.).

In this study, an ammonia and hydrogen co-fired gas turbine was developed in the existing gas turbine unit of a Fergana Combined Heat and Power (CHP) plant with a capacity of 7.6 MW.

First, a process flow diagram of the gas turbine cycle was developed using Aspen HYSYS software to determine the technical specifications of each component of the cycle, CO_2 emissions, etc. Four scenarios were investigated by setting the fuel mixture based on energy content to 100 % natural gas (NG), 30 % (ammonia) NH_3 and 70 % NG, 30 % (hydrogen) H_2 and 70 % NG, and 30 % NH_3, 30 % H_2, and 40 % NG.

Second, the economic parameters of each scenario were calculated to understand the sensitive costs of all expenditures (i.e., fuel expenses) for operating the system.

Thirdly, a model of a combustion chamber was designed by using Ansys® Chemkin-Pro software for evaluating and analyzing combustion and post-combustion values of each scenario.

Finally, a comparative analysis was conducted by discussing the emissions related to the technical parameters of the combustor and gas turbine itself to identify the most optimal power output within one of the mentioned fuel mixture scenarios.

3.2 Materials and Methods

Figure 25 depicts the process flow diagram of a multi-fuel co-firing gas turbine cycle based on an existing Fergana CHP plant designed on the Aspen HYSYS software tool. Peng-Robinson fluid package was used in software to determine the enthalpy and entropy of fluid and fluid mixtures in the proposed system. The cycle consists of an air compressor, fuel combustor, and gas turbine units. The installed capacity of the gas turbine unit was 7.6 MW, and all technical specifications were given for scenarios 1, 2, 3, and 4.

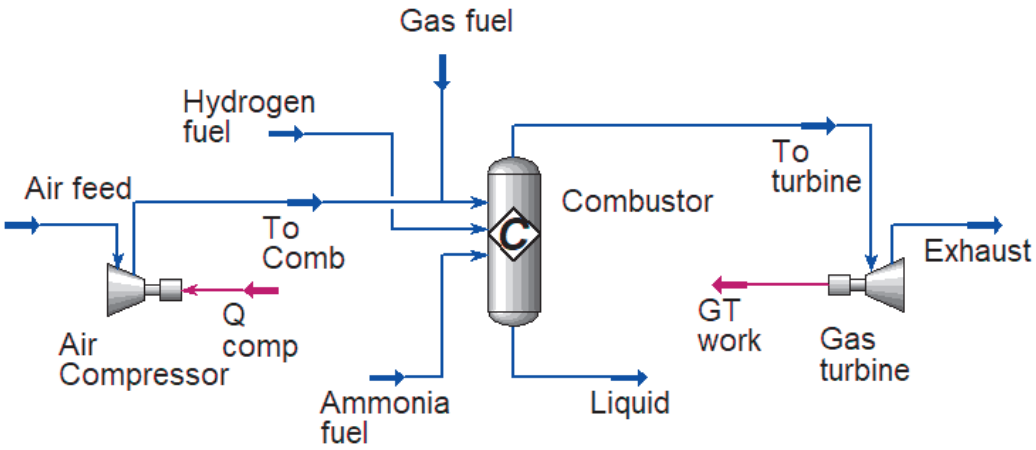

Figure 25. Process flow of natural gas, ammonia, and hydrogen co-firing CHP plant.

The main technical parameters of the air compressor and gas turbine of the Fergana CHP under different scenario models are listed in Table 7.

Table 7. Technical specifications of the air compressor and gas turbine of the power plant.

	Scenario 1 (reference model)		**Scenario 2**		**Scenario 3**		**Scenario 4**	
Parameters	**Air compressor**	**Gas turbine**	**Air compressor**	**Gas turbine**	**Air compressor**	**Gas turbine**	**Air compressor**	**Gas turbine**
Feed temperature (°C)	30	1312	30	1315	30	1322	30	1334
Feed pressure (bar)	1.3	20.28	1.3	20.28	1.3	20.28	1.3	20.28
Product temperature (°C)	431.7	750.8	431.7	752.6	431.7	757.2	431.7	765.9
Product pressure (bar)	20.28	2.026	20.28	2.026	20.28	2.026	20.28	2.026
Adiabatic efficiency (%)	85	85	85	85	85.4	85.4	85.4	85.4

Mass flow of working medium (kg/h)	90,000.00	92,327.93	87,463.00	90,247.10	87,654.00	89,796.61	82,660.00	90,247.10
Pressure ratio	15.6	-	15.6	-	15.6	-	15.6	-
Polytropic efficiency (%)	89.5	81	89.5	81	89.5	81.4	89.5	81.4
Power (kW)	10,621.40	18,227.30	10,322.40	17,983.67	10,344.54	17,922.73	9,755.17	17,392.81

As mentioned in the study objectives, 100 % NG combustion in scenario 1; 30 % NH_3 and 70 % NG fuel blend in scenario 2; 30 % H_2 and 70 % NG fuel mixture in scenario 3; and 30 %

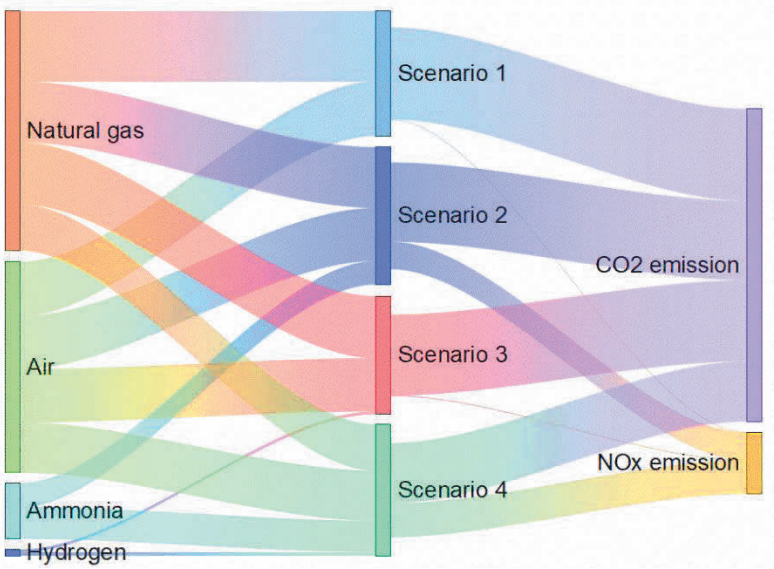

Figure 26. Overview of methodology for evaluating emission in four scenarios.

NH_3, 30 % H_2, and 40 % NG in scenario 4 were applied and analyzed in the operating Fergana CHP plant (Figure 26).

As for the composition of each fuel, NG with a composition of CH_4, C_2H_6, C_3H_8, C_4H_{10}, and CO_2 had mole fractions of 88%, 2%, 5%, 0.6%, and 4.4%, respectively. In the case of the composition of ammonia (NH_3) and hydrogen (H_2), both were considered pure and 100 % fuel for model simulations. The air used for compression contained 21% O_2 and 79% N_2.

Analysis of combustion and post-combustion cases was conducted by developing models

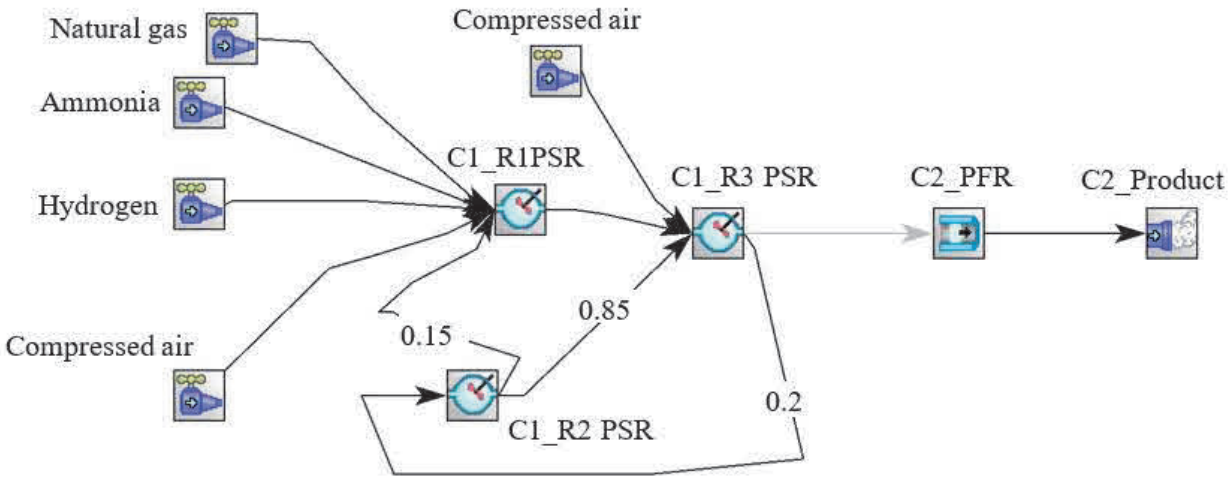

Figure 27. Process flow diagram of gas turbine with multi fuel combustion approaches.

using the Ansys Chemkin-Pro software tool and applying the GRImech 3.0, mechanism to analyze

the chemical kinetics of each scenario. GRImech 3.0 mechanism includes five elements, namely C, H, O, N, and Ar, 53 chemical species, and 325 reactions for a detailed analysis of the chemical pathway of each model point [89,90]. Figure 27 depicts the Perfectly Stirred Reactor (PSR) - Plug Flow Reactor (PFR) network for simulating the gas turbine combustor, covering the mixing and flow features of the working medium.

Based on the structure of the gas turbine network depicted in Figure 27, there are two clusters including a flame, a recirculation zone in the first cluster, and a second cluster with a single PFR. The first cluster has an Reactor (R)1 PSR designed as a premixing zone and an R2 PSR and R3 PSR for recirculation and flame zones, respectively. Figure 28 shows a comprehensive diagram of the developed models for analyzing combustion and post-combustion features. Each model had corresponding fuel blending approaches and the air was delivered in staging method for complying with low NOx emission from gas turbine network.

In this study structure of CHP plant is investigated by taking into consideration of each

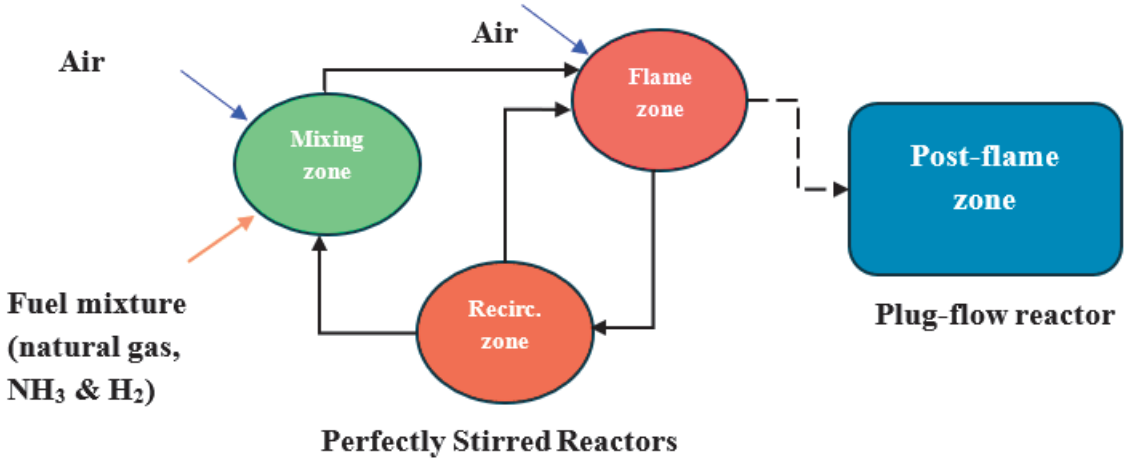

Figure 28. Diagram of gas turbine network with mixing, flame, and post flame zones.

component efficiency (e.g., thermal efficiency of the Brayton cycle, energy generation in the cycle, electricity consumed by the compressor of air, heat energy consumed by the gas turbine unit, and isentropic (ideal) (ηc & ηt) and polytropic (ηc/p & ηt/p) efficiency of the compressor and gas turbine units respectively) [29-31,91,92]. Because the current study emphasizes the evaluation of emissions, the CO_2 emissions of each model were determined using Equation (22):

Equation 22. CO_2 emission rate of the multi-fuel fired gas turbine.

$$CO_2 emission\ rate = Q \times EF \tag{22}$$

where Q (energy/time) is the input energy of the system and EF (kg CO_2/energy) is the emission factor of the fuel used in the system [93].

The Levelized Cost of Electricity (LCOE) for each scenario was determined using Equation (23) [94]:

Equation 23. Levelized cost of the multi-fuel fired gas turbine.

$$LCOE = \frac{\sum_{t=1}^{n} \frac{I_t + M_t + F_t}{(1+r)^t}}{\sum_{t=1}^{n} \frac{E_t}{(1+r)^t}} \tag{23}$$

Where I_t is the cost of investment and construction work in t years, M_t is the cost of operation and maintenance in t years, F_t is expenses on using fuel in t years, E_t is the total power output in t years, r is the discount rate of the selected technology, and n is the lifetime of the selected technology.

3.3 Results and Discussion

In this section, the energy and mass balance of each model are presented and described to compare them considering the emissions and efficiencies of the compressor and gas turbine. In addition, the flame and post-flame zones are discussed, and the optimal emission approach is stated. Figure 29 depicts the share of each fuel type applied to all study scenarios.

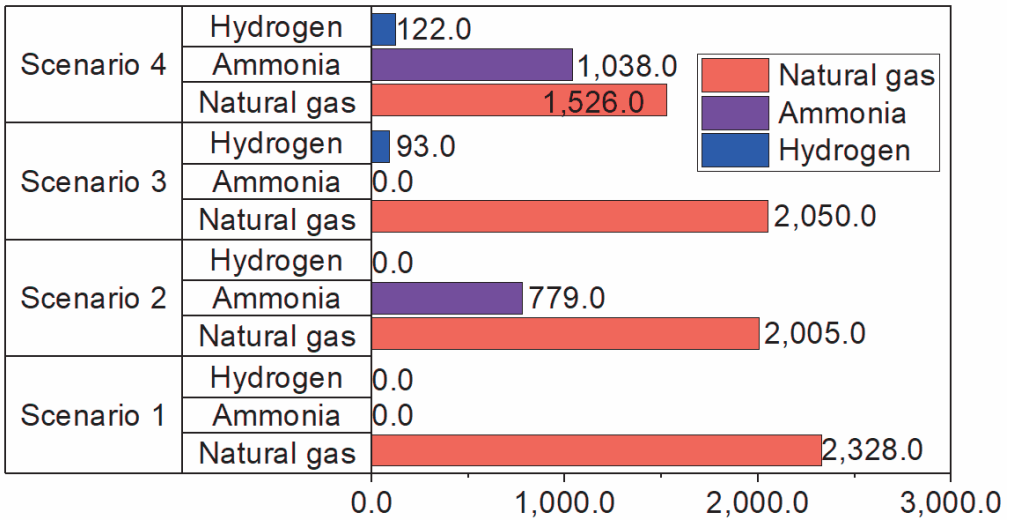

Figure 29. Fuel share and blending options for all investigated scenarios (kg/h).

3.3.1 Outcome of Scenario 1

In scenario 1, the fuel composition included NG only, and Figure 29 depicts the share of each selected fuel for the current research work.

The following reaction equations for the combustion of NG were used [95]:

Equation 24. Reaction of methane (CH_4) combustion.

$$CH_4(g) + 2O_2\ (g)\ \rightarrow CO_2(g) + 2H_2O\ (l) \quad (24)$$

Equation 25. Reaction of ethane (C_2H_6) combustion.

$$2C_2H_6(g) + 7O_2\ (g)\ \rightarrow 4CO_2(g) + 6H_2O\ (l) \quad (25)$$

Equation 26. Reaction of propane (C_3H_8) combustion.

$$C_3H_8(g) + 5O_2\ (g)\ \rightarrow 3CO_2(g) + 4H_2O\ (l) \quad (26)$$

Equation 27. Reaction of n-butane (C_4H_{10}) combustion.

$$2C_4H_{10}(g) + 13O_2\ (g)\ \rightarrow 8CO_2(g) + 10H_2O\ (l) \quad (27)$$

Equation 28. Reaction of n-pentane (C_5H_{12}) combustion.

$$C_5H_{12}(g) + 8O_2\ (g)\ \rightarrow 5CO_2(g) + 6H_2O\ (l) \quad (28)$$

Table 8 presents the material stream for scenario 1 (100 % NG combustion approach).

Table 8. Material stream in Scenario 1.

Name	Air feed	To Turbine	Gas fuel	To combustion	Exhaust
Vapor fraction	1	1	1	1	1
Temperature [°C]	30	1,313.00	30	431.4	752.1
Pressure [bar]	1.30	20.28	20.30	20.28	2.026
Molar flow [kgmole/h]	3,120.00	3.249.00	121.2	3,120.00	3,249.00
Mass flow [kg/h]	90,000.00	92,327.93	2,328.00	90,000.00	92,327.93
Standard liquid volume flow [m3/h]	104.0	108.7	6,804.00	104.0	108.7
Heat flow [kcal/h]	101,141.00	6,571,510.97	-2,640,017.81	9,211,529.07	-9,082,823.26

Table 9 lists the mol fraction of the material flow within the entire system under Scenario 1.

Table 9. Composition of mol fractions of the model under Scenario 1.

Name	Air feed	To turbine	Gas fuel	To combustion	Exhaust
Methane	0.00	0.00	0,8800	0.00	0.00
Propane	0.00	0.00	0.05	0.00	0.00
Ethane	0.00	0.00	0.02	0.00	0.00
n-Butane	0.00	0.00	0.006	0.00	0.00
n-Pentane	0.00	0.00	0,00	0.00	0.00
Oxygen	0.21	0.1226	0,00	0.21	0.1226
Nitrogen	0.79	0.7585	0,00	0.79	0.7585
CO_2	0.00	0.0424	0.044	0.00	0.0424
H_2O	0.00	0.0765	0.00	0.00	0.0765

Table 10 lists the energy flows in the system and the balance is closed. Total gained energy in the cycle accounted for 6,543,468.02 kcal/h or 7,604.96 kW.

Table 10. Energy balance of the system under Scenario 1.

Inlet Streams	Energy Flow [kcal/h]	Outlet Streams	Energy Flow [kcal/h]
Air Feed	101,141.01	**Exhaust**	-9,082,345.11
Q Compressor	9,110,388.07	**Gas turbine work**	15,653,856.08
Gas fuel	-2,640,017.81	**-**	-

As for the rate of production of NO emissions from Scenario 1, in Figure 30, it was mentioned that reaction $NO+O+M \Leftrightarrow NO_2+M$ was mostly dominating in NO emissions with a rate of 0.00429 mole/m^3-sec, while reaction $HO_2+NO \Leftrightarrow NO_2+OH$ was contributing to consumption of NO accounting for -0.00596 mole/m^3-sec. Similar methods for identifying sensitive reactions in

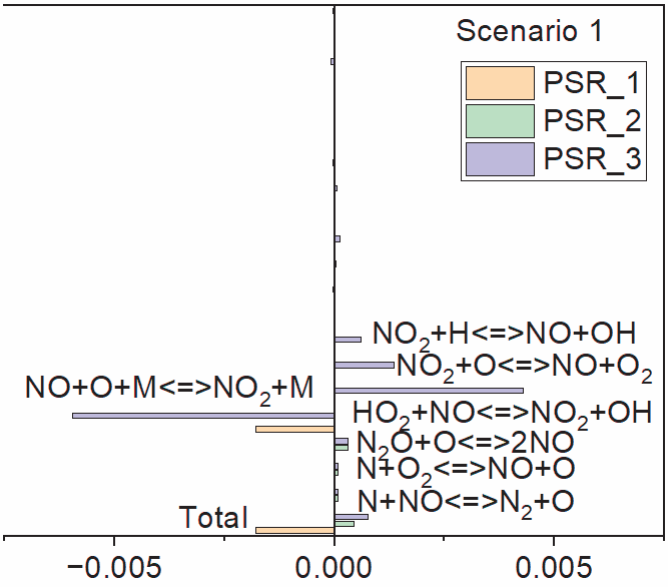

Figure 30. Rate of production of NO (mole/m3-sec) in Scenario 1.

the combustion of different fuels in a fuel mixture have also been investigated previously by Li et al. [96-98].

3.3.2 Outcome of Scenario 2

In scenario 2 fuel composition included NG 70 % vol. and NH_3 30 % vol.

In the model, in addition to the reaction equation set of combustion of natural gas following the reaction equation of combustion of ammonia was used [99]:

Equation 29. Ammonia (NH_3) combustion.

$$4NH_3(g) + 3O_2\ (g)\ \rightarrow 2N_2(g) + 6H_2O\ (g) \qquad (29)$$

Table 11 covers the material stream of Scenario 2 (70 % natural gas and 30 % NH_3 combustion approach).

Table 11. Material stream in Scenario 2.

Name	Air feed	To Turbine	Gas fuel	Ammonia fuel	To combustion	Exhaust
Vapor fraction	1	1	1	1	1	1
Temperature [°C]	30	1,316.00	30	30	431.4	753.8
Pressure [bar]	1.30	20.28	20.30	20.30	20.28	2.026
Molar flow [kgmole/h]	3,032.00	3,200.00	104.4	45.77	3,032.00	3,200.00
Mass flow [kg/h]	87,463.00	90,247.10	2,005.00	779.5	87,463.00	90,247.10
Standard liquid volume flow [m3/h]	101.1	106.2	5.860	1.265	101.1	106.2
Heat flow [kcal/h]	98,289.95	5,951,196.22	-2,273,726.68	-726,886.06	8,951,866.30	-9,494,267.59

Table 12 shows the composition of mole fractions of the selected system within Scenario 2.

Table 12. Composition of mole fractions of the model under Scenario 2.

Name	Air feed	To turbine	Gas fuel	Ammonia fuel	To combustion	Exhaust
Methane	0.00	0.00	0,8800	0.00	0.00	0.00
Propane	0.00	0.00	0.05	0.00	0.00	0.00
Ethane	0.00	0.00	0.02	0.00	0.00	0.00
n-Butane	0.00	0.00	0.006	0.00	0.00	0.00
n-Pentane	0.00	0.00	0,00	0.00	0.00	0.00
Oxygen	0.21	0.1191	0,00	0.00	0.21	0.1191
Nitrogen	0.79	0.7555	0,00	0.00	0.79	0.7757
CO_2	0.00	0.0371	0.044	0.00	0.00	0.0371
H2O	0.00	0.0883	0.00	0.00	0.00	0.0883
Ammonia	0.00	0.00	0.00	1.00	0.00	0.00

Table 13 covers the energy flows of the system within Scenario 2. The total energy gained in the cycle accounted for 6,591,434.85 kcal/h or 7,660.71 kW. The system's energy balance was also closed. Composition of mol fractions of the model under Scenario 2.

Table 13. Energy balance of the system under Scenario 2.

Inlet Streams	Energy Flow [kcal/h]	Outlet Streams	Energy Flow [kcal/h]
Air Feed	98,289.95	**Exhaust**	-9,493,814.97
Q Compressor	8,853,576.35	**Gas turbine work**	15,445,011.20
Gas fuel	-2,273,726.68	-	-
Ammonia fuel	-726,886.06		

In the case of NO emission of the model within Scenario 2, in Figure 31, it was mentioned that reaction NO+O+M⇔NO_2+M was dominant among all reactions at a rate of 3.50E-01 mole/m^3-sec, while reaction HO_2+NO⇔NO_2+OH was contributing to consumption of NO accounting for -0.679 mole/m^3-sec. As mentioned by Zhang et al. the presence of free radicals and their content fluctuation are directly related to the proportion of ammonia in a fuel mixture [100]. The presence of the intermediate product, HNO, in Figure 31 indicates the formation of NO during

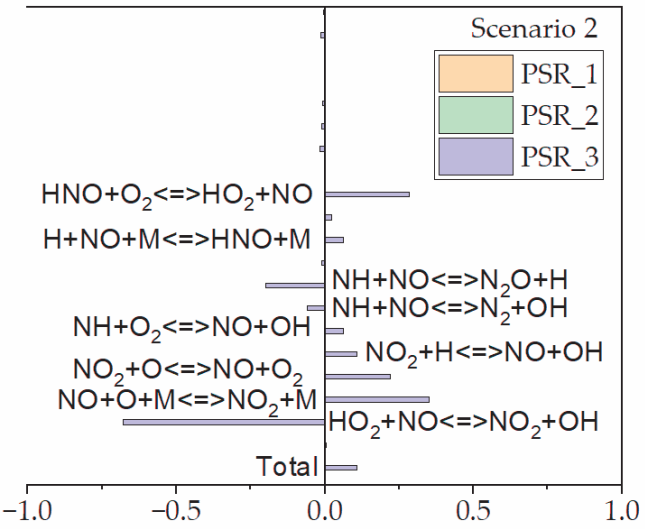

Figure 31. Rate of production of NO (mol/m3-sec) in Scenario 2.

NH3 combustion. Cecere et al. also mentioned several intermediate products (e.g., CN, HCN,

HNO, and NHi) produced during the combustion of ammonia, which after oxidation, contribute to the formation of NO emissions [101-103].

3.3.3 Outcome of Scenario 3

In scenario 3 fuel composition included NG 70 % vol. and H_2 30 % vol.

In the model, in addition to the reaction equation set for the combustion of natural gas following reaction equation of combustion of hydrogen was used [104]:

Equation 30. Combustion of hydrogen (H_2) in the gas turbine.

$$2H_2(g) + O_2\ (g)\ \rightarrow 2H_2O\ (l) \tag{30}$$

Table 14 presents the material stream of the system under Scenario 3.

Table 14. Material stream in Scenario 3.

Name	Air feed	To Turbine	Gas fuel	Hydrogen fuel	To combustion	Exhaust
Vapor fraction	1	1	1	1	1	1
Temperature [°C]	30	1,323.00	30	30	431.4	758.4
Pressure [bar]	1.30	20.28	20.30	20.30	20.28	2.026
Molar flow [kgmole/h]	3,038.00	3,175.00	106.7	46.13	3,038.00	3,175.00
Mass flow [kg/h]	87,654.00	89,796.61	2,050.00	93.00	87,654.00	89,796.61
Standard liquid volume flow [m3/h]	101.3	105.6	5.9913	1.331	101.3	105.6
Heat flow [kcal/h]	98,504.59	6,648,216.93	-2,324,757.95	1,560.00	8,971,415.22	-8,744,811.50

Table 15 lists the composition of the mole fractions of the selected fuel and air in each unit.

Table 15. Composition of mole fractions of the model under Scenario 3.

Name	Air feed	To turbine	Gas fuel	Hydrogen fuel	To combustion	Exhaust
Methane	0.00	0.00	0,8800	0.00	0.00	0.00
Propane	0.00	0.00	0.05	0.00	0.00	0.00
Ethane	0.00	0.00	0.02	0.00	0.00	0.00
n-Butane	0.00	0.00	0.006	0.00	0.00	0.00
n-Pentane	0.00	0.00	0,00	0.00	0.00	0.00
Oxygen	0.21	0.1224	0,00	0.00	0.21	0.1224
Nitrogen	0.79	0.7559	0,00	0.00	0.79	0.7559
CO_2	0.00	0.0382	0.044	0.00	0.00	0.0382
H_2O	0.00	0.0834	0.00	0.00	0.00	0.0834
Hydrogen	0.00	0.00	0.00	1.00	0.00	0.00

Table 16 displays the energy flows within the system for Scenario 2. The total energy gained in the cycle amounted to 6,519,553.33 kcal/h or 7,577.16 kW, and the system's energy balance was successfully closed.

Table 16. Energy balance of system under Scenario 3.

Inlet Streams	Energy Flow [kcal/h]	Outlet Streams	Energy Flow [kcal/h]
Air Feed	98,504.59	**Exhaust**	-8,744,247.02
Q Compressor	8,872,910.62	**Gas turbine work**	15,392,463.95
Gas fuel	-2,324,757.95	**-**	-
Hydrogen fuel	1,559.67		

In the analysis of NO emissions for Scenario 3, the dominant reaction differed from scenarios 1 and 2. Specifically, the reaction HO_2+NO ⇔ NO_2+OH was found to be predominant

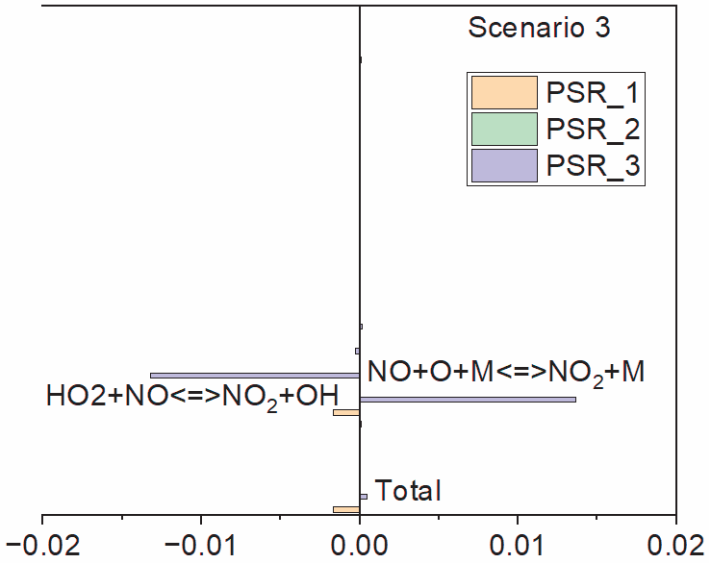

Figure 32. Rate of NO production (mol/m3-sec) in Scenario 3.

among all reactions, with a rate of 0.0136 mol/m3-sec. Additionally, the reaction NO+O+M ⇔ NO_2+M was identified as consuming NO emissions, accounting for -0.0132 mole/m3-sec. The total NO emissions were significantly lower than those in Scenarios 1 and 2. Figure 32 illustrates the behavior of chemical reactions in Scenario 3. In a study by Ma et al., various free radicals, including H, O, and OH, were identified as factors influencing the trend of NO emissions after the dilution of hydrogen in the fuel blends [105]. Karam Ghareh Gheshlaghi and Tahsini also emphasized the dominant NO emission reaction in H_2 and CH_4 combustion with varying fuel compositions [78].

3.3.4 Outcome of Scenario 4

In Scenario 4, the fuel composition included 40% vol. NG, 30% vol. NH3, and 30% vol. H2. For this scenario, Equations (3), (4), (5), (6), (7), (8), and (9) were employed. Only the volume fraction of each fuel was identified based on the fuel-blending approach for each scenario.

Table 17 presents the material stream details of the model under Scenario 4, where the fuel mixture consisted of NG, NH_3, and H_2 fuels in the proportions of 40%, 30%, and 30% vol., respectively.

Table 17. Material stream in Scenario 4.

Name	Air feed	To Turbine	Gas fuel	Hydrogen fuel	Ammonia fuel	To combustion	Exhaust
Vapor fraction	1	1	1	1	1	1	1
Temperature [°C]	30	1,335.0	30	30	30	431.4	767.1
Pressure [bar]	1.30	20.28	20.30	20.30	20.30	20.28	2.028
Molar flow [kgmole/h]	2,865.0	3,057.0	79.44	60.52	60.95	2,865.0	3,057.0
Mass flow [kg/h]	82,660.0	85,345.64	1,526.0	122.0	1,038.0	82,660.0	85,345.64
Standard liquid volume flow [m3/h]	95.56	100.2	4,460.0	1,746.0	1,685.0	95.56	100.2
Heat flow [kcal/h]	92,892.4	5,763,833.6	-1,730,527.2	2,046.0	-967,962.9	8,460,277.7	-9,174,178.4

Table 18 provides the details of the composition of the mole fraction of each working agent in the model under Scenario 4.

Table 18. Composition of mole fractions of the model under Scenario 4.

Name	Air feed	To turbine	Gas fuel	Ammonia fuel	Hydrogen fuel	To combustion	Exhaust
Methane	0.00	0.00	0,8800	0.00	0.00	0.00	0.00
Propane	0.00	0.00	0.05	0.00	0.00	0.00	0.00
Ethane	0.00	0.00	0.02	0.00	0.00	0.00	0.00
n-Butane	0.00	0.00	0.006	0.00	0.00	0.00	0.00
n-Pentane	0.00	0.00	0,00	0.00	0.00	0.00	0.00
Oxygen	0.21	0.1169	0,00	0.00	0.00	0.21	0.1169
Nitrogen	0.79	0.7505	0,00	0.00	0.00	0.79	0.7505
CO_2	0.00	0.0296	0.044	0.00	0.00	0.00	0.0296
H_2O	0.00	0.1030	0.00	0.00	0.00	0.00	0.1030
Ammonia	0.00	0.00	0.00	1.00	0.00	0.00	0.00
Hydrogen	0.00	0.00	0.00	0.00	1.00	0.00	0.00

Table 19 displays the energy flows within the system for Scenario 4. The total energy gained in the cycle amounted to 6,570,626.70 kcal/h or 7,636.53 kW and the system's energy balance was closed.

Table 19. The energy balance of the system under Scenario 4.

Inlet Streams	Energy Flow [kcal/h]	Outlet Streams	Energy Flow [kcal/h]
Air Feed	92,892.39	**Exhaust**	-9,174,178.34
Q Compressor	8,367,385.31	**Gas turbine work**	14,938,012.01
Gas fuel	-1,730,527.14	**-**	-
Ammonia fuel	-967,962.91		
Hydrogen fuel	2,046.02		

In the final Scenario 4, NO emissions exhibited a certain level of complexity. In Figure 33, several dominating reactions within the diverse fuel blending options can be observed. Ultimately,

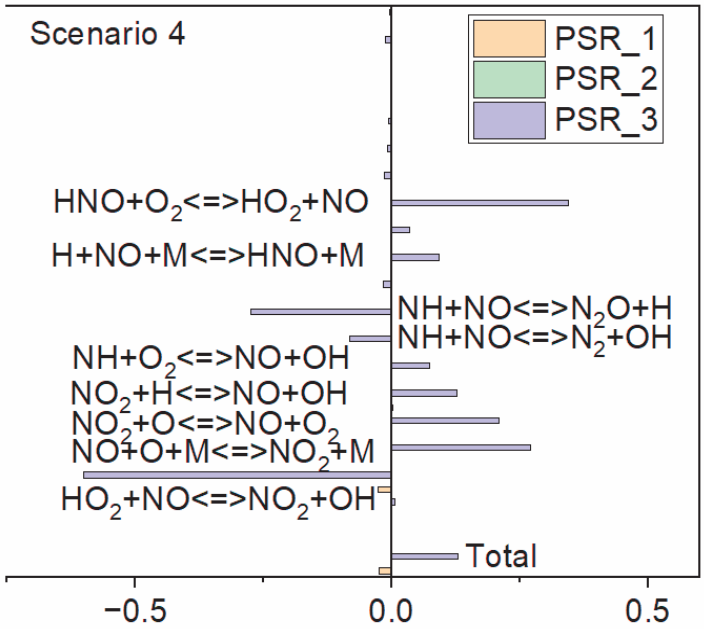

Figure 33. Rate of production of NO (mole/m3-sec) in Scenario 4.

the reaction HNO+O_3 ⇔ HO_2+NO emerged as dominant compared to other reactions, rated at 0.345 mole/m3-sec, while the reaction HO_2+NO ⇔ NO_2+OH played a significant role in reducing NO emissions, with a rate of -0.601 mole/m3-sec. The total NO emission represented the highest NO emission scenario compared to Scenarios 1, 2, and 3. As mentioned earlier, in Scenario 4, variations in the amount of free radicals were observed after premixing ammonia and hydrogen in a fuel mixture. Similar to Scenario 2, the presence of the intermediate product HNO resulting from ammonia combustion contributes to the formation of NOx emissions. Cecere et al. [101-103] also mentioned the role of HNO produced during ammonia combustion in the development of NOx emissions.

3.4.5 Technical, economic, and environmental analyses

The findings of each scenario differed from one another in various aspects. For example, comparing the Levelized Cost of Electricity (LCOE) to CO_2 emissions provided insight into how

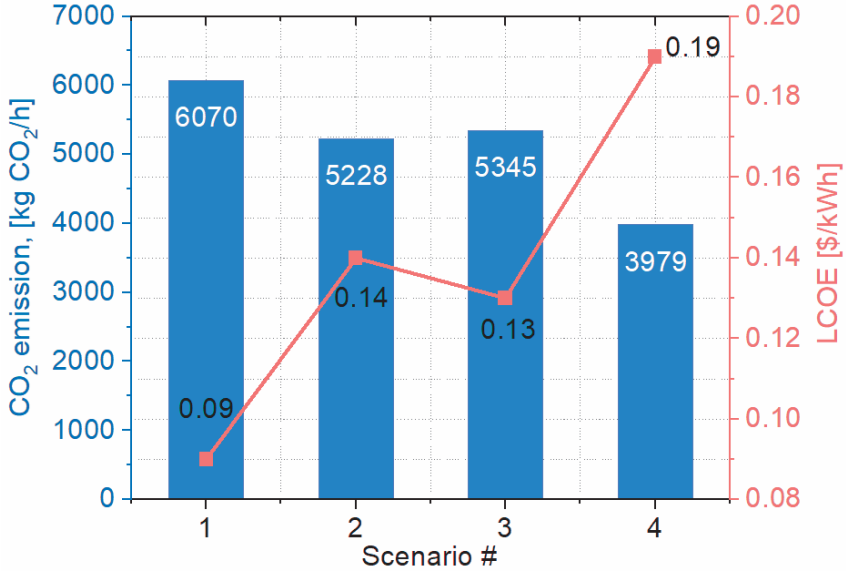

Figure 34. CO_2 emission [kg CO_2/h] and LCOE [$/kWh] of all scenarios.

a greater reduction in emissions contributes to an increase in LCOE. Figure 34 illustrates the relationship between LCOE and CO_2 emissions for all scenarios. In Scenario 1, which had the highest CO_2 emission at 6,070.00 kg/h, the LCOE was the lowest at 0.09 USD/kWh. On the other hand, Scenario 4, featuring a multi-fuel blending option (NG 40% vol., NH_3 30% vol., and H_2 30% vol.), emitted 3,979.00 kg CO_2/h, contributing positively to the system's performance. However, it had the highest LCOE at 0.19 USD/kWh, representing a less attractive point due to the high cost of alternative fuels. For instance, the sale price of ammonia per ton was 5 million Uzbek So'm (UZS) or 410 USD, based on quotes received from a local ammonia manufacturer's dealer in Uzbekistan as of October 18, 2023. Additionally, the sale price of hydrogen fuel ranged from 2.5 to 3 USD per kg in Uzbekistan [106]. To gauge the feasibility of implementing Scenarios 2, 3, and 4, an additional study similar to Kim et al. [107] must be conducted among residents. This study aims to identify additional willingness to pay for purchasing electricity generated with alternative fuels, considering the fuel blending options mentioned above. From an emissions standpoint, Koc et al.'s study on co-firing hydrogen in a gas turbine with 50 MW at 50 bar resulted in 52.17 tons of CO_2/h or 1.0434 CO_2/kWh [108]. In comparison, the current study yielded 5.345 tons of CO_2/h or 0.70 kg CO_2/kWh.

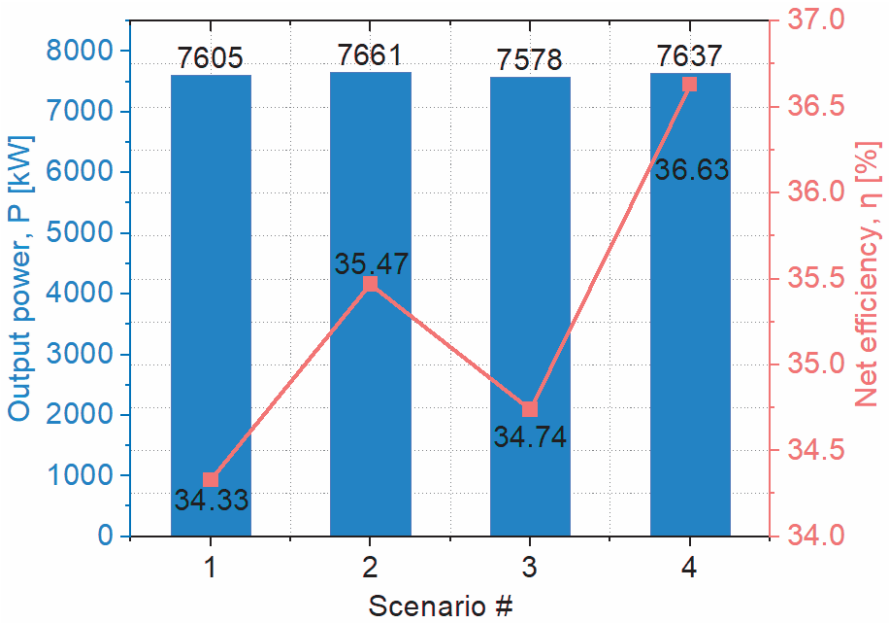

Figure 35. Relationship of output power and net efficiency of all scenarios.

On the other hand, the output capacity of each model yielded values that closely approached the range of design parameters for the selected gas turbine unit. Figure 35 illustrates the relationship between the output power and net efficiency of each model. From Figure 35, we can observe variations in output capacity, with Scenario 2 resulting in the highest capacity at 7,662.00 kW, while Scenarios 1, 3, and 4 generated 7,606.00 kW, 7,578.00 kW, and 7,638.00 kW, respectively. Regarding the net efficiency of all scenarios, Scenarios 1, 2, 3, and 4 amounted to 34.33%, 35.47%, 34.74%, and 36.63%, respectively. Comparing each case, output capacity is directly proportional to the net efficiency of the system. From the perspectives of CO_2 emissions versus output power and net efficiency for all scenarios, CO_2 emissions in Scenarios 1 and 4 were directly proportional to the fluctuations in output power and net efficiency. However, Scenarios 2 and 3 exhibited unusual behavioral outcomes, with CO_2 emissions at 5,228.00 kg/h and 5,345.00 kg/h, respectively. This is attributed to the consumption of NG share in Scenarios 2 and 3, accounting for 2,005.00 kg/h and 2,050 kg/h, respectively. The most attractive scenario demonstrated a significant reduction in CO_2 emissions, with Scenario 4 resulting in the lowest emissions at 3,979.00 kg/h, which is 35% lower than the baseline Scenario 1. Umyshev et al. also mentioned the possibility of reducing emissions to 0.53 kgCO_2/kWh through the modernization of existing gas turbine units [109]. On the other hand, Scenarios 2 and 3 resulted in a reduction of CO_2 emissions by 14% and 12%, respectively, compared to Scenario 1 (baseline case). Regarding

capacity fluctuations compared to the initial reference model (Scenario 1), Scenarios 2, 3, and 4 exhibited a 0.7% increase, a 0.37% reduction, and a 0.42% increase, respectively.

Regarding the analysis of the cost of annual fuel consumption per scenario, expenses on fuel for Scenario 4 amounted to 4.8 million USD/year, including 0.9 million USD/year for NG, 2.1 million USD/year for NH_3, and 1.8 million USD/year for H_2 consumptions. Figure 36 provides more details on all scenarios in terms of total annual fuel consumption and a breakdown of the costs for each scenario.

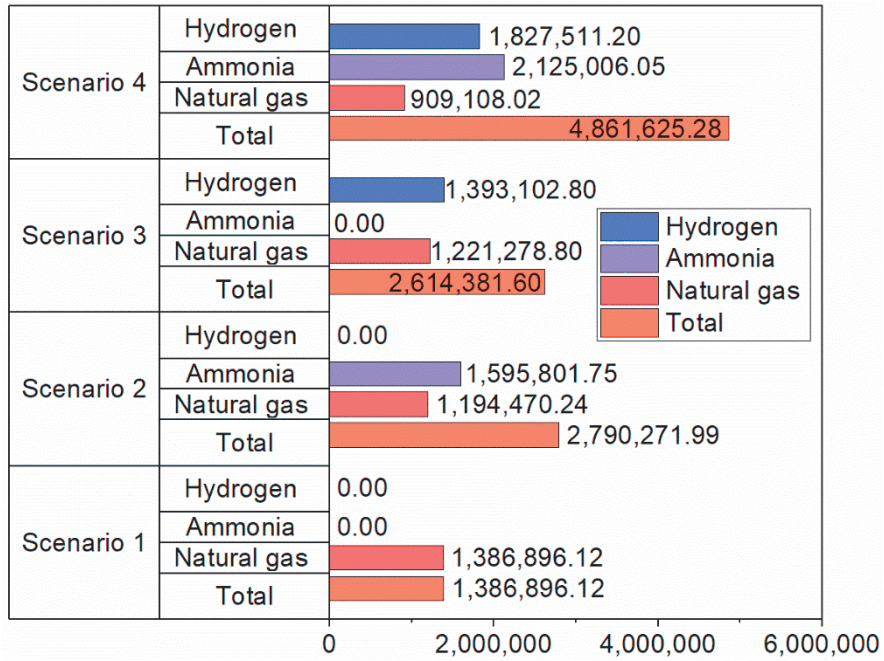

Figure 36. Comparison of costs on fuel consumption per each scenario ($/year).

As seen in Figure 36, Scenario 1 represents the most economically attractive case with 100% NG consumption and annual fuel expenditures of 1.38 million USD. Concerning fuel consumption costs for Scenarios 2 and 3, a slight difference is observed. When comparing the costs of NH_3 and H_2, NH_3 in Scenario 2 required 1.59 million USD/year, while H_2 in Scenario 3 required 1.39 million USD/year. Based on the comparative economic evaluations of NH_3 and H_2 by Bartels [110], the estimated 182-day storage cost for NH_3 and H_2 is 0.51 USD/kg-H_2 for ammonia and 14.00 USD/kg-H_2, respectively. Regarding transportation expenses of ammonia and hydrogen, Bartels [110] evaluated 0.70-3.22 USD/kg for H_2, and 0.0344 USD/kg for NH_3 transportation via pipelines. Referring to previous findings on NH_3 and H_2 handling expenses, it is more attractive to rely on ammonia rather than hydrogen [111]. Scenario 2 in the current study can be considered more attractive when compared to Scenario 3 with H_2 combustion in the fuel blending approach. Considering net efficiency pertaining to output power in Fig. 11, Scenario 4 demonstrated the highest efficiency at a rate of 36.67%, while Scenarios 1, 2, and 3 resulted in 34.33 %, 35.47 %, and 34.74 %, respectively.

From the perspectives of H_2 production in the case of Uzbekistan within minimum and maximum scenarios, it was estimated to produce between 494 and 2,093.00 thousand tons per annum, requiring Carbon Capture, Utilization, and Storage (CCUS) between 4 and 8 Million tons (Mt) CO_2 per annum respectively [106]. In this estimation, several approaches to hydrogen production were considered, including production based on electrolysis sourced from renewable electricity, nuclear electricity, NG, Steam Methane Reforming (SMR) including CCUS. The requirement for the mentioned H_2 production is to secure 72,051.00 GWh of renewable electricity per annum, 1,530.00 GWh of nuclear electricity per annum, and 4 billion cubic meters per annum of NG solely for this sector, while the entire country's annual production accounted for 74.3 GWh in 2022 [112]. This represents about 10 % of the required electricity for achieving the potential production of H_2 with the maximum scenario. From view viewpoint of emission per unit of produced H_2 using the SMR method, it is estimated to generate 10 kg CO_2 per 1 kg of H_2 or 10

tons CO_2/ton of H_2 production [106]. To provide sustainable H_2 supply for the 7.6 MW gas turbine unit's year-round operation, it is necessary to secure H_2 supply between 464.35 and 609.17 tons under Scenarios 3 and 4, respectively, representing only a 30 % vol. share of the fuel contribution into the fuel blend.

In the case of NH_3 production in Uzbekistan, a report prepared by the Center of Hydrometeorological Service (Uzhydromet) at the Cabinet of Ministers of the Republic of Uzbekistan and sponsored by the United Nations Environmental Program (UNEP) and the Global Environment Facility (GEF) mentioned a total of 1,065.1 tons of NH_3 production in 2005 and 1.317 tons of CO_2 per ton of NH_3 production [113]. Recently statistics on NH_3 production in Uzbekistan for the year 2022 from January to August reported 1,096.5 tons of NH_3 production [114], slightly more than the indicators reported by Uzhydromet. Comparing emissions from H_2 and NH_3 production in Uzbekistan, 7.5 times more CO_2 emissions can be found, as discussed above.

In terms of the efficiency of each unit within the CHP plant, it is important to evaluate the performance of the compressor and gas turbine, including their polytropic and isentropic efficiencies. The pressure ratio of a gas turbine plays a crucial role in evaluating its performance and efficiencies, with the polytropic efficiency of the compressor typically being lower than the isentropic efficiency, and vice versa for the gas turbine. As mentioned by Boyce, a compressor with a pressure ratio of 15.6 and 89.54 % polytropic efficiency will result in 85.4 % isentropic efficiency [115]. The reason for the identical efficiencies of the air compressor and the gas turbine is setting of the same pressure ratio and achieving very similar gas turbine inlet temperature (i.e., Scenarios 1, 2, 3, and 4 accounted for 1,313.00 °C, 1,316.00 °C, 1,323.00 °C, and 1,335.00 °C respectively).

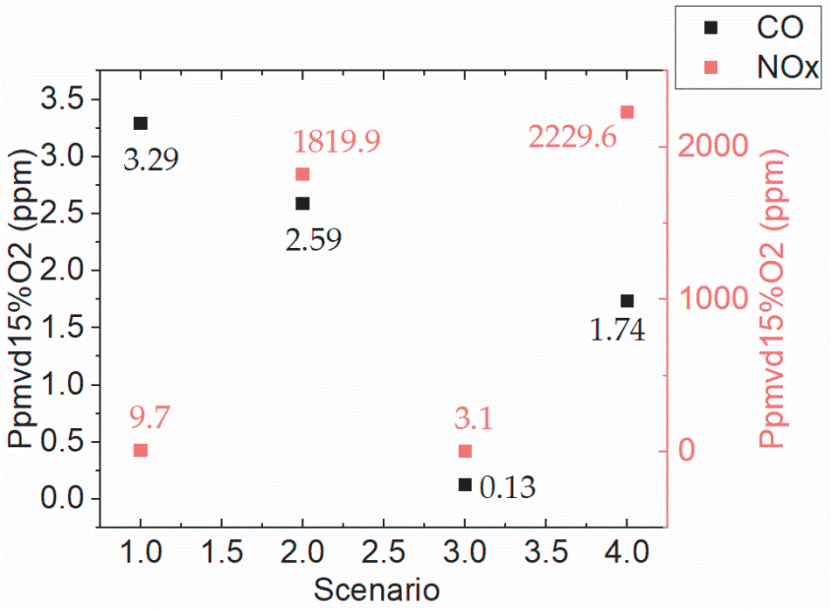

Figure 37. NOx and CO emissions in all scenarios.

A technical review of Mitsubishi Heavy Industries also reported on the possibility of combining NH_3 and H_2 in the fuel mixture of natural gas-fired gas turbines for the decarbonization of energy systems based on gas turbine technologies. They also mentioned limitations on increasing the share of NH_3 in the fuel mixture (e.g., up to 30 % vol.) to avoid enlarging of the combustor due to large amounts of NO_x emissions and rich-lean combustion exhaust products. Therefore, it was proposed to focus on a limited share of NH_3 or an increased share of H_2 in a fuel mixture [33]. The current study's findings on NOx emissions at a 15 % O_2 level demonstrate a clear picture for identifying cost-effective and environmentally friendly scenarios. Figure 37 illustrates the trend of NOx and CO emissions for each scenario, where Scenarios 1,2 3, and 4 resulted in 9.7 ppm at 15 % O_2, 1819.9 ppm at 15 % O_2, 3.1 ppm at 15 % O_2, and 2229.6 ppm at 15 % O_2 respectively. Scenario 1 (reference model) fell within the requirements of the gas turbine manufacturer [116], while Scenarios 2 and 4 exceeded the regulatory parameters of the gas turbine.

On the other hand, NOx emissions of Scenario 3 accounted for 3.1 ppm at 15 % O_2, which is a threefold reduction compared to Scenario 1's NOx emissions. If hydrogen and natural gas are mixed, combustion kinetics are enhanced because of hydrogen has wide flammability range and

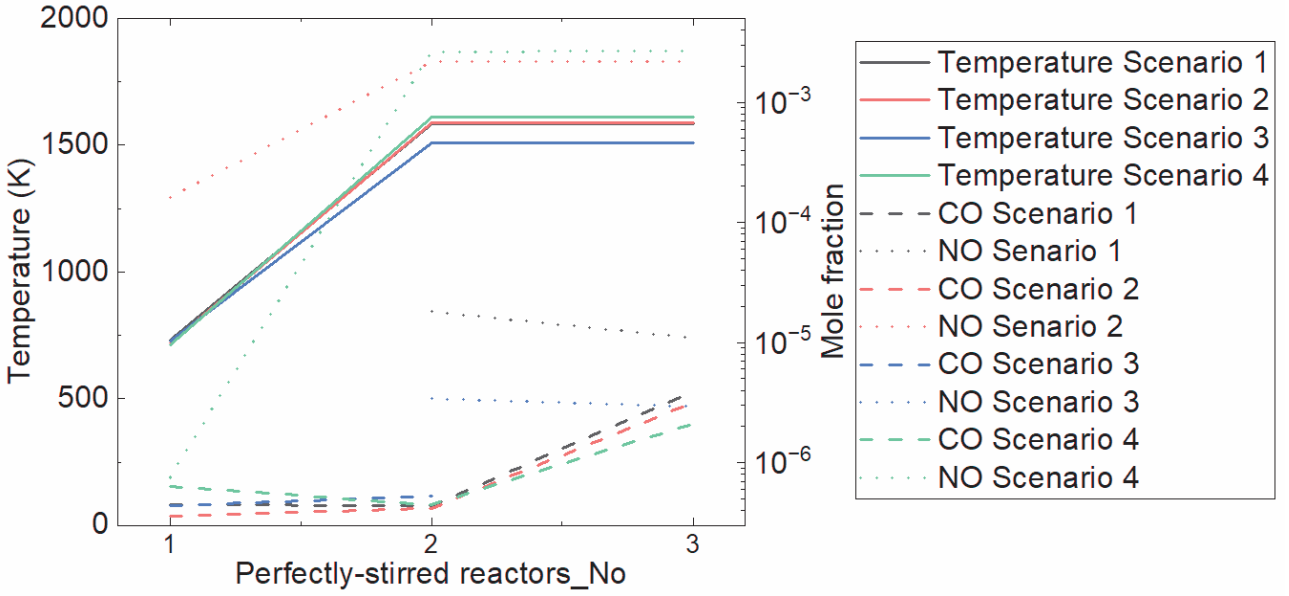

Figure 38. Temperature, NO and CO mole fraction fluctuation in all PSRs.

high diffusivity. Then improved combustion can result in more complete burning of the fuel blend, which in turn reduces CO and NO emissions. Regarding the current study's outcomes, unburned hydrocarbons in Scenarios 1, 2, 3, and 4 resulted in concentrations of 0.001093655 ppmvd, 0.000971534 ppmvd, 0.00000000167174 ppmvd, and 0.0005314867 ppmvd, respectively. Therefore, emissions in Scenario 3 were the lowest compared to the other cases. De Simio et al. also emphasized the role of H_2 co-firing in reducing the amount of unburned hydrocarbons [117]. Liu et al. emphasized gradual reduction of reaction activation energy by increasing the hydrogen share in methane combustion [118]. In Figure 38, the trend of temperature, NO, and CO emissions of all PSRs has been illustrated for each scenario. Since fuel blending was different in every scenario, NO emissions significantly varied, but values of CO emissions were in a close range.

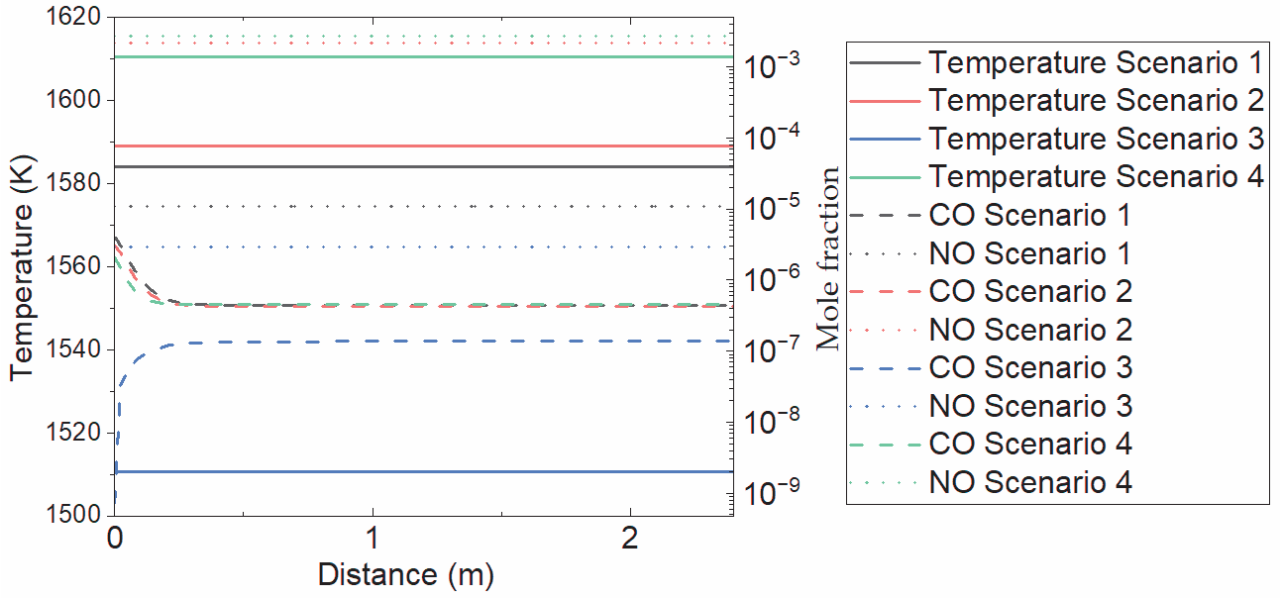

Figure 39. NO and CO mole fractions and temperature in Plug Flow Reactors of all scenarios.

From Figure 38, it is also possible to make the correct selection of scenarios for the decarbonization of existing power units. Moreover, NO and CO emissions in the post-combustion zone have been

depicted in Figure 39, showing steady values within temperature ranges. NO emissions of Scenarios 2 and 4 had the highest values and Scenario 3 resulted in the lowest emissions. The findings of Bastani et al. on co-firing NH_3 with methane in a gas turbine also mentioned less impact on CO emission variations [119]. In the current study findings, CO emissions were also observed with an insignificant range of differences.

On the other hand, temperatures in all scenarios remained stable within the range of the flame combustion zone distance (i.e. 2.4 m). In the Aspen HYSYS Scenario 3 model, the temperature in the combustor resulted in 1,323.00 ℃, but in the Ansys Chemkin Pro Scenario 3 model, the temperature in the combustor or PSR3 accounted for 1,510.00 K or 1,236.00 ℃. Since Ansys Chemkin Pro is specialized for designing and analyzing the combustion process, the values generated with the Chemkin Pro models will be taken into consideration for conclusion.

From the perspective of storing H_2 on-site, studies by Kolbantseva et al. concluded on the feasibility of blending 20 % vol. of H_2 in a NG fuel mixture for maintaining stable and safe operation in an existing power plant in Russia. It was also proposed to deliver 20 % vol. of H_2 and 80 % vol. of NG as a single mixture in a single existing pipeline due to the lack of available area for storing the required amount of H_2 [120].

In the case of the health safety of H_2 and NH_3 at an existing power plant, there are currently major issues related to the utilization of NH_3 fuel, such as respiratory diseases, etc. However, up-to-date studies by Jin et al. [121] on H_2 fuel have declared the absence of a threat to environmental and human health. That is why prioritizing the co-firing of H_2 fuel in a fuel mixture will be most advantageous due to its merits. The findings have been published in International Hydrogen of Hydrogen Energy (International Journal of Hydrogen Energy, Vol. 61, pp 432-443).

3.5 Conclusion

In this study, the effects of selecting different fuel blends on the operation of the existing Fergana Combined Heat and Power (CHP) plant, including emissions, Levelized Cost of Electricity (LCOE), output power, and net efficiency, have been investigated. The research involved developing a design model and simulating various fuel blends within four scenarios. Considering the discussion of the results, the following findings are summarized:

- Output power in all scenarios varied from each other. Scenario 4, with a fuel blend including ammonia (NH_3) and hydrogen (H_2), resulted in the highest output power. In co-firing a single alternative fuel, such as NH_3 in a fuel mix, exceeded the output power of the reference case, but H_2 co-firing resulted in the lowest output power among all cases.
- The specific fuel consumption in Scenarios 1, 2, 3, and 4 amounted to 0.31 kg/kWh, 0.38 kg/kWh, 0.39 kg/kWh, and 0.51 kg/kWh, respectively.
- CO_2 emissions varied in each scenario because of the fraction of fossil fuels. It was observed that Scenario 4, comprising NH_3 and H_2 blends in natural gas (NG), emitted the lowest CO_2, while Scenarios 2 and 3 were in the middle range of the reduction of CO_2 emissions.
- The lowest NOx emissions at 15% O_2 were noticed in the case of H_2 co-firing with NG. On the other hand, scenarios with NH_3 and H_2 co-firing emitted the highest NOx emissions. It was negatively affecting the further implementation of scenarios with NH_3 blending options. Findings were different than previous studies because technical parameters such as temperature and pressure of the working agent, and amount of unburned hydrocarbons in exhaust gas were also different.
- Since the electric efficiency of each model depends on the amount of inlet heat and output power of the system, the heat input into the system was highest in the case of the scenario with 100 % NG combustion, but electric efficiency was the lowest compared to other scenarios. The most attractive point was Scenario 4, where NH_3 and H_2 co-firing took place. In this case, input heat into the system was the lowest, but output power and electric efficiency were the highest among all scenarios.

From an economic point of view, reference Scenario 1 maintained a cost-effective level, while Scenario 4, with the highest output power and electric efficiency, resulted in the highest LCOE per kWh of generated electricity. On the other hand, scenarios with NH_3 and H_2 combustion were taking place in the middle range of LCOE compared to other scenarios. The main reason for the evolving LCOE pertaining to blending NH_3 and H_2 with NG was the high cost of production of each type of fuel.

Considering the technical, economic, and emission parameters of each scenario, scenario 4, NH_3 and H_2 co-firing case, was the most attractive one. However, the outcome of combustion kinetics analyses dramatically changed the final decision, and the scenario with H_2 co-firing demonstrated attractive performance and favorable combustion kinetics at this moment. It is advisable to consider advancements in the exhaust gas denitrification process or the optimization of ammonia combustion, either alone or in blends with other fuels, in the future. Until solutions related to controlling excess NOx emissions in gas turbine technology are resolved, more detailed studies on 100 % H_2 combustion can also be conducted to diversify alternative fuel options for existing gas turbine technologies worldwide.

Chapter 4. Comparative Technical and Economic Analyses of Hydrogen-based Steel and Power Sectors

4.1 Introduction

Making iron and steel produces 7% of the world's CO_2 emissions and 16% of all emissions from industries [23]. The usual way of making steel, known as the Blast Furnace-Basic Oxygen Furnace (BF-BOF) route, is responsible for 70.8% of steel made from ore globally [34]. In this process, a lot of carbon-intensive coke is used to turn iron ore into steel. This makes it one of the industries that emit a lot of carbon, producing over 1.8 tons of CO_2 for every ton of liquid steel made [23,35]. Technology developers are trying to find better ways to make iron and steel, like directly reducing iron ore. Different methods, like using carbon monoxide with natural gas or other carbon-based materials, are being explored for this type of production [36]. A strategy for reducing carbon emissions in the steel sector involves substituting hydrogen fuel for carbon monoxide in the process of reducing iron ore to produce sponge iron, which is then utilized in the manufacturing of liquid steel.

Within the context of the present study focusing on the hydrogen-based reduction of iron ore, it becomes crucial to assess and comprehend the potential for hydrogen production in this process, recognizing that it varies across different countries. The stoichiometric consumption of hydrogen in the reduction process amounts to 54 kg per ton of liquid steel production. Presently, the predominant method for large-scale hydrogen production is Steam Methane Reforming (SMR), a process that relies on fossil fuels. However, this approach is met with reluctance in many countries worldwide. As an alternative, numerous new initiatives emphasize the use of electrolyzers for generating green hydrogen [43]. Furthermore, certain authors conducted tests on the reduction rate of iron ore utilizing the moving-bed principle, observing the reducibility of iron within a temperature range of 500–1000 °C [122]. Initial assessments of the HYBRIT project affirmed the viability of the HDRI-EAF route, exemplified in the conditions of Sweden and Finland [123]. In the realm of EAF decarbonization, Echterhof's review [124] proposed the integration of biomass or alternative sources, replacing fossil fuel-based carbon in the steel-making process. Regarding the cost analysis of steel produced through the HDRI-EAF route with hydrogen as a reducing agent, reported figures indicated a Capital Expenditure (CAPEX) ranging from 118.7 USD/t steel at high cost to 111.9 USD/t steel at low cost [125]. As for the Levelized Cost of Production (LCOP) of the HDRI-EAF route, Vogl et al. [61] stated a range of 361–640 EUR per ton of steel production, while Bhaskar et al.'s study [126] found the LCOP at 669 USD/tls. Another study by Bhaskar et al. [127] reported a range between 622 USD/tls and 722 USD/tls, considering different electricity purchase schemes for HDRI-EAF route consumption.

Conversely, the power sector recorded the highest CO2 emissions in 2022, totaling 14.6 gigatons, surpassing emissions from other economic sectors [128]. A strategy for curbing CO2 emissions in the power sector involves substituting fossil fuels with alternatives such as hydrogen, biofuels, ammonia, and other sustainable fuels [33,71,129,130]. The investigation of hydrogen combustion in gas turbines dates back several decades. In 1937, Dr. Hans von Ohain conducted research on hydrogen fuel combustion in a gas turbine, encountering a significant challenge related to the burnout of metal components in the hot sections of the gas turbine unit [28].

This study delves into the optimization of processes with hydrogen assistance and

compares production costs between two sectors—the steel and power sectors—utilizing energy and mass balance calculations.

Firstly, a process flow diagram is devised, and the mass and energy balance of the process are calculated for each unit.

Secondly, operational parameters for HDRI-EAF and 100% hydrogen-fired gas turbine systems are optimized for application in economic analyses.

Thirdly, technical and economic assessments of a hydrogen-fired gas turbine are executed using the Aspen HYSYS tool. Additionally, a combustion kinetics model for a 100% hydrogen-fired gas turbine is developed using the Ansys Chemkin Pro tool.

Finally, comparative analyses are carried out, taking into consideration the levelized cost of production for each product (i.e., steel and electricity).

4.2 Materials and Methods

4.2.1 The structure of the Tebinbulak DRI-EAF for the development of the HDRI-EAF route.

A new mining and metallurgical complex, based on the Tebinbulak mine, is currently under development following the Presidential Decrees # PP-3473 dated January 12, 2018, and # PP-459

Figure 40. 3-D layout of Tebinbulak metallurgical plan, Uzbekistan (under development).

dated December 28, 2022 [131] of the Republic of Uzbekistan [132]. Figure 40 depicts the 3-D layout of the new metallurgical plant, which is based on the Direct Reduction Iron Ore (DRI) – Electric Arc Furnace (EAF) technology and is scheduled to commence operations in 2027. It is the first and currently the only DRI-EAF route-based metallurgical plant in Uzbekistan. Therefore, the Hydrogen Direct Reduction Iron Ore – Electric Arc Furnace route can be designed, considering the technical specifications of the targeted prospective metallurgical plant. More details of the process flow diagram of the metallurgical plant are presented in Figure 41. The Tebinbulak

metallurgical plant comprises several units, including iron ore mining, a beneficiation plant, a pelletizing plant, a direct reduction plant, a submerged electric arc furnace plant, a basic oxygen

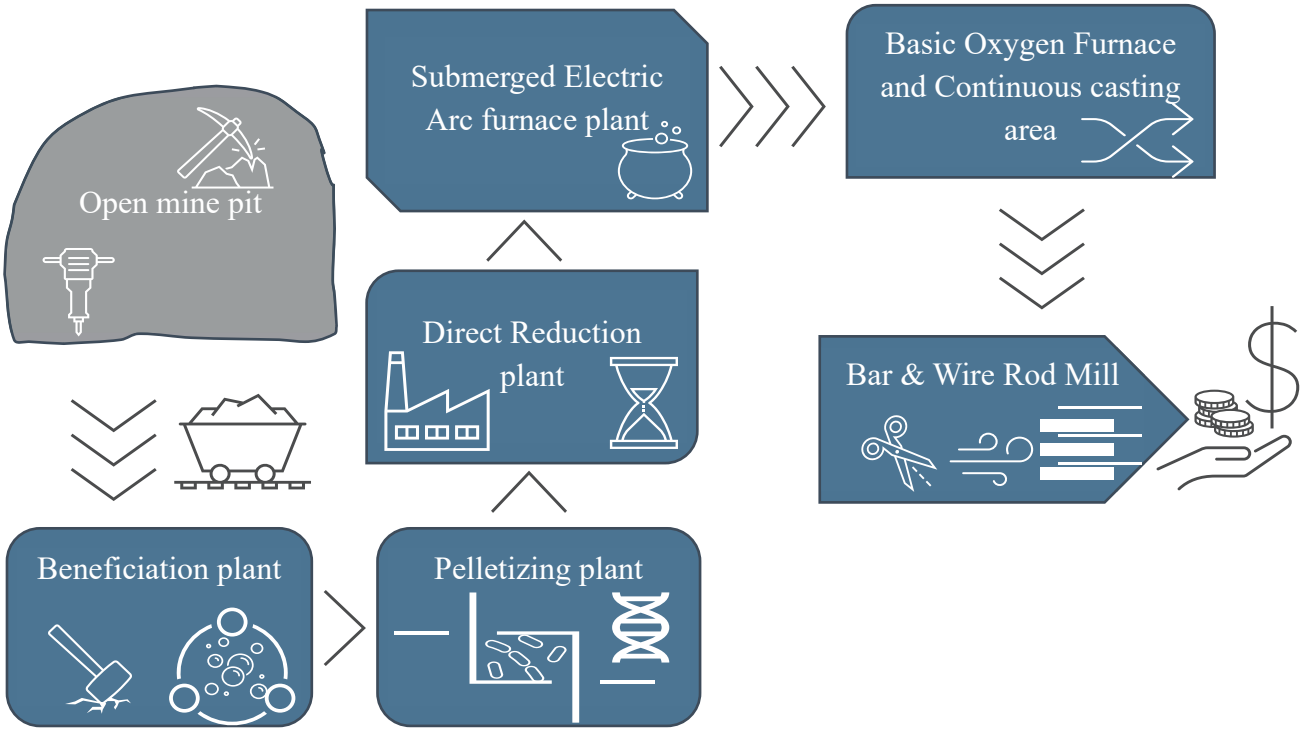

Figure 41. Process flow diagram of Tebinbulak mining and metallurgical complex in Uzbekistan.

furnace plant, and a continuous casting area for shaping target products (e.g., rebar, wire, corners, channels, etc.). The annual plan involves extracting 58 million tons of iron ore, producing 3.6 million tons of direct-reduced iron (sponge iron) from that amount. Half of the 3.6 million tons of direct-reduced iron will be used for producing 1.5 million tons of finished products, while the remaining 1.8 million tons of direct-reduced iron will be sent to another metallurgical plant in Bekabad city, Uzbekistan, as feed material for steel production [133]. Additional technical specifications for the plant can be found in Table 20.

Table 20. Technical specification of Tebinbulak metallurgical plant.

#	**Specifications**	**Value**
1	Type of metallurgical plant	DRI-SAF-BOF
2	Steel production	3,000,000.00 t/year
		375.00 t/h
3	Required DRI for steel production	3,600,000.00 t/year
		450.00 t/h
4	Iron ore mass flow (after beneficiation process)	5,145,945.94 t/year
		643.24 t/h
5	Operation hours	8,000.00 hours/year
6	Total Fe in Fe_2O_3 after beneficiation, concentrate	67.4 %
7	Implementation period	2022-2027

In the current research, the mass flow of input materials is calculated based on the annual production volume of finished products (steel) due to the limited availability of input parameters for the Tebinbulak metallurgical plant.

To find economic effect of steel sector-based on hydrogen fuel, it is necessary to evaluate the Levelized Cost of Production (LCOP) of steel, which is determined by the following Equation [127,134]:

Equation 31. Levelized cost of production of steel.

$$\mathrm{LCOP} = \frac{\mathrm{C_{capex}} * \mathrm{ACC} + \mathrm{C_{opex}} + \mathrm{C_{maint}} + \mathrm{C_{labor}} + \mathrm{C_{emission}}}{\text{Annual steel production}} \quad (31)$$

Where, C_{capex} represents the total investment cost, encompassing the cost of all main and auxiliary units in the route, ACC is an annuity factor. On the other hand, C_{opex}, C_{maint}, C_{labor} and $C_{emission}$ are costs associated with the operation, maintenance, labor, and emissions within the route respectively. The annuity factor of the route is determined by the following equation [127,134]:

Equation 32. Annuity factor of HDRI-EAF route.

$$\mathrm{ACC} = \frac{\mathrm{r} * (1+\mathrm{r})^{\mathrm{n}}}{(1+\mathrm{r})^{\mathrm{n}} - 1} \quad (32)$$

Where, r is the discount rate, and n is plant life. In this study, the life span of the HDRI-EAF route-based plant is considered to be 20 years, with a discount rate is 10 %.

Additionally, the Net Present Value (NPV) of the plant is crucial for the accurate calculation of LCOP over the selected life span period, and it is determined by the following equation [127]:

Equation 33. Net present value (NPV) of HDRI-EAF route.

$$\mathrm{NPV} = \sum_{\mathrm{n=1}}^{\mathrm{n}} \frac{\mathrm{CF}}{(1+\mathrm{r})^{\mathrm{n}}} \quad (33)$$

Where, CF, r and n represent cumulative cash flow, discount rate and the life span of the plant respectively.

4.2.2 100 % hydrogen-fired gas turbine modeling and specification

The gas turbine unit of the existing Combined Heat and Power (CHP) plant [116] with a 7.6 kW capacity has been selected for developing a 100 % hydrogen-fired gas turbine model. Based on the technical specification of the existing plant, a new model has been designed to evaluate the performance of the cycle. Aspen HYSYS software, utilizing the Peng-Robinson fluid package, was employed to evaluate the technical parameters of the designed model, including the enthalpy and entropy of fluid and fluid mixtures in the cycle. Figure 42 depicts the process flow diagram of the 100 % hydrogen-fired gas turbine unit. Technical specifications of the cycle, based on 100 % hydrogen combustion, are provided in Table 21. Considering the given technical specification, the

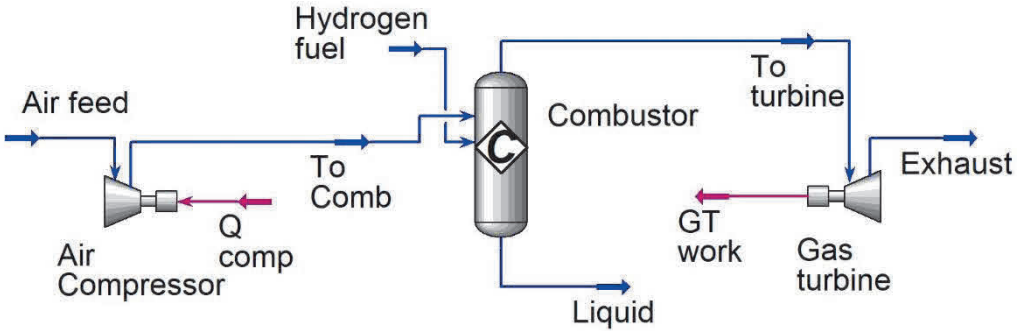

Figure 42. Process flow diagram of 100% hydrogen fired combined heat and power plant.

specific fuel consumption in the designed model accounted for 1.24 kg/kWh compared to 0.31 kg/kWh in the reference case (i.e., 100 % natural gas-fired CHP plant).

In the model, the following reaction equation for the combustion of hydrogen was used (Equation 30 is identical to Equation 30) [104]:

$$2H_2(g) + O_2\ (g) \rightarrow 2H_2O\ (l) \quad (30)$$

Table 21. Technical specifications of the air compressor and gas turbine for the 100 % hydrogen-fired CHP plant.

Parameters	Air compressor	Gas turbine
Feed temperature (°C)	30	1312
Feed pressure (bar)	1.0	15.60
Product temperature (°C)	431.6	802.2
Product pressure (bar)	15.60	2.026
Adiabatic efficiency (%)	85.4	85.4
Mass flow of working medium (kg/h)	85,000.00	85,929.58
Pressure ratio	15.6	-
Polytropic efficiency (%)	89.5	81.97
Power (kWe)	10,025.37	17,149.23

In the analysis of the combustion process analyses in the design model, another model has been developed using Ansys Chemkin Pro software for evaluating NOx emissions when the cycle is fully operated on hydrogen fuel. Since there is no CO_2 emission from the 100 % hydrogen-fired CHP plant, the anticipation of NO_x emission becomes a critical consideration, aligning with

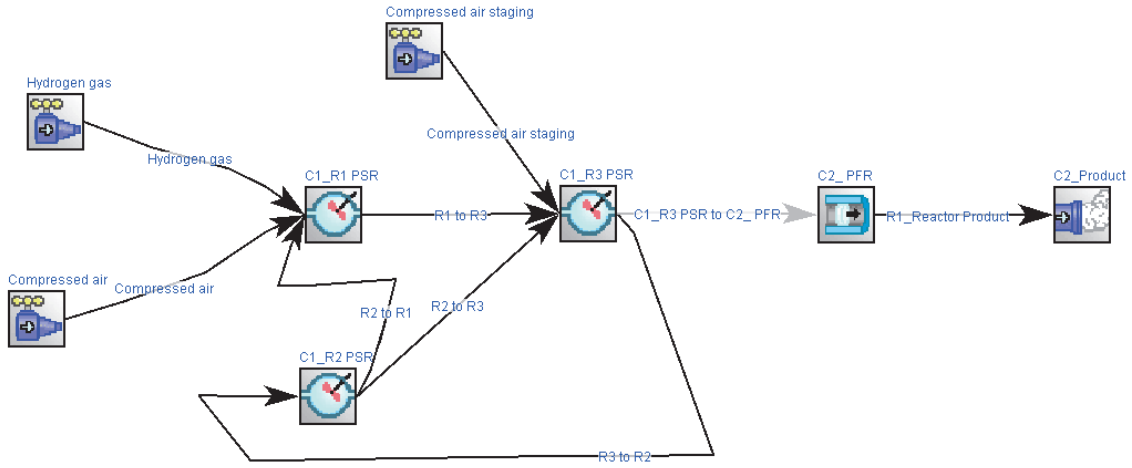

Figure 43. Process flow diagram of a gas turbine with multi-fuel combustion approaches.

regulatory requirement for the power sector. Figure 43 illustrates the process flow diagram of the gas turbine network developed using Ansys Chemkin Pro software. To mitigate NO_x emissions, the model employs the staging of inlet air method. Additionally, an exhaust gas recycling method has been applied to reduce the amount of unburned gases in the exhaust gas. Figure 44 illustrates the method for investigating combustion kinetics in the gas turbine network. The network comprises three zones: the mixing zone, flame, and post flame zones. In the mixing zone, air and hydrogen are premixed and then sent to the flame zone. In the flame zone, a portion of the air is allocated to reduce thermal NO_x formation, and some exhaust gases are recycled to ensure the complete combustion of the working fuel in the network. The developed model has been simulated by applying the GRImech 3.0 mechanism, which includes 5 elements (C, H, O, N and Ar), 53

chemical species, and 325 reactions for analyzing the chemical kinetics of the network [89]. Figure 8 includes several units, namely Perfectly Stirred Reactors (PSR), divided into three parts. PSR R1 represents the Mixing, PSR R2 represents the Recirculation zone, and PSR R3 represents the

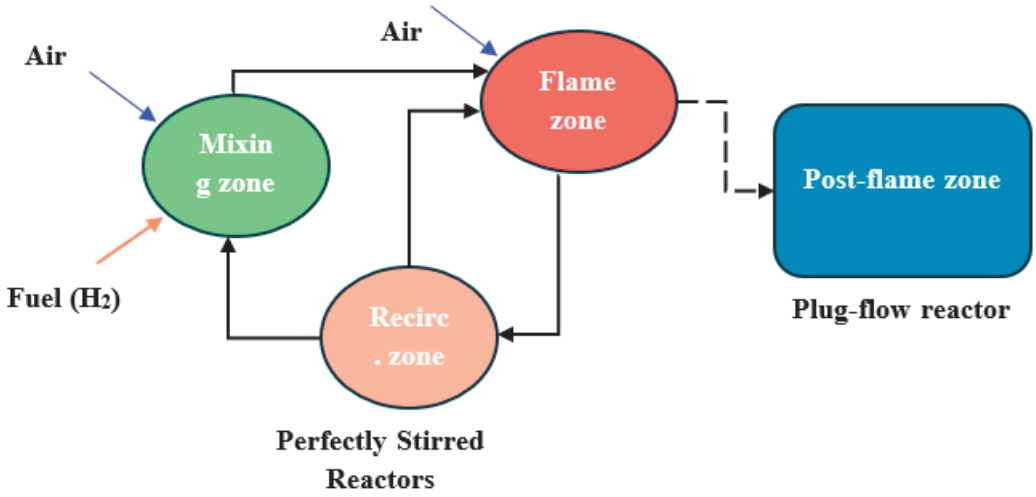

Figure 44. Process flow diagram of gas turbine network describing three target zones: mixing, flame, and post flame zones.

Flame zone of the gas network based on the illustration given in Figure 44.

The thermal efficiency of the gas turbine network is determined using the following equation:

Equation 34. Thermal efficiency of gas turbine.

$$\eta = \frac{\text{Work done}}{\text{Heat input}} \text{ or } \eta = 1 - \left(\frac{P1}{P2}\right)^{\frac{\gamma-1}{\gamma}} \tag{34}$$

Where $\frac{P2}{P1}$ is the pressure ratio of the cycle, which ranges between 11 and 16, γ is the adiabatic constant [31]. Total power output from the cycle can be calculated from the following equation:

Equation 35. Total power output of CHP.

$$W = W_{turbine} - W_{compressor} \tag{35}$$

Where $W_{turbine}$ is the power generated by the gas turbine's generator, and $W_{compressor}$ is the power consumed by the air compression unit.

In turn, the power consumed by the air compressor, $W_{compressor}$, is found from the following equation:

Equation 36. Power consumption of the air compressor.

$$W = \text{Heat flow}_{outlet} - \text{Heat flow}_{inlet} \tag{36}$$

In the case of the power generated by the gas turbine generator, $W_{turbine}$, it is found from the following equation:

Equation 37. Power output of gas turbine unit generator.

$$W = \text{Heat flow}_{inlet} - \text{Heat flow}_{outlet} \tag{37}$$

The isentropic (ideal) efficiency of the compressor (η_c) is determined from the following equation:

Equation 38. Isentropic efficiency of the compressor.

$$\eta_c = \frac{\text{Power required}_{ideal}}{\text{Power required}_{actual}} \times 100\% = \frac{(\varepsilon_{pc})^{\frac{\gamma-1}{\gamma}} - 1}{(\varepsilon_{pc})^{\frac{\gamma-1}{\gamma} \times \frac{1}{\eta_{c/p}}} - 1} \times 100\% \quad (38)$$

Where ε_{pc} is the pressure ratio of a compressor, and γ and $\eta_{c/p}$ are the ratio of specific heats and is the polytropic efficiency of the compressor, respectively. Since "adiabatic" and "isentropic" efficiencies are used interchangeably, isentropic power is considered as an ideal power.

As for the polytropic efficiency of the compressor ($\eta_{c/p}$), it is determined by the following equation:

Equation 39. Polytropic efficiency of the compressor.

$$\eta_{c/p} = \frac{\text{Work input}_{ideal}}{\text{Work input}_{actual}} \times 100\% = \frac{n}{n-1} \times \frac{\gamma-1}{\gamma} \times 100\% \quad (39)$$

In the case of the isentropic efficiency of gas turbine (η_t), it is determined by the following equation:

Equation 40. Isentropic efficiency of gas turbine.

$$\eta_t = \frac{\text{Work produced}_{actual}}{\text{Work output}_{ideal}} \times 100\% \quad (40)$$

On the other hand, the polytropic efficiency of the gas turbine ($\eta_{t/p}$) is determined by the following equation:

Equation 41. Polytropic efficiency of the gas turbine.

$$\eta_{t/p} = \frac{n-1}{n} \times \frac{\gamma}{\gamma-1} \times 100\% \quad (41)$$

Where, n and γ are the polytropic index and the ratio of specific heats, respectively.

An expression relating the isentropic and polytropic efficiencies of the gas turbine, with emphasis on the pressure ratio, is calculated from the following equation:

Equation 42. The Isentropic efficiency of the gas turbine as a function of the polytropic efficiency of the gas turbine and compression ratio.

$$\eta_t = \frac{1 - (\frac{1}{\varepsilon_{pt}})^{\frac{\gamma-1}{\gamma} \times \eta_{t/p}}}{1 - (\frac{1}{\varepsilon_{pt}})^{\frac{\gamma-1}{\gamma}}} \times 100\% \quad (42)$$

Where ε_{pt} and γ are the ratios of pressure and specific heats of a gas turbine, and $\eta_{t/p}$ is the gas turbine's polytropic efficiency [91,92].

Since the evaluation of CO_2 emissions from the cycle is one of parameter of decarbonization studies, the CO_2 emission of the model has been determined from the following equation (Equation 22 is identical to Equation 22):

$$CO_2 \text{emission rate} = Q \times EF \quad (22)$$

Where, Q (energy/time) represents the input energy in the system, and EF (kg CO_2/energy) is the emission factor of the fuel used in the system [93].

Regarding the economic features of the model, the Levelized Cost of Electricity (LCOE) is a criterion, and the following equation provides detailed information [94] (Equation 23 is identical to Equation 23):

$$\mathrm{LCOE} = \frac{\sum_{t=1}^{n} \frac{I_t + M_t + F_t}{(1+r)^t}}{\sum_{t=1}^{n} \frac{E_t}{(1+r)^t}} \quad (23)$$

Where I_t is the capital expenditure, including the cost of investment and construction works over t years, M_t is the operational expenditure, including the cost of operation and maintenance over t years, F_t is the operational expenditure, including expenses on using fuel over t years, E_t is the total power output over t years, r and n are the rate of discount and the lifespan of the technology, respectively.

4.3 Results and discussion

In this section, the results and discussions derived from two distinct approaches are presented: the use of hydrogen fuel as a reducing agent in the steel industry and as a working agent for combustion in the power sector. Initially, the details on mass and energy balance, along with optimized reduction process results are provided. The energy consumption and the speed of reduction with findings from previous studies, emphasizing the innovative nature of our approach are compared. Subsequently, the Levelized Cost of Production (LCOP) for 1 ton of liquid steel, enabling a comparison with the cost of generating 1 kWh of electricity from a gas turbine unit running exclusively on hydrogen fuel is calculated. This comparison aims to offer insights into the prospects of each sector. Additionally, this section covers the development of a 100% hydrogen-fired gas turbine unit with optimized operational conditions. The assumption is made that the gas turbine operates stably under the 100% hydrogen combustion mode, drawing support from a previous study that successfully demonstrated such operation [135,136].

4.3.1 Optimized operational condition of HDRI-EAF

Due to limited available input parameters of new metallurgical plant in Uzbekistan, it was not possible to conduct wide range of sensitive analysis. Nevertheless, the proposed operational parameters of the plant were calculated using output product amount. Table 22 shows the optimal operational parameters of HDRI-EAF based on Tebinbulak metallurgical plant.

Table 22. Operation related specification of HDRI-EAF.

Name of specification	Unit	Value
Required Iron ore	t/h	643.24
Required sponge iron for steel production	t/h	450.00
Target steel production	t/h	375.00
Require hydrogen amount for steel production	t/h	24.32
Required hydrogen amount for steel production during sunshine hours (7h)	t/h	83.39
Electricity required by electrolyzer efficiency (2020) per hour	kWh	4,420,077.22
Electricity required by electrolyzer efficiency (2030) per hour	kWh	3,752,895.75
Required hydrogen storage	kgH2/h	59,073.36
Required electricity for compressions of hydrogen per hour	kWh	55,264.32
Required hydrogen production and storage hours	h	7
Number of hours of hydrogen production is not taking place	h	17
Required operation hours of HDRI-EAF per year	h	8000
Required amount of ultrapure water per kg of hydrogen production (practical)	kg	9 (13)
Required amount of ultrapure water	t/h	316.21

In the optimization process, green hydrogen production occurs during the 7 hours of available sunshine in Uzbekistan. In this case, the electricity needed for green hydrogen production is planned to be sourced from a solar PV plant.

4.3.2 Levelized cost of production of HDRI-EAF

In addition to the optimization of the HDRI-EAF process, the evaluation of the cost of steel is also an important factor towards successful commercialization and implementation of this route in developed and emerging countries.

Table 23. HDRI-EAF capital expenditure specification.

Capital cost (assumptions)			
Equipment name	Unit	Cost	Reference
Electrolyzer	USD/kW	450	Melnikov, 2023 [106]
Electrolyzer stack replacement cost	USD/kW	200	IRENA, 2021 [137,138], Krishnan et al., 2023 [139]
Shaft furnace	USD/tsteel/year	260	Kruger et al., 2020 [140]
Electric air furnace	USD/tsteel/year	200	Kruger et al., 2020 [140]
Hydrogen storage tank	USD kg/H_2	400	Feng, 2022 [141]
Hydorgen compressor	USD kg/H_2	2545	Christensen, 2020 [142]

Table 23 shows a summary of investment costs illustrating the capital expenditure of the HDRI-EAF route. The case of Uzbekistan was applied in this study by using available costs of each unit and materials. In the economic evaluations, additional units have been added to the calculations, such as hydrogen storage and compression units. Table 24 shows details of operational expenditure of HDRI-EAF.

Table 24. HDRI-EAF operational expenditure specification.

Operational cost (assumptions)			
Item name	Unit	Cost	Reference
Iron ore	USD/t	138	Kolisnichenko, 2023 [143]
Electrolyzer efficiency (2020)	kWh/kgH_2	53	Bhaskar et al., 2022 [127]
Electrolyzer efficiency (2030)	kWh/kg H_2	45	Bhaskar et al., 2022 [127] Monitor Deloitte, 2021 [144]
Hydrogen fuel	USD/kg	2.5-3	Melnikov, 2023 [106]
Ultrapure water for H_2 production	USD/kg	0.08	Flagma.uz, 2024 [145]
Required H_2 storage capacity	kgH2/7h	413,513.51	Based on calculation
DRI OPEX	USD/tls	12	Cavaliere, 2019 [146]
Electric air furnace OPEX	USD/tls	33	Cavaliere, 2019 [146]
Hydrogen storage OPEX	% of H_2 storage CAPEX	2	Elsheikh, 2023 [147]
Emission price	USD/tCO_2	11	Anderson et al., 2022 [148]
Grid emission factor (Uzbekistan)	gCO_2/kWh	400	IRENA, 2023 [149]

Based on the latest reports, the cost of stack replacement is about 45 % of the total capital expenditure of the alkaline electrolyzer unit [137]. In economic evaluation studies, the technical specifications of the Tebinbulak DRI-EAF project (under development) have been selected for the case study in the current investigations [133]. Due to limited data from the selected case study, additional technical specifications of DRI-EAF have been used for the current study [150]. Current

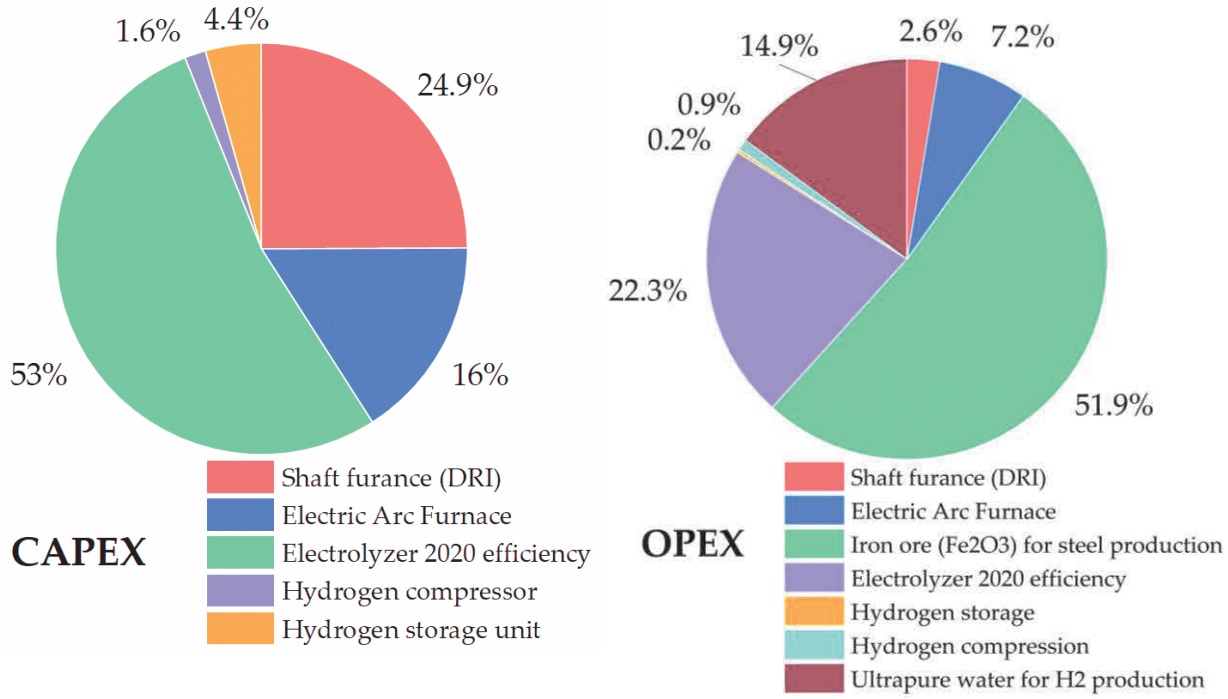

Figure 45. Capital and operational expenditure of HDRI-EAF with electrolyzer unit of 2020 efficiency.

available alkaline electrolyzer [137,138,151] with 2020 efficiency have a stack with a lifetime period of 60,000.00-80,000.00 hours, and the electrolyzer units in the current study are operated during sunshine hours with an overall 51,100.00 hours in the 20 years of HDRI-EAF's lifespan period. Operational expenditures on stack replacement for electrolyzer were not included in the calculations of LCOP. There are some assumptions applied in LCOP calculations. For example, the Uzbek commodity exchange does not have several products on sale, namely iron ore, electrolyzer, hydrogen fuel, ultrapure water, hydrogen compression and storage units, shaft furnace, EAF, etc. Calculations on the economic indicators of the route, in the case of the Tebinbulak project (under development) [133] in Uzbekistan with an annual 3 million tons of liquid steel production, resulted in 633.68 USD/tls of LCOP. The original project does not include hydrogen fuel as a reducing agent, but in this study, green hydrogen was introduced instead of the designated fossil fuel. Figure 45 shows the capital and operational expenditure of the HDRI-EAF route based on applying electrolyzer units with 2020 efficiency (53 kWh/kgH_2). Due to limited data from the ongoing project in Tebinbulak, it was not possible to acquire the project-based capital and operational expenditures on the shaft furnace, electric arc furnace, and local iron ore price. As a result, the HDRI-EAF route with an electrolyzer of 2020 efficiency requires an overall investment of 3,752,345,559.85 USD or 1,250.78 USD/tls and 1,369,478,570.51 USD/year of operational costs.

In the case of economic analysis of the HDRI-EAF route with an electrolyzer of 2030 efficiency (45 kWh/kgH_2), it accounted for 606.30 USD/tls of LCOP (Figure 46). In this route with

an electrolyzer of 2030 efficiency, the total investment requires 3,452,113,899.61 USD or 1,150.70 USD/tls, and operational expenditure of 1,323,453,056.99 USD/year. In the calculations, solar PV electricity with a 0.027 USD/kWh rate was used for producing hydrogen with electrolyzer.

Taking into account the LCOP in two cases, it ranged between 606.30 USD/tls and 633.68 USD/tls for the case of Uzbekistan, while conventional steel production at Uzmetkombinat in Bekabad city, Uzbekistan, provided a LCOP of finished product at 406 USD/tls [152].

4.3.3 Optimized operation of 100 % hydrogen-fired gas turbine model

In this section, the results of optimization strategies for the 100 % hydrogen-fired gas

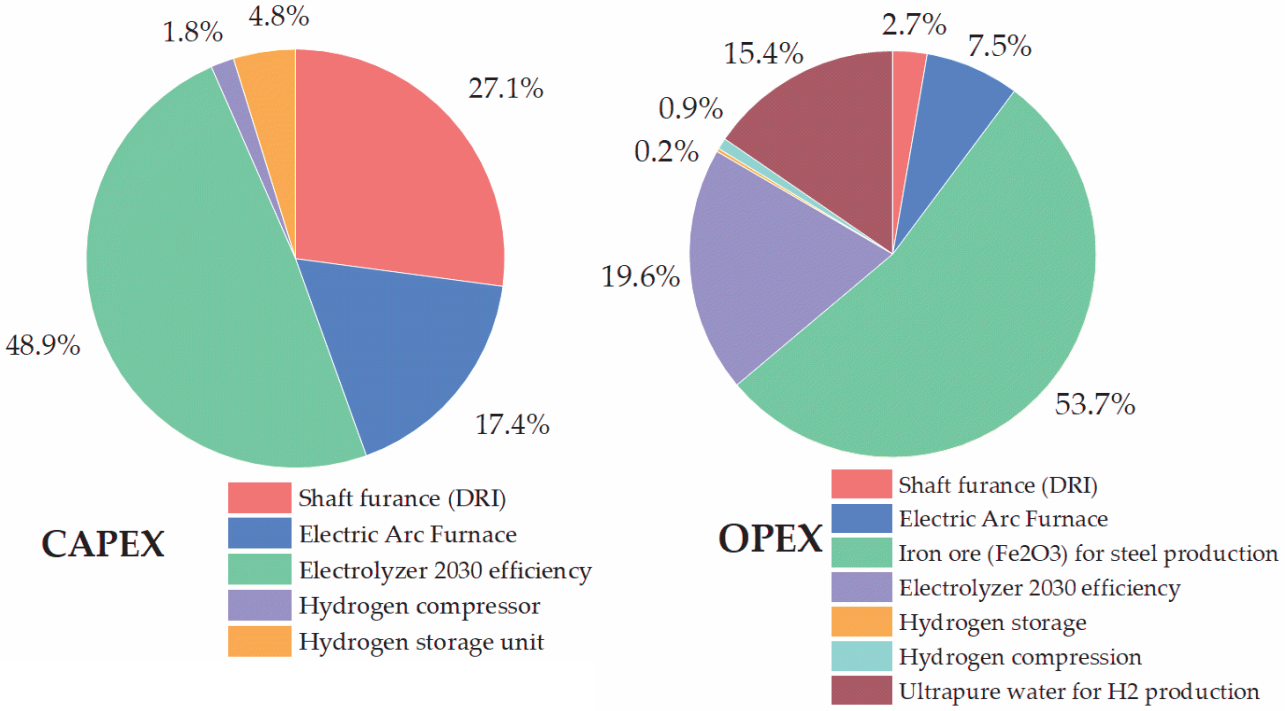

Figure 46. Capital and operational expenditure of HDRI-EAF with electrolyzer unit of 2030 efficiency.

turbine cycle were described based on the simulation model developed using Aspen HYSYS and Ansys Chemkin Pro software tools. Table 25 shows the main results of the mass stream of the model.

Table 25. Material stream of 100 % hydrogen-fired gas turbine model developed on Aspen HYSYS.

Name	Air feed	To Turbine	Hydrogen fuel	To combustion	Exhaust
Vapor fraction	1	1	1	1	1
Temperature [°C]	30	1,400.0	30	431.6	862.7
Pressure [bar]	1.00	15.6	20.3	15.6	2.026
Molar flow [kgmole/h]	2,955.0	3,186.0	461.3	2,955.0	3,186.0
Mass flow [kg/h]	85,000.0	85,929.5	930.0	85,000.0	85,929.5
Liquid volume flow [m3/h]	98.9	100.8	13.3	98.96	100.8
Heat flow [kcal/h]	97,479.9	8,739,123.2	15,596.7	8,723,526.6	-6,016,452.3

Table 26 includes energy flows of the model. In the model, the total flow of the inlet stream accounted for 8,739,123.33 kcal/h or 10,156.80 kW. The system's energy balance was also closed.

Table 26. Energy balance of 100 % hydrogen-fired gas turbine model developed on Aspen HYSYS.

Inlet Streams	Energy Flow [kcal/h]	Outlet Streams	Energy Flow [kcal/h]
Air Feed	97,479.95	Exhaust	-6,016,452.39
Q Compressor	8,626,046.65	Gas turbine work	14,755,575.72
Hydrogen fuel	15,596.73		

In terms of finding the optimized condition for the operation of the 100 % hydrogen-fired gas turbine unit, Figure 47 shows different electric efficiencies at different power outputs of the

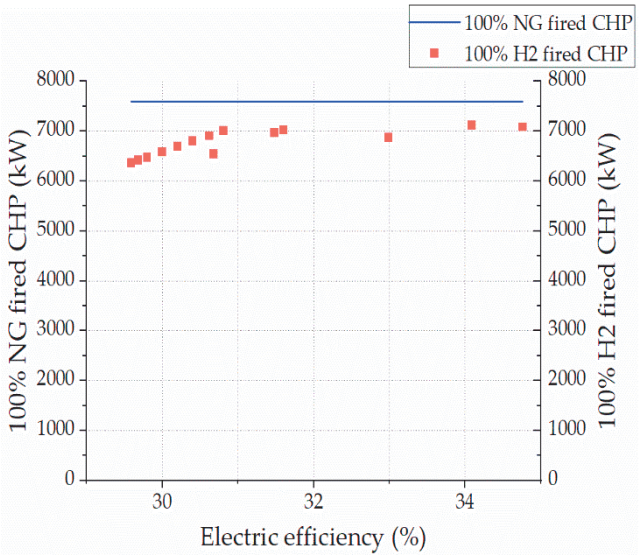

Figure 48. Comparison of natural and hydrogen gas-fired cycles power output over fluctuating electric efficiency of target model.

100 % hydrogen-fired gas turbine in comparison with the benchmark power output based on the 100 % natural gas-fired gas turbine cycle. The main optimization criteria in the target model were

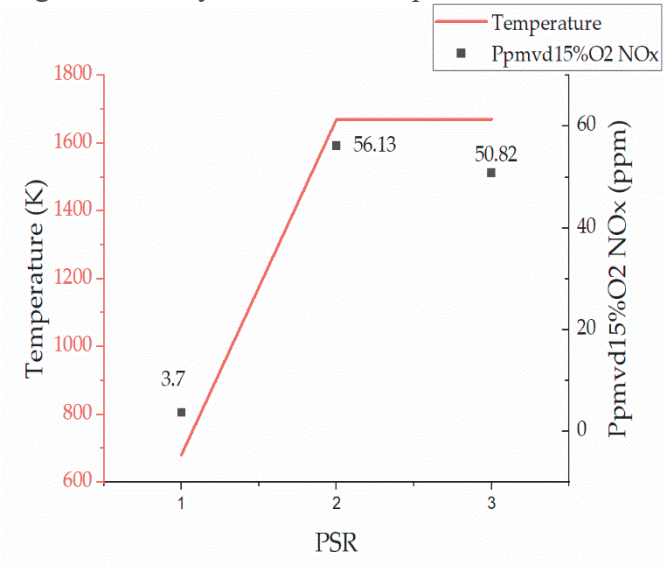

Figure 47. NOx emissions vs Temperature in three zones (PSRs 1,2 and 3).

staying within the range of the inlet temperature of the gas turbine unit. Analyzing all fingins, the condition with a 1,400 ℃ inlet temperature resulted in a 34.10 % electric efficiency (93.73 % achievability of the reference model power output of 7,600.00 kW), 7,123.86 kW power output, 930.00 kg/h mass flow of hydrogen, and 85,000.00 kg/h mass flow of air. As mentioned earlier, there is no CO_2 emission in the exhaust gases of the model. On the other hand, the cycle presents challenges with NOx emissions. Figure 48 shows the fluctuation of NO_x emissions at three points, namely Perfectly-Stirred Reactor (PSR) 1, 2 and 3. The ultimate value of NOx at 15% O_2 is rated at 50.82 ppm, which is higher than the required benchmark (9.9 ppm at 15% O_2) set by the gas turbine manufacturer [116]. However, the 50.82 ppm of NOx emissions at 15 % O_2 is still lower than the latest findings of Banihabib et al. [136], which reported 62 ppm of NOx emissions at 15 % O_2. Therefore, the result of the lowest NOx emissions at 15 % O_2 is still significant and novel.

Table 27. Capital expenditure of 100 % hydrogen-fired gas turbine with a 7.6MW output capacity.

Capital cost (assumptions)			
Equipment name	Unit	Cost	Reference
Electrolyzer	USD/kW	450	Melnikov, 2023 [106]
Electrolyzer stack replacement cost	USD/kW	200	IRENA, 2021 [137,138], Krishnan et al., 2023 [139]
CHP CAPEX (electrolyzer units 2020)	USD/kW/year	14,223.77	Calculation results
CHP CAPEX (electrolyzer units 2030)	USD/kW/year	12,612.45	Calculation results
Hydrogen storage tank	USD kg/H_2	400	Feng, 2022 [141]
Hydrogen Compressor	USD kg/H_2	2545	Christensen, 2020 [142]

Regarding the economic indicators of the model, calculations included capital and operating expenditures. Table 27 provides details of capital expenditures for the successful operation of the 100 % hydrogen-fired gas turbine unit.

As Uzbekistan has an average of 7 hours of sunshine daily [153], it is necessary to consider the required hydrogen storage capacity (15,810.00 kg of H_2 per 7 hours or 2,258.57 kg of H_2 per hour) for storing the necessary amount of hydrogen to use during the unavailable sunshine operation hours of the CHP plant. Taking into consideration the necessary amount of hydrogen production, it is required to have an electrolyzer unit with a 168.99 MW capacity in the case of one with an efficiency of 2020 or a 143.48 MW capacity with an efficiency of 2030. From the stoichiometry of the reaction mentioned in equation 26, 9 kg of ultra-pure water is required to produce 1 kg of hydrogen. In practice, 10-13 kg of water is required to produce 1 kg of hydrogen, taking into consideration the losses in the electrolyzer unit [154]. Therefore, for the above-mentioned 100 % hydrogen-fired gas turbine unit, it is necessary to prepare 12,090.00 kg of ultra-pure water per hour.

On the other hand, Table 28 provides details of operational expenditure for running the 100 % hydrogen-fired gas turbine with a 7.6 MW installed capacity.

Table 28. Operational expenditure of 100 % hydrogen-fired gas turbine with a 7.6 MW capacity.

Operational cost (assumptions)			
Item name	Unit	Cost	Reference
Hydrogen fuel	USD/kg	2.5-3	Melnikov, 2023 [106]
Electrolyzer efficiency (2020)	kWh/kgH_2	53	Bhaskar et al., 2022 [127]
Electrolyzer efficiency (2030)	kWh/kgH_2	45	Bhaskar et al., 2022 [127]
			Monitor Deloitte, 2021 [144]
Required H_2 storage capacity	kgH2/h	2259	Based on calculation
Ultrapure water for H_2 production	USD/kg	0.08	Flagma.uz, 2024 [145]
Hydrogen compression unit 20.3 bar	kWh/kgH2	2.27	Calculation results
CHP OPEX (electrolyzer units 2020)	USD/kW/year	2432.27	Calculation results
CHP OPEX (electrolyzer units 2030)	USD/kW/year	2185.26	Calculation results
Emission price	USD/tCO_2	11	Anderson et al., 2022 [148]
Grid emission factor (Uzbekistan)	gCO_2/kWh	400	IRENA, 2023 [149]

Taking into consideration the condition of operating the existing gas turbine unit with a 7,123.86 kW output power capacity, using hydrogen as the main fuel, including electrolyzer units of 2020 efficiency, ultrapure water for hydrogen production, hydrogen compressor and storage, the LCOE accounted for 0.81 USD/kWh. In comparison, the LCOE of the first solar PV plant in Uzbekistan accounted for 0.027USD/kWh [106]. The reason for such a high LCOE from the 100 %

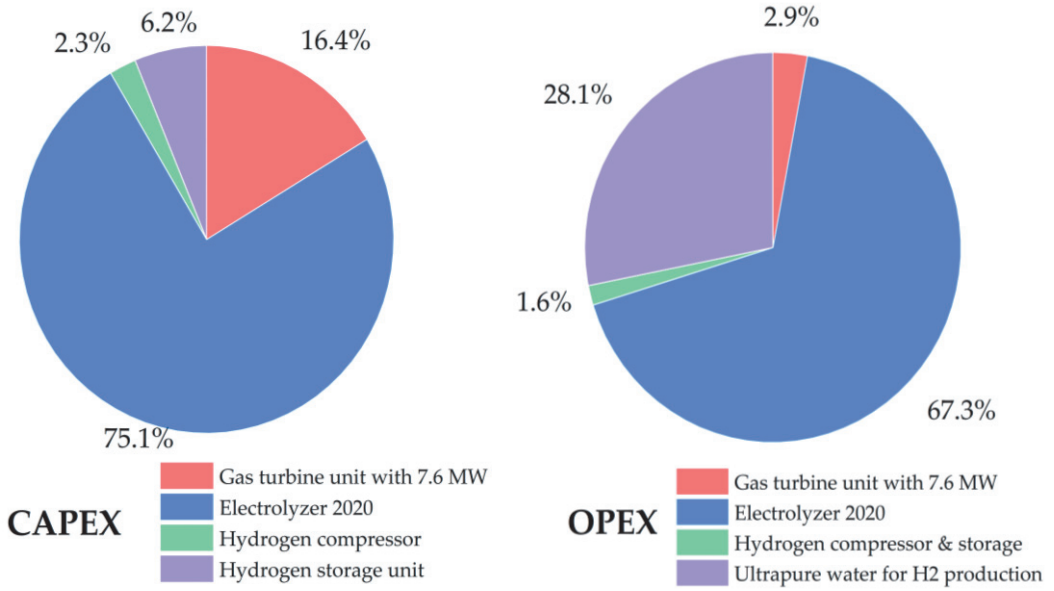

Figure 49. CAPEX and OPEX (electrolyzer efficiency 2020) of 100 % hydrogen-fired gas turbine.

hydrogen fired gas turbine is additional capital and operational expenditures, namely electrolyzer units, hydrogen compressor and storage tank, and feed materials for hydrogen production. Studies of Skordoulias et al. also found the LCOE of 100 % hydrogen-fired gas turbine in a similar range [155]. Figures 49 and 50 show a breakdown of capital and operational expenditures of the 100 % hydrogen-fired gas turbine with an emphasis on costs related to electrolyzer units with different efficiencies (i.e., 2020 and 2030). In the cost breakdown of CAPEX with an electolyzer of 2020 efficiency, the highest capital expenditure (75.1 %) belongs to the procurement of electrolyzer units, and the overall investment cost was 14,223.77 USD/kW. Therefore, electricity consumed by

the electrolyzer with an efficiency of 2020 accounted for 67.3 % in the cost breakdown of OPEX. On the other hand, the case with an electrolyzer of 2030 showed lower expenditures, such as 71.9 % of the electrolyzer share in CAPEX and 63.6 % of electrolyzer operational expenditures. The overall investment cost of the system was 12,612.45 USD/kW. Both cases are far from the overall CAPEX of the reference 100 % natural gas-fired gas turbine unit, which is 2,183.00 USD/kW. The reason for such high expenditure costs related to electrolyzer unit CAPEX and OPEX is the operation of electrolyzer units only during sunshine hours (7 hours) and the generation of green hydrogen.

A comparison of findings in both cases, applying hydrogen fuel for the full (100 %) replacement of fossil fuel consumption in the steel and power sectors, gives a good understanding of the future perspectives of each sector. As HDRI-EAF route's LCOP ranged between 606.30 USD/tls and 633.68 USD/tls, the impact of 1 kg of used hydrogen on the total hourly cost of steel ranged between 9.34 and 9.76 USD per kg of used hydrogen. In the case of the 100 % hydrogen-

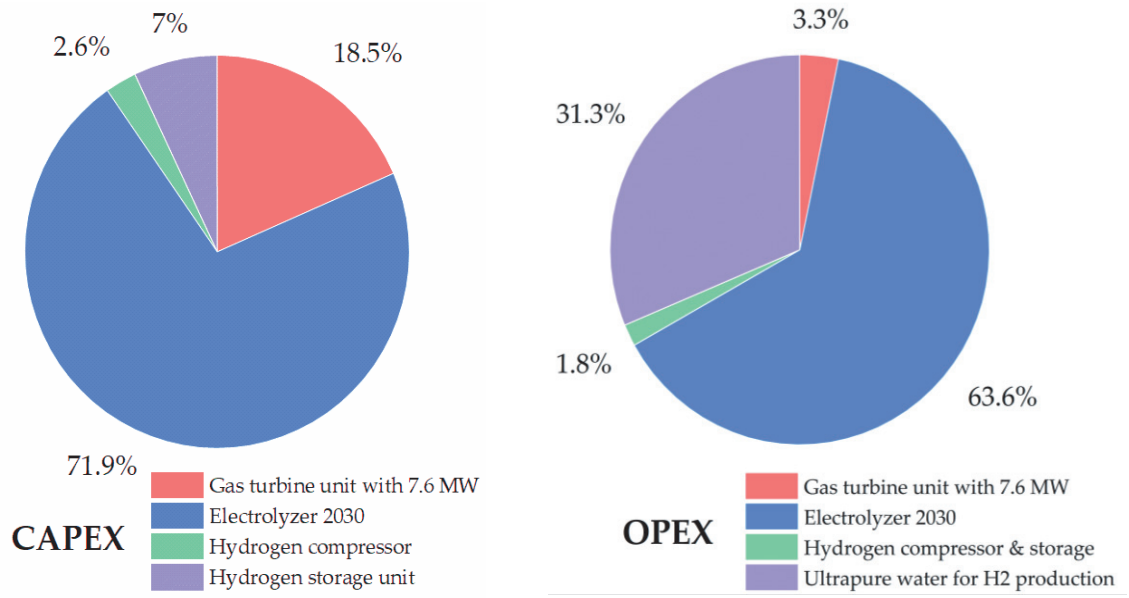

Figure 50. CAPEX and OPEX (electrolyzer efficiency 2030) of 100 % hydrogen-fired gas turbine.

fired gas turbine unit, LCOE ranged between 0.72 and 0.80 USD/kWh, and the impact of 1 kg of hydrogen fuel on the total hourly produced electricity amounted to a value in the range of 5.53 and 6.18 USD per kg of consumed hydrogen.

Since the investment cost to produce 1 kg of hydrogen fuel in the HDRI-EAF route and 100 % fired-gas turbine unit, in cases of electrolyzer units with 2020 and 2030 efficiency features, requires 91,116.42 USD/kgH_2 capacity and 78,773.57 USD/kgH_2 capacity respectively, the steel sector has a more attractive final product cost compared to the power sector.

From the viewpoint of the achievability of the required installed electrolyzer units, HDRI-EAF with electrolyzer units (2020 and 2030 efficiency rates) requires 4,420.07 MW and 3,752.89 MW respectively, while the 100 % hydrogen-fired gas turbine needs 168.99 MW of electrolyzer with 2020 efficiency and 143.48 MW in the case of the one with 2030 efficiency. As the recent largest alkaline electrolyzer-based hydrogen-producing plant with a 260 MW capacity in Xinjiang, northwest China [156] has failed in stable operation due to fluctuations in renewable energy output, from a technical and financial viewpoint, it is difficult to deploy hydrogen units for the prospective Tebinbulak DRI-EAF route at this moment. On the other hand, it is the first DRI-EAF route-based metallurgical plant in Uzbekistan, and there are no other small-scale DRI-EAF routes in the

country. In the case of applying hydrogen fuel in the power sector of Uzbekistan, there are several applicable gas turbines in existing power plants with capacities in the range of 7.6 MW to 650 MW gas turbine units [157]. Another positive development in this direction is ACWA Power launching the first green hydrogen project in Uzbekistan with a capacity of 3,000.00 tons of hydrogen production per year. In addition, ACWA Power is developing another pilot project for producing 3,000.00 tons of green ammonia per year and a subsequent project for 500,000.00 tons of green ammonia per year [158]. As the current study's 100 % hydrogen fired gas turbine model requires 4,643.67 tons of hydrogen per year for the demands of the CHP, this source of hydrogen and ammonia can be used in the power sector to replace fossil fuel. Future scenarios for 2030 from previous study of Giacomazzi et al. [70,159] also mention the possibility of reducing NOx emission below 25 ppmvd at 15 % O_2 with 100 % hydrogen combustion. Moreover, an issue related to the flashback phenomena of hydrogen combustion in a gas turbine must also be considered before transforming existing gas turbine units from conventional fuel to hydrogen [160]. Last but not least, hydrogen storage under high pressure in this study showed high costs, including expenses on the compression unit. Therefore, ammonia-based hydrogen storage can also be considered as a potential option based on previous studies [161-163]. The findings have been published in the Energies journal (Energies 2024, 17(5), 1242).

4.4 Conclusion

This research work aims to compare the effects of applying hydrogen fuel in the steel and power sectors of Uzbekistan. Firstly, the energy and mass balance of Hydrogen Direct Reduction Iron ore – Electric Arc Furnace (HDRI-EAF), analysis of energy consumption indicators of the process, and lab-scale experiments for optimizing the yield of reduction with an emphasis on residence time, temperature, and mass flow of hydrogen have been investigated. Secondly, optimized condition of the energy and mass balance of the 100 % hydrogen-fired gas turbine unit with a 7.6 MW installed capacity were found for analyzing the chemical kinetics in the hydrogen combustion process. Thirdly, the levelized cost of production of steel, in the example of prospective Tebinbulak DRI-EAF route-based metallurgical plant in Uzbekistan, was conducted to compare with the levelized cost of electricity of the 100 % hydrogen-fired gas turbine unit at Fergana CHP in Uzbekistan. After discussing all results from two different hydrogen-based industrials sectors, the following research findings are summarized:

- The total specific energy consumption of the HDRI-EAF route, as determined through energy and mass balance calculations, yielded a significantly lower value (2,679.69 kWh/tls) compared to previous findings in other studies.
- Optimizing iron ore reduction with hydrogen fuel in a laboratory condition experiment provided valuable expertise in handling hydrogen fuel in the process. This optimization resulted in a high reduction yield at lower temperature (770 °C) and within a limited residence time (7 minutes for two identical samples or 3.5 minutes per sample), compared to the experimental conditions of previous studies.
- In the case of the 100 % hydrogen-fired gas turbine, several simulations on Aspen HYSYS resulted in finding optimal condition with energy and mass balance for the cycle. The newly developed cycle was able to achieve nearly 93.73% of installed capacity (7.6 MW) of the gas turbine output power rate.
- As for emissions from the newly developed 100 % hydrogen-fired gas turbine cycle, no CO2 emissions were observed. Regarding NOx emissions at 15 % O2, the findings (50.82 ppmvd) exceeded the manufacturer's regulation (9.9 ppmvd) but remained lower than those demonstrated by a recently introduced novel 100 % hydrogen fired micro gas turbine (62 ppmvd).
- In the economic assessment of the HDRI-EAF route, two scenarios, each with different efficiency levels of electrolyzer units (2020 and 2030), have been investigated. The results show a lower Levelized Cost of Production (LCOP) of steel, ranging from 606.30 USD/tls to 633.68

USD/tls), compared to recently conducted studies on economic analysis of HDRI-EAF (which reported values from 622 USD/tls to 722 USD/tls).

- On the other hand, the 100 % hydrogen fired gas turbine resulted in LCOE ranging from 0.72 USD/kWh to 0.80 USD/kWh with hydrogen production on-site or 0.46 USD/kWh LCOE without hydrogen production on—site but procuring hydrogen from outside at 3 USD/kgH2, falling within a similar range to previous studies (from 0.50 USD/kWh to 0.75 USD/kWh). However, in comparison with the LCOE (from 0.027 USD/kWh to 0.08 USD/kWh) of conventional power plants in Uzbekistan, there is a significant difference that must be reduced in the future.
- Comparative analysis of LCOP of HDRI-EAF route and LCOE of 100 % hydrogen-fired gas turbine provided clear picture on capital and operational expenditure of each system. The effect of 1 kg of hydrogen was higher in the case of steel sector (from 9.34 to 9.76 USD per kg of used hydrogen) and lower in case of power sector (from 5.53 to 6.18 USD per kg of consumed hydrogen). Capacity of required electrolyzer units and availability of wide range of applicable technologies pointed to power sector transformation from fossil to hydrogen fuel in a short term. To prioritize the power sector, various aspects are emphasized, such as several existing gas turbine units in Uzbekistan with a wide range of capacity and significant CO2 emissions in the power sector, rather than the steel manufacturing sector.

Chapter 5. General Discussion and Conclusions

5.1 Discussion

The decarbonization of the most carbon-intensive industries, such as the steel and power sectors, is imperative for the sustainable development of these global industries. Initial steps involve conducting energy and mass balance evaluations for the Hydrogen Direct Reduction Iron Ore – Electric Arc Furnace (HDRI–EAF) route and performing experiments to optimize the reduction parameters of the process. The Specific Energy Consumption (SEC) of the HDRI–EAF was calculated as 2,679.69 kWh/tls. In comparison, earlier studies by Bhaskar et al. (2020) reported an SEC of 3.72 MWh/tls for HDRI-EAF [23], and Vogl et al. (2018) found an SEC of 3.48 MWh/tls [61]. The notable variation in SEC among studies is attributed to the use of different methodologies, including variations in the ratios of the actual flow rate of hydrogen to the stoichiometric flow rate required for the reduction reaction. Concerning the optimization of the reduction process, complete reduction of Fe_2O_3 can be achieved within 7 minutes using a hydrogen mass flow of 1 L/min for two identical samples of Fe_2O_3, each weighing 2.3622g, at a temperature of 770 °C. Regarding the optimization of the reduction process, earlier studies, such as the review by Heidari et al. (2021), indicated a 95% reduction in iron ore using 100% hydrogen in 5 minutes at 700 °C [40]. Wagner et al. (2006) achieved a 90% reduction of iron ore with 100% H2 at 800 °C within 3.5 minutes or 210 seconds [48]. Additionally, Patisson et al. (2020) reported a 50% and 40% reduction yield at 770 °C with 4.7 g of iron ore, using a mass flow of 2 L/min of H2/He (60/40 vol.) [43]. The differences in reduction yield and residence time noted in prior research, in contrast to the outcomes of the present study, can be ascribed to the utilization of distinct experimental configurations, varied iron ore compositions, and sample forms (fine or pellet), as well as discrepancies in the composition of the reducing agent, potentially involving diverse inert gases. The findings have been published in the Energies journal (Energies 2024, 17(5), 1242).

When considering strategies for decarbonizing the power sector, technical and economic considerations play a pivotal role in determining the most suitable and feasible scenario. In terms of technical parameters, aspects such as output power, CO_2 and NOx emissions, net efficiency, and specific fuel consumption undergo thorough examination and analysis utilizing Aspen HYSYS v8.8 and Ansys Chemkin Pro R1 software tools. Furthermore, the levelized cost of electricity for each scenario, incorporating various fuel blends, is calculated through discounted cash flow analysis. In the discussion of output power across all scenarios, Scenario 2 emerged as the most compelling choice, achieving the highest output capacity of 7,661.00 kW (100.73%). This surpassed the power output of Scenarios 1 (7,605.00 kW) (100%), 3 (7,578.00 kW) (99.64%), and 4 (7,637.00 kW) (100.42%). Comparing the findings of the current study with previous research, Ito et al. (2020) explored a combustor with a 2 MW capacity, achieving 2 MW with the co-firing of 20% vol. NH_3 [164]. In contrast, Azaria Haykal Ahmad et al. (2023) reported a 98.7% output power attainment with 30% vol. hydrogen co-firing in a gas turbine [165]. In the present study, a 99.64% output capacity was achieved with 30% vol. hydrogen co-firing. The slight difference in replacing natural gas with 30% vol. hydrogen can be attributed to various factors, including unit capacity, the distinct calorific value of the main fuel (natural gas), variations in inlet air temperature, differences in fluid packages, distinct inlet temperatures of the gas turbine, and other technical parameters.

CO_2 emissions in scenarios 1, 2, 3, and 4 were 6,070.00 kg/h (100%), 5,228.00 kg/h (86%), 5,345.00 kg/h (88%), and 3,979.00 kg/h (66%), respectively. Scenario 4 exhibited the highest reduction in CO_2 emissions compared to other scenarios. In a study by Koc et al. (2020), a hydrogen-co-firing gas turbine with 50 MW reported 1.0434 kg CO_2/kWh [108], while scenario 3 in the current study achieved 0.70 kg CO_2/kWh. Scenarios 1, 2, and 4 resulted in 0.79 kg CO_2/kWh, 0.68 kg CO_2/kWh, and 0.52 kg CO_2/kWh, respectively. The variation in CO_2 emissions per kWh among different fuel blends is linked to the combustion efficiency of each blend. Differences in CO_2/kWh compared to previous studies can be attributed to the composition of the used fuel and, notably, the turbine design, especially the software tool employed. The net efficiency in scenarios 1, 2, 3, and 4 varied, with values of 34.41 %, 35.52 %, 34.81 %, and 36.67 %, respectively. This variation can be traced back to the different inlet temperatures of the gas turbine in each scenario (1313 °C, 1316 °C, 1323 °C, and 1335 °C). Ammonia combustion, with its wide flammability limits, played a role in enhancing combustion efficiency. The Levelized Cost of Electricity (LCOE) for these scenarios was 0.09 USD/kWh, 0.14 USD/kWh, 0.13 USD/kWh, and 0.19 USD/kWh, respectively, mainly influenced by fuel cost. Among the provided fuels, natural gas proved to be the most cost-effective at 0.09 USD/kg. Specific fuel consumption in scenarios 1, 2, 3, and 4 was 0.31 kg/kWh, 0.38 kg/kWh, 0.39 kg/kWh, and 0.51 kg/kWh, respectively. The combustor design led to a higher required amount of fuel for hydrogen compared to ammonia, underscoring the suitability of ammonia for combustion. NOx emissions at 15 % O_2 in scenarios 1, 2, 3, and 4 were 9.7 ppm, 1819.9 ppm, 3.1 ppm, and 2229.6 ppm, respectively. Egawa et al. (2023) reported low NOx emissions with a 30 % vol. hydrogen co-firing gas turbine, while significant increases were noted under the NH_3 co-firing approach [166]. The notable NOx emissions in Scenarios 2 and 4 are associated with variations in the amount of free radicals observed after premixing ammonia and hydrogen in the fuel mixture. In Scenario 2, the presence of the intermediate product HNO resulting from ammonia combustion contributes to the formation of NOx emissions, explaining the significantly higher NOx emissions in Scenarios 2 and 4. Discussing the suitability of H_2 and NH_3 at a 30 % volume share, H_2 can be a suitable option, although it has some disadvantages such as the potential for easy leakage from junctions of the fuel handling units. Therefore, it is advisable to investigate inert gas and oxygen-based sealing methods in gas turbines to prevent hydrogen leakage. The findings have been published in International Journal of Hydrogen Energy (Vol. 61, pp. 432-443).

After identifying the appropriate and viable iron ore reduction and fuel-blending option, the next step is to assess the impact of introducing 1 kg of hydrogen in the steel and power sectors. This serves as an example for Uzbekistan, illustrating the transformation from conventional operation mode to a hydrogen-based mode. Hydrogen consumption in both the steel and power plant cases was reported at 0.06 kgH_2/kg of steel and 0.13 kgH_2/kWh, respectively. The HDRI-EAF theoretically requires 54 kg of H_2 to produce 1 ton of steel. However, in the new Tebinbulak metallurgical complex, the actual value stands at 60 kg of H_2 per ton of steel. In terms of hydrogen-based electricity generation, the theoretical requirement is 0.03 kg of H_2 to produce 1 kWh of electricity. The findings of this study reveal a higher consumption rate of 0.13 kg of H_2 for 1 kWh of electricity generation, largely influenced by the gas turbine combustor design limitations in Aspen HYSYS, lacking specific functions for new combustor options like multi-cluster or premixed. Capital expenditure (CAPEX) related to the product cost in hydrogen-based steel is 1.9 times higher than the cost of 1 ton of hydrogen-based steel and 3.5 times more than the cost of 1 kWh of hydrogen-based electricity. This substantial difference in CAPEX between the 100%

hydrogen-fired gas turbine and 1 kWh of electricity is attributed to the high hydrogen consumption in the power sector. Operational expenditure (OPEX) for the steel plant is 0.72 times the cost of 1 ton, while OPEX for the power plant is 0.6 times the cost of 1 kWh. The slightly elevated OPEX in the steel plant is linked to iron ore procurement costs. The cost impact of 1 kg of hydrogen is higher in the steel sector, increasing from 9.34 to 9.76 USD per kg of used hydrogen, and lower in the power sector, rising from 5.53 to 6.18 USD per kg of consumed hydrogen. If hydrogen fuel is not produced on-site and is purchased externally at \$3 per kgH_2, the Levelized Cost of Production (LCOP) in the steel plant case will be \$578/tls, and in the power plant case, it will be 0.46 USD/kWh. With this approach, the levelized cost of steel and electricity can decrease by 9% and 42.5%, respectively. The cost of 1 ton of hydrogen-based liquid steel is 1.49 times that of 1 ton of EAF-based steel (conventional). Additionally, the cost of 1 kWh of hydrogen-based electricity is 0.72 USD, which is 9 times the current sale price (0.08 USD/kWh) of electricity produced with a conventional approach in Uzbekistan. The findings have been published in the Energies journal (Energies 2024, 17(5), 1242).

5.2 Conclusions

After reviewing all the findings throughout the entire research, the following conclusions are summarized:

- The Specific Energy Consumption (SEC) of HDRI-EAF amounted to 2,679.69 kWh/tls. To reduce 1,428.00 kg of iron ore or produce 1 ton of liquid steel, 54 kg of H_2 is needed. Additionally, 483 kg of H_2O is required to produce 54 kg of H_2. To produce 1 ton of liquid steel, 999 kg of sponge iron and 1 kg of char are necessary.
- 7 minutes of residence time with a mass flow of 1 L/min of H_2 consumption for reducing two identical 2.3622g Fe_2O_3 samples are most optimally reduced, each with 99.70% and 99.33% yield of reduction at 770 °C.
- Four scenarios are developed. Scenario 1, Scenario 2, Scenario 3 and Scenario 4 with fuel blending of 100 % Natural gas (NG); 30% NH_3 & 70 % NG; 30% H_2 & 70% NG and 30% NH_3, 30% H_2 & 40 % NG. respectively. Output power in all scenarios varied from each other. Scenario 4, with a fuel blend including ammonia (NH_3) and hydrogen (H_2), resulted in the highest output power. In co-firing a single alternative fuel, such as NH_3 in a fuel mix, exceeded the output power of the reference case, but H_2 co-firing resulted in the lowest output power among all cases. Considering the technical, economic, and emission parameters of each scenario, scenario 4, NH_3 and H_2 co-firing case, was the most attractive one. However, the outcome of combustion kinetics analyses dramatically changed the final decision, and the scenario with H_2 co-firing demonstrated attractive performance and favorable combustion kinetics at this moment.
- Levelized cost of production of steel and electricity ranged from \$606.30/tls to \$633.68/tls and from \$0.72/kWh and \$0.80/kWh respectively. The cost impact of 1 kg of hydrogen was higher in the steel sector (increasing from 9.34 to 9.76 USD per kg of used hydrogen) and lower in the power sector (rising from 5.53 to 6.18 USD per kg of consumed hydrogen).
- The cost of 1 ton of hydrogen-based liquid steel is 1.49 times that of 1 ton of EAF-based steel (conventional). The cost of 1 kWh of hydrogen-based electricity is 0.72 USD, which is 9 times the current sale price (0.08 USD/kWh) of electricity produced with the conventional approach in Uzbekistan. The findings prioritize the application of hydrogen in the steel sector.

Considering the unavailability of the Direct Reduction Iron Ore – Electric Arc Furnace (DRI-EAF) route in Uzbekistan at this moment and the operation of a large-scale new DRI-EAF route-based metallurgical plant only in 2027, it is more feasible to start hydrogen-based power sector development in the short term. This is particularly relevant, especially with several gas turbines in existing power plants with capacities in the range of 7.6 MW to 650 MW available.

References

1. ClimateWatch. Global Greenhouse Gas Emission by Sector. Available online: https://ourworldindata.org/emissions-by-sector (accessed on 28 February 2024).
2. Vercammen, S. Steel. Available online: https://www.mckinsey.com/capabilities/sustainability/our-insights/spotting-green-business-opportunities-in-a-surging-net-zero-world/transition-to-net-zero/steel (accessed on 28 February 2024).
3. Finkelstein, J.; Frankel, D.; Noffsinger, J. How to decarbonize global power systems. Available online: https://www.mckinsey.com/industries/electric-power-and-natural-gas/our-insights/how-to-decarbonize-global-power-systems#/ (accessed on 28 February 2024).
4. Kurrer, C. *The potential of hydrogen for decarbonising steel production*; European Parliamentary Research Service: Scientific Foresight Unit (STOA), 2020; pp. 1-8.
5. IEA. Global Hydrogen Review 2023. **2023**, 1-174.
6. JERA. A World First: The First Step Toward Carbon-Free Thermal Power Generation. Available online: https://www.jera.co.jp/en/action/discover/025#:~:text=Ammonia%20(NH3)%20holds%20the,reducing%20their%20CO2%20emissions. (accessed on 28 February 2024).
7. Fujimori, T.; Suda, T. *Ammonia Energy Value Chain for Carbon Neutrality from Production to Utilization*; IHI Corporation: Tokyo, Japan, **2022**.
8. Mayer, P.; Ramirez, A.; Pezzella, G.; Winter, B.; Sarathy, S.M.; Gascon, J.; Bardow, A.P. Blue and green ammonia production: A techno-economic and life cycle assessment perspective. *Iscience* **2023**, *26*, 107389, doi:doi.org/10.1016/j.isci.2023.107389.
9. Black&Veatch. Ammonia: Fuel vs. Hydrogen Carrier. Available online: https://www.bv.com/perspectives/ammonia-fuel-vs-hydrogen-carrier/ (accessed on 01 March 2024).
10. Shah, J. Can Green Ammonia Solve India's Subsidies Woes? Available online: https://www.saurenergy.com/solar-energy-blog/can-green-ammonia-solve-indias-subsidies-woes (accessed on 01 March 2024).
11. Hydrogen-Newsletter. What is Steam Methane Reforming (SMR)? Available online: https://www.hydrogennewsletter.com/what-is-steam-methane-reforming-smr/ (accessed on 01 March 2024).
12. EERE, D. Hydrogen Production: Electrolysis. Available online: https://www.energy.gov/eere/fuelcells/hydrogen-production-electrolysis (accessed on 01 March 2024).
13. IRENA&AEA. *Innovation Outlook: Renewable Ammonia*; IRENA and AEA: International Renewable Energy Agency, Abu Dhabi & Ammonia Energy Association, Brooklyn, 2022.
14. Lüngen, H.B.; Schmöle, P. History, developments and processes of direct reduction of iron ores. **2022**, 1-18.
15. Midrex Technologies, I. *2021 World Direct Reduction Statistics*; Midrex Technologies, Inc.: New Jersey, the USA, **2022**; pp. 1-18.
16. Tanaka, H. Resources Trend and Use of Direct Reduced Iron in Steelmaking Process. **2015**, *33*, 1-7.

17. IEEFA. *Steelmakers seeking green steel*; The Institute for Energy Economics and Financial Analysis: www.ieefa.org, **2022**; pp. 1-2.
18. Nishioka, K.; Ujisawa, Y.; Tonomura, S.; Ishiwata, N.; Sikstrom, P.K. Sustainable Aspects of CO2 Ultimate Reduction in the Steelmaking Process (COURSE50 Project), Part 1: Hydrogen Reduction in the Blast Furnace. *Journal of Sustainable Metallurgy* **2016**, *2*, 200-208, doi:doi.org/10.1007/s40831-016-0061-9.
19. SSAB. HYBRIT®. A new revolutionary steelmaking technology. Available online: https://www.ssab.com/en/fossil-free-steel/insights/hybrit-a-new-revolutionary-steelmaking-technology (accessed on 01 March 2024).
20. H2greensteel. Powering a new, clean industrial revolution. Available online: https://www.h2greensteel.com/ (accessed on 01 March 2024).
21. ArcelorMittal. ArcelorMittal Projects. Available online: https://projects.arcelormittal.com/ (accessed on 01 March 2024).
22. TATASteel. *HISARNA: Building a sustainable steel industry*; TATA Steel: www.tatasteeleurope.com, **2020**; pp. 1-4.
23. Bhaskar, A.; Assadi, M.; Nikpey Somehsaraei, H.A.; Somehsaraei, H.N. Decarbonization of the Iron and Steel Industry with Direct Reduction of Iron Ore with Green Hydrogen. *Energies* **2020**, *13*, 758, doi:doi.org/10.3390/en13030758.
24. Digiesi, S.; Mummolo, G.; Vitti, M.S. Minimum Emissions Configuration of a Green Energy-Steel System: An Analytical Model. *Energies* **2022**, *15*, 3324, doi:doi.org/10.3390/en15093324.
25. de la Pena, B.; de la Peña, B.; Iriondo, A.; Galletebeitia, A.; Gutierrez, A.; Rodriguez, J.; Lluvia, I.; Vicente, A.B. Toward the Decarbonization of the Steel Sector: Development of an Artificial Intelligence Model Based on Hyperspectral Imaging at Fully Automated Scrap Characterization for Material Upgrading Operations. *Steel Research International* **2023**, *94*, doi:doi.org/10.1002/srin.202200943.
26. WSA. *Hydrogen (H2) - based ironmaking*; World Steel Association: https://worldsteel.org/, **2022**; pp. 1-2.
27. GTL-MIT. Early Gas Turbine History. Available online: https://www.gas-turbine-lab.mit.edu/early-gas-turbine-history (accessed on 01 March 2024).
28. Langston, L.S. As the Turbine Turns... Hydrogen-Fueled Gas Turbines. *Mechanical Engineering* **2019**, *141*, 52-54, doi:doi.org/10.1115/1.2019-MAR-6.
29. Radovanovic, M. *Sustainable Energy Management - Planning, Implementation, Control, and Security*, 2nd Edition ed.; **2022**.
30. US. Deparment of Energy, E.E.R.E. Combined Heat and Power Technology Fact Sheet Series. **2017**, *DOE/EE-1692*.
31. ScienceFact.net. Brayton Cycle. Available online: https://www.sciencefacts.net/brayton-cycle.html (accessed on 22 September 2023).
32. Linkevics, O.; Grebesa, P.; Andersons; Janis; Mezulis; Ansis. Decarbonisation options of existing thermal power plant burning natural gas. *Advances in Carbon Capture Utilization and Storage* **2023**, *1*, 9–21, doi:doi.org/10.21595/accus.2022.23058.
33. Matsumoto, T.; Kawakami, T.; Takeishi, H.; Miura, K.; Nakamura, S.; Yuri, M. *Development of Hydrogen/Ammonia-firing Gas Turbine for Carbon Neutrality - Mitsubishi Heavy Industries Technical Review*; Mitsubishi Heavy Industries: **2022**; p. 13.
34. Basson, E. *2022 World Steel in Figures*; World Steel Association: **2022**.
35. Holappa, L. A General Vision for Reduction of Energy Consumption and CO2 Emissions from the Steel Industry. *Metals* **2020**, *10*, 1117, doi:doi.org/10.3390/met10091117.
36. Small, M. Direct Reduction of Iron-Ore. *Journal of Metals* **1981**, *33*, 67-75, doi:doi.org/10.1007/BF03354411.
37. Eisl, R.; Hochwimmer, M.; Oppeneiger, C.; Buchberger, D. Hydrogen Based Direct Iron Ore Reduction Plant Simulation. *BHM Berg- und Hüttenmännische Monatshefte* **2022**, *167*, 92-98, doi:10.1007/s00501-022-01199-2.

38. Yamashita, S. Hyfor Pilot Plant Starts Operation – Next Step In Carbon-Free Hydrogen Reduction
Steelmaking. Available online: https://www.primetals.com/jp/%E3%83%97%E3%83%AC%E3%82%B9-%E3%83%A1%E3%83%87%E3%82%A3%E3%82%A2/%E6%9C%80%E6%96%B0%E6%83%85%E5%A0%B1/hyfor-pilot-plant-under-operation-the-next-step-for-carbon-free-hydrogen-based-direct-reduction-is-done (accessed on 12 December 2023).
39. Spreitzer, D.; Wurm, J.; Hiebl, B.; Rein, N.; Wolfinger, T.; Sterrer, W.; Fleischanderl, A. HYFOR – Hydrogen-based Fine-Ore Reduction. Available online: https://www.mhi.co.jp/technology/review/pdf/e592/e592070.pdf (accessed on 16 December 2023).
40. Heidari, A.; Niknahad, N.; Iljana, M.; Fabritius, T.A. A Review on the Kinetics of Iron Ore Reduction by Hydrogen. *Materials* **2021**, *14*, 7540, doi:doi.org/10.3390/ma14247540.
41. Ma, K.; Deng, J.; Wang, G.; Zhou, Q.I.; Xu, J.K.H.; Xu, J. Utilization and impacts of hydrogen in the ironmaking processes: A review from lab-scale basics to industrial practices. *International Journal of Hydrogen Energy* **2021**, *46*, 26646-26664, doi:doi.org/10.1016/j.ijhydene.2021.05.095.
42. Hessels, C.J.M.; Homan, T.A.M.; Deen, N.G.; Tang, Y.C.J.M.; Tang, Y. Reduction kinetics of combusted iron powder using hydrogen. *Power Technology* **2022**, *407*, 117540, doi:doi.org/10.1016/j.powtec.2022.117540.
43. Patisson, F.; Mirgaux, O.F. Hydrogen Ironmaking: How It Works. *Metals* **2020**, *10*, 922, doi:doi.org/10.3390/met10070922.
44. Spreitzer, D.; Schenk, J.D. Reduction of Iron Oxides with Hydrogen—A Review. *Steel Research International* **2019**, *90*, 1900108, doi:doi.org/10.1002/srin.201900108.
45. Yi, S.-H.; Lee, W.-J.; Lee, Y.-S.; Kim, W.-H.S.H.; Kim, W.-H. Hydrogen-Based Reduction Ironmaking Process and Conversion Technology. *Korean Journal of Metals and Materials* **2021**, *59*, 41-53, doi:dx.doi.org/10.3365/KJMM.2021.59.1.41.
46. Patisson, F.; Mirgaux, O.; Birat, J.-P.F. Hydrogen steelmaking. Part 1: Physical chemistry and process metallurgy. *Matériaux Techniques* **2021**, *109*, 303, doi:doi.org/10.1051/mattech/2021025.
47. Ishii, K.; Akiyama, T.; Kashiwaya, Y.; Kondo, S.-i. The Rates of Reduction of Iron-Ore and Water-Gas Shift Reaction. *Hokkaido University Faculty of Engineering Bulletin* **1986**, *71*, S97-S97, doi:hdl.handle.net/2115/38021.
48. Wagner, D.; Devisme, O.; Patisson, F.; Ablitzer, D. A laboratory study of the reduction of iron oxides by hydrogen. *Sohn International Symposium* **2006**, 111-120, doi:hal.science/hal-00265636.
49. Zakeri, A.; Coley, K.S.; Tafaghodi, L.A. Hydrogen-Based Direct Reduction of Iron Oxides: A Review on the Influence of Impurities. *Sustainability* **2023**, *15*, 13047, doi:doi.org/10.3390/su151713047.
50. Zheng, H.; Schenk, J.; Daghagheleh, O.; Taferner, B.H. Parameter Optimization for Hydrogen-Induced Fluidized Bed Reduction of Magnetite Iron Ore Fines. *Metals* **2023**, *13*, 339, doi:doi.org/10.3390/met13020339.
51. Alikulov, K.; Xuan Tran, D. O-17 Achievement of theoretical hydrogen consumption in Hydrogen Direct Reduction of Iron Ore. In Proceedings of the 18th Biomass Science Conference, Maebashi, Japan, **2022**; pp. 37-38.
52. Boretti, A. The perspective of hydrogen direct reduction of iron. *Journal of Cleaner Production* **2023**, *429*, 139585, doi:doi.org/10.1016/j.jclepro.2023.139585.
53. Felder, R.M.; Rousseau, R.W. *Elementary principles of chemical processes*, 3rd ed.; John Wiley: New York ; Chichester, **2000**; pp. xxvi, 675 p.
54. Smith, J.M.; Van Ness, H.C.; Abbott, M.M. *Introduction to chemical engineering thermodynamics*, 7th ed.; McGraw-Hill: Boston, **2005**; pp. xviii, 817 p.

55. National Institute of Standards and Technology (U.S.). *NIST chemistry webbook*, June 2005 ed.; National Institute of Standards and Technology: Washington, D.C., **2005**; p. electronic text.
56. Dutta, S.K.; Ghosh, A.S.K.; Ghosh, A. A New Method for Measurement of Degree of Reduction in Composite Pellets of Iron Ore with Carbonaceous Matter. *ISIJ International* **1993**, *33*, 1104-1106, doi:doi.org/10.2355/isijinternational.33.1104.
57. Li, S.; Zhang, H.; Nie, J.; Dewil, R.; Baeyens, J.; Deng, Y.S. The Direct Reduction of Iron Ore with Hydrogen. *Sustainability* **2021**, *13*, 8866, doi:doi.org/10.3390/su13168866.
58. Rechberger, K.; Spanlang, A.; Sasiain Conde, A.; Wolfmeir, H.; Harris, C.K. Green Hydrogen-Based Direct Reduction for Low-Carbon Steelmaking. *Steel Research International* **2020**, *91*, 2000110, doi:doi.org/10.1002/srin.202000110.
59. Pimm, A.J.; Cockerill, T.T.; Gale, W.F.A.J.; Gale, W.F. Energy system requirements of fossil-free steelmaking using hydrogen direct reduction. *Journal of cleaner production* **2021**, *312*, 127665, doi:doi.org/10.1016/j.jclepro.2021.127665.
60. Souza Filho, I.R.; Springer, H.; Ma, Y.; Mahajan, A.; Da Silva, C.C.; Kulse, M.; Raabe, D.I.R.; Hauke, H.; Raabe, D. Green steel at its crossroads: Hybrid hydrogen-based reduction of iron ores. *Journal of cleaner production* **2022**, *340*, 130805, doi:doi.org/10.1016/j.jclepro.2022.130805.
61. Vogl, V.; Åhman, M.; Nilsson, L.J.V.; Ahman, M.; Nilsson, L.J. Assessment of hydrogen direct reduction for fossil-free steelmaking. *Journal of cleaner production* **2018**, *203*, 736-745, doi:doi.org/10.1016/j.jclepro.2018.08.279.
62. FCON CO., L. Mass Flow Controller 1000 Series. Available online: http://www.fcon-inc.jp/en/en_MFC/1000/1000.html (accessed on December 13, 2023).
63. Cavaliere, P.; Perrone, A.; Marsano, D.P. Effect of reducing atmosphere on the direct reduction of iron oxides pellets. *Powder Technology* **2023**, *426*, 118650, doi:doi.org/10.1016/j.powtec.2023.118650.
64. Sarkar, A.; Chavan, V.; Pai, N.N.; Prakash, A.; Hazra, B.; Raut, P.; Sunilkumar, D.; Sivananda, C.; Kundu, S.; Nag, S.; et al. Reduction of Iron Ore Pellets: A Microstructural Perspective? *Metallurgical and Materials Transactions A - Physical Metallurgy and Materials Science* **2024**, *55*, 537-549, doi:doi.org/10.1007/s11661-023-07265-9.
65. Sohn, H.Y. Energy Consumption and CO2 Emissions in Ironmaking and Development of a Novel Flash Technology. *Metals* **2020**, *10*, 54, doi:doi.org/10.3390/met10010054.
66. Wang, K.; Li, F.; Zhou, T.; Ao, Y.K.F.; Ao, Y. Numerical Study of Combustion and Emission Characteristics for Hydrogen Mixed Fuel in the Methane-Fueled Gas Turbine Combustor. *Aerospace* **2023**, *10*, 72, doi:doi.org/10.3390/aerospace10010072.
67. Sampath, P.; Shum, F. Combustion Performance of Hydrogen in a Small Gas-Turbine Combustor. *International Journal of Hydrogen Energy* **1985**, *10*, 829-837, doi:doi.org/10.1016/0360-3199(85)90172-7.
68. Moliere, M.; Molière, M. The Fuel Flexibility of Gas Turbines: A Review and Retrospective Outlook. *Energies* **2023**, *16*, 3962, doi:10.3390/en16093962.
69. Giacomazzi, E.; Messina, G. Hydrogen and the fuel-flexibility dilemma in gas turbines. **2021**, 125-129, doi:DOI 10.12910/EAI2021-024.
70. Giacomazzi, E.; Troiani, G.; Di Nardo, A.; Calchetti, G.; Cecere, D.; Messina, G.; Carpenella, S.E. Hydrogen Combustion: Features and Barriers to Its Exploitation in the Energy Transition. *Energies* **2023**, *16*, 7174, doi:10.3390/en16207174.
71. MHI.LTD. *Hydrogen Power Generation Handbook*, 2nd Edition ed.; MHI.LTD Energy Systems: **2021**; Volume METP-01GT02E1-A-0, (1.0)21-09, ZEG.
72. Aziz, M.; Juangsa, F.B.; Irhamna, A.R.; Irsyad, A.R.; Hariana, H.; Darmawan, A.M. Ammonia utilization technology for thermal power generation: A review. *Journal of the Energy Institute* **2023**, *111*, 101365, doi:doi.org/10.1016/j.joei.2023.101365.

73. Erdemir, D.; Dincer, I. A perspective on the use of ammonia as a clean fuel: Challenges and solutions. *International Journal of Energy Research* **2021**, *45*, 4827-4834, doi:doi.org/10.1002/er.6232.
74. Aalrebei, O.F.; Fawwaz Aalrebei, O.; Hamdan Al Assaf, A.; Amhamed, A.; Swaminathan, N.; Hewlett, S.O.F.; Al Assaf, A.H.; Hewlett, S. Ammonia-hydrogen-air gas turbine cycle and control analyses. *International Journal of Hydrogen Energy* **2022**, *47*, 8603-8620, doi:doi.org/10.1016/j.ijhydene.2021.12.190.
75. Ditaranto, M.; Heggset, T.; Berstad, D.M. Concept of hydrogen fired gas turbine cycle with exhaust gas recirculation: Assessment of process performance. *Energy* **2020**, *192*, 116646, doi:doi.org/10.1016/j.energy.2019.116646.
76. Lee, H.; Lee, M.-J. Recent Advances in Ammonia Combustion Technology in Thermal Power Generation System for Carbon Emission Reduction. *Energies* **2021**, *14*, 5604, doi:10.3390/en14185604.
77. Bayramoglu, K.; Bayramoğlu, K.; Bahlekeh, A.; Masera, K. Numerical investigation of the hydrogen, ammonia and methane fuel blends on the combustion emissions and performance. *International Journal of Hydrogen Energy* **2023**, *48*, 39586-39598, doi:10.1016/j.ijhydene.2023.06.079.
78. Karam Ghareh Gheshlaghi, M.; Tahsini, A.M. Numerical investigation of hydrogen addition effects to a methane-fueled high-pressure combustion chamber. *International Journal of Hydrogen Energy* **2023**, *48*, 33732-33745, doi:doi.org/10.1016/j.ijhydene.2023.05.119.
79. Aminov, Z.; Nakagoshi, N.; Xuan, T.D.; Higashi, O.; Alikulov, K.Z. Evaluation of the energy efficiency of combined cycle gas turbine. Case study of Tashkent thermal power plant, Uzbekistan. *Applied Thermal Engineering* **2016**, *103*, 501-509, doi:10.1016/j.applthermaleng.2016.03.158.
80. Matjanov, E. Gas turbine efficiency enhancement using absorption chiller. Case study for Tashkent CHP. *Energy* **2020**, *192*, 116625, doi:10.1016/j.energy.2019.116625.
81. Tang, G.; Jin, P.; Bao, Y.; Chai, W.S.; Zhou, L.G. Experimental investigation of premixed combustion limits of hydrogen and methane additives in ammonia. *International Journal of Hydrogen Energy* **2021**, *46*, 20765-20776, doi:doi.org/10.1016/j.ijhydene.2021.03.154.
82. Gurakov, N.I.; Kolomzarov, O.V.; Idrisov, D.V.; Novichkova, S.S.; Emirova, L.S.; Abrashkin, V.Y.; Matveev, S.S.; Fokin, N.I.; Simin, N.O.; Ivanovskii, A.A.; et al. Numerical and Experimental Study of Combustion of Methane-Hydrogen Mixtures in a Model Combustion Chamber of a Gas-Turbine Power Plant. *Combustion Explosion and Shock Waves* **2023**, *59*, 137-144, doi:doi.org/10.1134/S001050822302003X.
83. Sanli, A.; Yılmaz, I.T.; Gümüş, M.A.; Yilmaz, I.T.; Gümüs, M. Assessment of combustion and exhaust emissions in a common-rail diesel engine fueled with methane and hydrogen/methane mixtures under different compression ratio. *International Journal of Hydrogen Energy* **2020**, *45*, 3263-3283, doi:doi.org/10.1016/j.ijhydene.2019.11.222.
84. Kurien, C.; Varma, P.S.; Mittal, M.C. Effect of ammonia energy fractions on combustion stability and engine characteristics of gaseous (ammonia/methane) fuelled spark ignition engine. *International Journal of Hydrogen Energy* **2023**, *48*, 1391-1400, doi:doi.org/10.1016/j.ijhydene.2022.10.032.
85. Fuzesi, D.; Füzesi, D.; Józsa, V.; Csemány, D. Numerical investigation on the effect of hydrogen share in NH3/H2 blends in a turbulent lean-premixed swirl burner. *International Journal of Hydrogen Energy* **2024**, *49*, 816-827, doi:doi.org/10.1016/j.ijhydene.2023.09.091.
86. Wang, J.; Liu, H.; Wei, Z.E.; Pan, K.; Ji, W.; Jiang, Y.I.; Ye, D.; Wang, H.J.H.; Wang, H.N. Mapping the research on the spontaneous combustion of high-pressure hydrogen leakage: A bibliometric analysis. *International Journal of Hydrogen Energy* **2024**, *50*, 1006-1028, doi:doi.org/10.1016/j.ijhydene.2023.08.196.

87. Xi, Z.; Lian, T.; Shi, X.; Liu, Z.; Han, S.; Yang, X.; Zhang, J.; Li, W.; Mei, B.; Li, Y.Z.Y.; et al. Co-firing hydrogen and dimethyl ether in a gas turbine model combustor: Influence of hydrogen content and comparison with methane. *International Journal of Hydrogen Energy* **2022**, *47*, 38432-38444, doi:doi.org/10.1016/j.ijhydene.2022.09.012.
88. Luo, H.; Chang, F.; Jin, Y.U.; Ogata, Y.; Matsumura, Y.; Ichikawa, T.; Kim, W.; Nakashimada, Y.; Nishida, K.H.L.; Nishida, K. Experimental investigation on performance of hydrogen additions in natural gas combustion combined with CO2. *International Journal of Hydrogen Energy* **2021**, *46*, 34958-34969, doi:doi.org/10.1016/j.ijhydene.2021.08.037.
89. CHEMKIN®Software. *CHEMKIN-Pro 15112 Tutorials Manual, Reaction Design*; San Diego, 2011.
90. Smith, G.P.; Golden, D.M.; Frenklach, M.; Moriarty, N.W.; Eiteneer, B.; Goldenberg, M.; Bowman, C.T.; Hanson, R.K.; Song, S.; Gardiner, W.C.; et al. GRI-Mech 3.0. **2011**.
91. Campbell, J.M.; Hubbard, R.A. *Gas conditioning and processing*, 8th ed.; John M. Campbell and Company: Norman, Okla., 1966; pp. xii, 440 pages.
92. Association, G.P.S. Engineering Data Book. **2004**.
93. HYSYS, A. *Process Utility Manager*, 8.8; **2023**.
94. Solar-Edition. What is LCOE, Levelized Cost of Energy? The Concept Explained & Formula …. Available online: https://solaredition.com/what-is-lcoe/ (accessed on 24 October 2023).
95. ESAPyronics. An Introduction to Combustion. **2015**, 4.
96. Li, N.; Deng, H.; Xu, Z.; Yan, M.; Shengnan, w.; Sun, G.; Wen, X.; Wang, F.; Chen, G.N.N.; Wei, S.; et al. Experimental study on NH3/H2/air, NH3/CO/air, NH3/H2/CO/air premix combustion in a closed pipe and dynamic simulation at high temperature and pressure. *International Journal of Hydrogen Energy* **2023**, *48*, 34551-34564, doi:10.1016/j.ijhydene.2023.05.213.
97. Ueda, A.; Nisida, K.; Matsumura, Y.; Ichikawa, T.; Nakashimada, Y.; Endo, T.; Kim, W.A. Effects of hydrogen and carbon dioxide on the laminar burning velocities of methane-air mixtures. *Journal of the Energy Institute* **2021**, *99*, 178-185, doi:10.1016/j.joei.2021.09.007.
98. Karan, A.; Dayma, G.; Chauveau, C.; Halter, F. High-pressure and temperature ammonia flame speeds. In Proceedings of the 13th Asia-Pacific Conference on Combustion (ASPACC), Abu Dhabi, United Arab Emirates, **2021**.
99. Kobayashi, H.; Hayakawa, A.; Somarathne, K.D.Kunkuma A.; Okafor, E.H. Science and technology of ammonia combustion. *Proceedings of the Combustion Institute* **2019**, *37*, 109-133, doi:doi.org/10.1016/j.proci.2018.09.029.
100. Zhang, Y.; Zhao, D.; Li, Q.; Huang, M.; Hao, Q.; Du, J.; Song, Y.; Ming, Z.; Wang, J.Y.F.; Wang, J.H. Premixed combustion and emission characteristics of methane diluted with ammonia under F-class gas turbine relevant operating condition. *Frontiers in Energy Research* **2023**, *11*, doi:10.3389/fenrg.2023.1120108.
101. Cecere, D.; Carpenella, S.; Giacomazzi, E.; Stagni, A.; Di Nardo, A.; Calchetti, G. Effects of hydrogen blending and exhaust gas recirculation on NOx emissions in laminar and turbulent CH4/Air flames at 25 bar. *International Journal of Hydrogen Energy* **2023**, *49*, doi:doi.org/10.1016/j.ijhydene.2023.10.172.
102. Valera-Medina, A.; Vigueras-Zuniga, M.-O.; Shi, H.; Mashruk, S.; Alnajideen, M.; Alnasif, A.; Davies, J.; Wang, Y.; Zhu, X.; Yang, W.; et al. Ammonia combustion in furnaces: A review. *International Journal of Hydrogen Energy* **2023**, *49*, 1597-1618, doi:doi.org/10.1016/j.ijhydene.2023.10.241.
103. Mashruk, S.; Vigueras Zuniga, M.O.; Tejeda-del-Cueto, M.E.; Xiao, H.; Yu, C.; Maas, U.; Valera-Medina, A.S.; Valera Medina, A. Combustion features of CH4/NH3/H2 ternary blends. *International Journal of Hydrogen Energy* **2022**, *47*, 30315-30327, doi:doi.org/10.1016/j.ijhydene.2022.03.254.

104. Fukutani, S.; Kunioshi, N.; Jinno, H.S. Mechanism of Combustion Reactions in Hydrogen-Air Premixed Flames. *Bulletin of the Chemical Society of Japan* **1990**, *63*, 2191-2198, doi:10.1246/bcsj.63.2191.
105. Ma, F.; Guo, L.; Li, Z.; Zeng, X.; Zheng, Z.; Li, W.; Zhao, F.; Yu, W.F. A Review of Current Advances in Ammonia Combustion from the Fundamentals to Applications in Internal Combustion Engines. *Energies* **2023**, *16*, 6304, doi:10.3390/en16176304.
106. Melnikov, Y. *Sustainable Hydrogen Production Pathways in Eastern Europe, the Caucasus and Central Asia*; United Nations Economic Comission for Europe: Geneva, **2023**; p. 110.
107. Kim, Y.-K.; Kim, J.-H.; Yoo, S.-H.Y.K.; Yoo, S.H. Public perspective on co-firing hydrogen with natural gas in power plants in South Korea. *International Journal of Hydrogen Energy* **2023**, *48*, 4119-4128, doi:10.1016/j.ijhydene.2022.10.266.
108. Koc, Y.; Koç, Y.; Yağlı, H.; Görgülü, A.; Koç, A.Y.; Yagli, H. Analysing the performance, fuel cost and emission parameters of the 50 MW simple and recuperative gas turbine cycles using natural gas and hydrogen as fuel. *International Journal of Hydrogen Energy* **2020**, *45*, 22138-22147, doi:10.1016/j.ijhydene.2020.05.267.
109. Umyshev, D.R.; Osipov, E.V.; Kibarin, A.A.; Korobkov, M.S.; Khodanova, T.V.; Duisenbek, Z.S.D.R.; Duisenbek, Z.S. Techno-Economic Analysis of the Modernization Options of a Gas Turbine Power Plant Using Aspen HYSYS. *Energies* **2023**, *16*, 2704, doi:doi.org/10.3390/en16062704.
110. Bartels, J. A feasibility study of implementing an Ammonia Economy. Iowa State University, Iowa State University, **2008**.
111. Kojima, Y.; Yamaguchi, M.Y. Ammonia as a hydrogen energy carrier. *International Journal of Hydrogen Energy* **2022**, *47*, 22832-22839, doi:doi.org/10.1016/j.ijhydene.2022.05.096.
112. Statista. Total power generation in Uzbekistan from 2016 to 2022. Available online: https://www.statista.com/statistics/1299178/uzbekistan-electricity-generation/#:~:text=Power%20plants%20in%20Uzbekistan%20generated,increased%20each%20year%20under%20consideration. (accessed on 24 October 2023).
113. UNFCCC. *Project «Uzbekistan: Preparation of the Second National Communication under UN Framework Convention on Climate Change (UNFCCC)», National GHG Inventory Report 2000*; Center of Hydrometeorological Service (Uzhydromet) at the Cabinet of Ministers of the Republic of Uzbekistan: Tashkent, 2008; p. 144.
114. SAU. For 8 months, 1,096.5 thousand tons of anhydrous ammonia were produced. Available online: https://stat.uz/en/press-center/news-of-committee/27801-8-oyda-1-096-5-ming-tonna-suvsiz-ammiak-ishlab-chiqarilgan-3 (accessed on 24 October 2023).
115. Boyce, M.P. *Gas turbine engineering handbook*, 2nd ed.; Gulf Professional Pub.: Boston, MA, 2002; pp. xv, 799 p.
116. KHI. GPB80D. Available online: https://kga.com.my/wp-content/uploads/2020/10/GPB80D-200227.pdf (accessed on 22 November 2023).
117. De Simio, L.; Iannaccone, S.; Guido, C.; Napolitano, P.; Maiello, A. Natural Gas/Hydrogen blends for heavy-duty spark ignition engines: Performance and emissions analysis. *International Journal of Hydrogen Energy* **2023**, *50*, 743-757, doi:doi.org/10.1016/j.ijhydene.2023.06.194.
118. Liu, X.; Zhao, M.; Feng, M.; Zhu, Y.X.T.; Zhu, Y.J. Study on mechanisms of methane/hydrogen blended combustion using reactive molecular dynamics simulation. *International Journal of Hydrogen Energy* **2023**, *48*, 1625-1635, doi:doi.org/10.1016/j.ijhydene.2022.10.050.
119. Bastani, M.; Tabejamaat, S.; Ashini, H. Numerical and experimental study of combustion and emission characteristics of ammonia/methane fuel mixture in micro gas turbine combustor. *International Journal of Hydrogen Energy* **2023**, *49*, 1399-1415, doi:doi.org/10.1016/j.ijhydene.2023.09.319.

120. Kolbantseva, D.; Treschev, D.; Trescheva, M.; Anikina, I.; Kolbantsev, Y.; Kalmykov, K.; Aleshina, A.; Kalyutik, A.; Vladimirov, I.D. Analysis of Technologies for Hydrogen Consumption, Transition and Storage at Operating Thermal Power Plants. *Energies* **2022**, *15*, 3671, doi:10.3390/en15103671.
121. Jin, C.; Li, X.; Xu, T.; Dong, J.; Geng, Z.; Liu, J.; Ding, C.; Hu, J.; El Alaoui, A.; Zhao, Q.; et al. Zero-Carbon and Carbon-Neutral Fuels: A Review of Combustion Products and Cytotoxicity. *Energies* **2023**, *16*, 6507, doi:10.3390/en16186507.
122. Sohn, H.Y.; Roy, S.H.Y.; Roy, S. Development of a Moving-Bed Ironmaking Process for Direct Gaseous Reduction of Iron Ore Concentrate. *Metals* **2022**, *12*, 1889, doi:doi.org/10.3390/met12111889.
123. Pei, M.; Petäjäniemi, M.; Regnell, A.; Wijk, O.M. Toward a Fossil Free Future with HYBRIT: Development of Iron and Steelmaking Technology in Sweden and Finland. *Metals* **2020**, *10*, 972, doi:doi.org/10.3390/met10070972.
124. Echterhof, T. Review on the Use of Alternative Carbon Sources in EAF Steelmaking. *Metals* **2021**, *11*, 222, doi:doi.org/10.3390/met11020222.
125. Gielen, D.; Saygin, D.; Taibi, E.; Birat, J.D. Renewables-based decarbonization and relocation of iron and steel making: A case study. *Journal of Industrial Ecology* **2020**, *24*, 1113-1125, doi:10.110.1111/jiec.12997111/jiec.12.
126. Bhaskar, A.; Assadi, M.; Somehsaraei, H.N.A.; Somehsaraei, H.N. Can methane pyrolysis based hydrogen production lead to the decarbonisation of iron and steel industry? *Energy Conversion and Management: X* **2021**, *10*, 100079, doi:doi.org/10.1016/j.ecmx.2021.100079.
127. Bhaskar, A.; Abhishek, R.; Assadi, M.; Somehesaraei, H.N.A.; Somehesaraei, H.N. Decarbonizing primary steel production : Techno-economic assessment of a hydrogen based green steel production plant in Norway. *Journal of Cleaner Production* **2022**, *350*, 131339, doi:doi.org/10.1016/j.jclepro.2022.131339.
128. IEA. CO2 Emissions in 2022. Available online: https://www.iea.org/reports/co2-emissions-in-2022 (accessed on 27 December 2023).
129. Skabelund, B.B.; Jenkins, C.D.; Stechel, E.B.; Milcarek, R.J.B.B.; Milcarek, R.J. Thermodynamic and emission analysis of a hydrogen/methane fueled gas turbine. *Energy Conversion and Management: X* **2023**, *19*, 100394, doi:doi.org/10.1016/j.ecmx.2023.100394.
130. Nose, M.; Kawakami, T.; Nakamura, S.; Kuroki, H.; Kataoka, M.; Yuri, M. *Development of Hydrogen/Ammonia Firing Gas Turbine for Decarbonized Society*; Mitsubishi Heavy Industries: Mitsubishi Heavy Industries, **2021**.
131. Triangul-Metals. Tebinbulak Mining and Metallurgical Complex. Available online: https://www.triangulmetals.com/en (accessed on 22 February 2024).
132. JSC"O'zbekiston_temir_yo'llari". "Tebinbulak" Mining and Metallurgical complex: Implementation stages of the investment project. Available online: https://railway.uz/en/informatsionnaya_sluzhba/novosti/21873/ (accessed on 22 February 2024).
133. EnterEngineering. Design of Tebinbulak concentration plant is approaching “the home stretch”. Available online: https://www.ent-en.com/en/page/publication/210# (accessed on 10 January 2024).
134. Toktarova, A.; Karlsson, I.; Rootzén, J.; Göransson, L.; Odenberger, M.; Johnsson, F.A. Pathways for Low-Carbon Transition of the Steel Industry-A Swedish Case Study. *Energies* **2020**, *13*, 3840, doi:doi.org/10.3390/en13153840.
135. Banihabib, R.; Assadi, M.R. A Hydrogen-Fueled Micro Gas Turbine Unit for Carbon-Free Heat and Power Generation. *Sustainability* **2022**, *14*, 13305, doi:doi.org/10.3390/su142013305.
136. Banihabib, R.; Lingstädt, T.; Wersland, M.; Kutne, P.; Assadi, M. Development and testing of a 100 kW fuel-flexible micro gas turbine running on 100% hydrogen. *International*

Journal of Hydrogen Energy **2024**, *49*, 92-111, doi:doi.org/10.1016/j.ijhydene.2023.06.317.
137. IRENA. Making the breakthrough: Green hydrogen policies and technology costs. **2021**.
138. IRENA. *Green Hydrogen Cost Reduction: Scaling up Electrolysers to Meet the 1.5ºC Climate Goal*; 978-92-9260-295-6; International Renewable Energy Agency: Abu Dhabi, **2020**; pp. 1-103.
139. Krishnan, S.; Koning, V.; Kramer, G.J. Present and future cost of alkaline and PEM electrolyser stacks. *International Journal of Hydrogen Energy* **2023**, *48*, 32313-32330, doi:doi.org/10.1016/j.ijhydene.2023.05.031.
140. Kruger, A.; Krüger, A.; Andersson, J.; Grönkvist, S.; Cornell, A. Integration of water electrolysis for fossil-free steel production. *International Journal of Hydrogen Energy* **2020**, *45*, 29966-29977, doi:doi.org/10.1016/j.ijhydene.2020.08.116.
141. Feng, Z. *Economically Viable Intermediate to Long Duration Hydrogen Energy Storage Solutions for Fossil Fueled Assets*; WE New Energy Inc: Knoxville, TN, United States, **2022**.
142. Christensen, A. *Assessment of Hydrogen Production Costs from Electrolysis: United States and Europe*; International Council on Clean Transportation: https://theicct.org, **2020**.
143. Kolisnichenko, V. Iron ore prices on the Dalian Exchange reached $138/t. Available online: https://gmk.center/en/news/iron-ore-prices-on-the-dalian-exchange-reached-138-t/ (accessed on 06 January 2024).
144. Monitor-Deloitte. *Fueling the future of mobility: hydrogen electrolyzers*; Monitor Deloitte: https://www2.deloitte.com/, **2021**; p. 27.
145. Flagma. Highly purified deionized water. Available online: https://flagma.uz/ru/deionizirovannaya-voda-vysokoy-stepeni-ochistki-o1931903.html (accessed on 07 January 2024).
146. Cavaliere, P. Direct Reduced Iron: Most Efficient Technologies for Greenhouse Emissions Abatement. *Clean Ironmaking and Steelmaking Processes* **2019**, 419–484, doi:doi.org/10.1007/978-3-030-21209-4_8.
147. Elsheikh, H.; Eveloy, V.H. Renewable hydrogen based direct iron ore reduction and steel making with grid assistance. *Energy Conversion and Management* **2023**, *297*, 117544, doi:doi.org/10.1016/j.enconman.2023.117544
148. Anderson, G.; Ma, J.; Mirzoev, T.; Zhu, L.; Zhunussova, K. A Low-Carbon Future for the Middle East and Central Asia: What Are the Options? *International Monetary Fund Departmental Papers* **2022**, 52.
149. IRENA. Energy Profile - Uzbekistan. Available online: https://www.irena.org/-/media/Files/IRENA/Agency/Statistics/Statistical_Profiles/Asia/Uzbekistan_Asia_RE_SP.pdf (accessed on 21 December 2023).
150. Midrex. MIDREX® Direct Reduction Plants 2022 Operations Summary. Available online: https://www.midrex.com/tech-article/midrex-direct-reduction-plants-2022-operations-summary/ (accessed on 09 January 2024).
151. Rolo, I.; Costa, V.A.F.; Brito, F.P. Hydrogen-Based Energy Systems: Current Technology Development Status, Opportunities and Challenges. *Energies* **2024**, *17 (1)*, doi:doi.org/10.3390/en17010180.
152. Pirmatov, R.; Ahmedov, D.; Budey, T. *Business Plan of JSC "UZMETKOMBINAT" for 2023*; JSC "UZMETKOMBINAT": www.uzbeksteel.uz, **2022**; pp. 1-33.
153. Meteonorm-8. Meteorological dataset of Uzbekistan. **2020**.
154. Eurowater. Water treatment for hydrogen production: FAQ - water treatment and hydrogen production. Available online: https://www.eurowater.com/en/hydrogen-production#:~:text=89%25%20of%20the%20mass%20is,due%20to%20losses%20and%20inefficiencies. (accessed on 06 January 2024).

155. Skordoulias, N.; Koytsoumpa, E.I.; Karellas, S.N. Techno-economic evaluation of medium scale power to hydrogen to combined heat and power generation systems. *International Journal of Hydrogen Energy* **2022**, *47*, 26871-26890, doi:10.1016/j.ijhydene.2022.06.057.
156. Collins, L. EXCLUSIVE | World's largest green hydrogen project 'has major problems due to its Chinese electrolysers': BNEF. Available online: https://www.hydrogeninsight.com/production/exclusive-worlds-largest-green-hydrogen-project-has-major-problems-due-to-its-chinese-electrolysers-bnef/2-1-1566679 (accessed on 13 January 2024).
157. JSC"TPP". *Business Plan of Joint-Stock Company "Thermal Power Plants" for 2023*; Joint-Stock Company "Thermal Power Plants": https://tpp.uz, **2022**; pp. 1-25.
158. Čučuk, A. ACWA Power launches Uzbekistan's first green hydrogen project. Available online: https://www.offshore-energy.biz/acwa-power-launches-uzbekistans-first-green-hydrogen-project/ (accessed on 14 January 2024).
159. Cecere, D.; Giacomazzi, E.; Di Nardo, A.; Calchetti, G.D. Gas Turbine Combustion Technologies for Hydrogen Blends. *Energies* **2023**, *16*, 6829, doi:doi.org/10.3390/en16196829.
160. Serbin, S.; Radchenko, M.; Pavlenko, A.; Burunsuz, K.; Radchenko, A.; Chen, D.S. Improving Ecological Efficiency of Gas Turbine Power System by Combusting Hydrogen and Hydrogen-Natural Gas Mixtures. *Energies* **2023**, *16*, 3618, doi:doi.org/10.3390/en16093618.
161. Aziz, M.; Wijayanta, A.T.; Nandiyanto, A.B.D.M.; Nandiyanto, A. Ammonia as Effective Hydrogen Storage: A Review on Production, Storage and Utilization. *Energies* **2020**, *13*, 3062, doi:doi.org/10.3390/en13123062.
162. Negro, V.; Noussan, M.; Chiaramonti, D.V. The Potential Role of Ammonia for Hydrogen Storage and Transport: A Critical Review of Challenges and Opportunities. *Energies* **2023**, *16*, 6192, doi:10.3390/en16176192.
163. Hasan, M.H.; Mahlia, T.M.I.; Mofijur, M.; Rizwanul Fattah, I.M.; Handayani, F.; Ong, H.C.; Silitonga, A.S.M.H.; Mahlia, T.; Silitonga, A.S. A Comprehensive Review on the Recent Development of Ammonia as a Renewable Energy Carrier. *Energies* **2021**, *14*, 3732, doi:10.3390/en14133732.
164. ITO, S.; UCHIDA, M.; SUDA, T.; FUJIMORI, T. Development of Ammonia Gas Turbine Co-Generation Technology. *IHI Engineering Review* **2020**, *53*, 1-6.
165. Ahmad, A.H.; Darmanto, P.S.; Juangsa, F.B.A.H.; Juangsa, F.B. Thermodynamic Study on Decarbonization of Combined Cycle Power Plant. *Journal of Engineering and Technological Sciences* **2023**, *55*, 613-626, doi:doi.org/10.5614/j.eng.technol.sci.2023.55.5.10.
166. Egawa, T.; Nagahashi, H.; Hayashi, A.; Fukuba, S.; Sato, K.; Nakamura, S. Hydrogen/Ammonia-fired Gas Turbine Initiatives for Carbon Neutrality. *Mitsubishi Heavy Industries Technical Review* **2023**, *60*, 1-12.